

**Books/Book Chapters/Conference Papers 2014-15**

SI No.	Name of the Teacher	Title of the Paper/Books/Book Chapter	Title of the proceedings of the conference	Name of the conference	National/ International	Year of publication	ISBN/ISSN number of the proceeding	Affiliating Institute at the time of publication	Name of the Publisher
1	Dr. V.R. Sastry, Dr. D. Venkat Reddy, and G. Raghu Chandra	Rock Blasting Geological Discontinuities & Influence on Blasting			International	18 SEPTEMBER S2014	ISBN: 978-93-5361-241-2	National Institute of Technology Karnataka, Surathkal	National Institute of Technology Karnataka, Surathkal
2	Y Madhu Maheswara Reddy, R Moses Kruparam, M Amresh Reddy	Design, Simulation And Analysis Of Automatic Multifastener Device	International Conference on Advances in Engineering and Technology-(ICAET 2014)	ICAET 2014,	International	2-3 May 2014	ISBN No.: 978-1-4799-4949-6 @ 2014 IEEE	Nagapattinam. Chennai	EGS Pillai Engineering College
3	B. Naik, K.K.Khatua and Kamel Miri	Prediction of Energy loss along the non-prismatic reach of a compound channel using ANN	River Flow-2014	International conference on Fluvial Hydraulics	International	3-5 September 2014.	ISBN 9781138026742	EPFL , Lausanne, Switzerland.	Taylor & Francis Group, London, ISBN 978-1-138-02674-2
4	Dr.G.Aravind	"Structural and Dielectric studies of Nickel Substituted Lithium nano ferrites by low temperature combustion	Innovative Trends in Applied Physical, Chemical, Mechanical, Statistical Sciences and Emerging Energy Technology for Sustainable Development" APCMSET-2014	Innovative Trends in Applied Physical, Chemical, Mechanical, Statistical Sciences and Emerging Energy Technology for Sustainable Development" APCMSET-2014	International	Jul/14	ISBN: 978-93-83083-88-6	Methodist College of Engg and Tech., Hyd	Excellent Publishing House, New Delhi
5	Md. Fakhruddin H. N.	Waste cooking oil as feedstock to produce biodiesel & Saponification reaction as by product		International Conference on Trend Setting Innovations in Chemical Sciences & Technology – Application in Pharma Industry (TSCST-APT)	International	16th - 18th DECEMBER,2015		Methodist College of Engg and Tech., Hyd	Institute of Science & Technology (Autonomous) Jawaharlal Nehru Technological University, Hyderabad – 58, Telangana State, India

**PRINCIPAL**  
 METHODIST COLLEGE OF ENGG. & TECH.  
 King Kot Road, Hyd, Hyderabad.

**Books/Book Chapters/Conference Papers 2014-15**

SI No.	Name of the Teacher	Title of the Paper/Books/Book Chapter	Title of the proceedings of the conference	Name of the conference	National/ International	Year of publication	ISBN/ISSN number of the proceeding	Affiliating Institute at the time of publication	Name of the Publisher
6	Md. Fakhruddin H. N.	Modified CI Engine Performance by Varying Injection Timing		International Conference on Advance Research in Technology and Engineering – ICARTE	International	20/Mar/15	ISSN 2349-9303	Methodist College of Engg and Tech., Hyd	INTERNATIONAL CONFERENCE ON ADVANCE RESEARCH IN TECHNOLOGY AND ENGINEERING
7	K Srinivasa Raghavan	Performance of CI engine with and without swirl in crown of piston with varying injection timing		An International Conference & Exhibition on Cutting Edge Technological Challenges in MEchanical Engineering (CETCME-2015)	International	21st to 22nd March 2015		Noida Institute of Engineering and Technology, Greater Noida	
8	B.Naik, K.K.Khatua	Water Surface Profile Computation In Non-prismatic Compound Channels	ICWRCOE 2015	International conference on water resources, coastal and ocean engineering	International	12th to 14th March 2015	ISSN 2214-241X	National Institute of Technology, Suratkal	
9	T. Sravan Kumar , I. Srikanth and Rayavarapu Prasad Rao	Realization of FIR Filter using High Speed Low Power Floating point Arithmetic unit	International Conference on Electrical, Electronics, Signal, Communication and Optimization (EESCO-2015)	International Conference on Electrical, Electronics, Signal, Communication and Optimization (EESCO-2015)	International	24-25 Jan. 2015	ISBN 978-1-479-7678- 2/15	Methodist College of Engg and Tech., Hyd	IEEE
10	Abinash Mohanta, Bandita Naik, K.C. Patra and K.K. Khatu	Experimental and Numerical Study of Flow in Prismatic and Non-prismatic Section of a Converging Compound Channel	SITCBE – 2014	2nd International Conference On “Sustainable Innovative Techniques In Civil and Environmental Engineering	International	4-5 JANUARY 2014	ISSN 2278-3652	JNU, New Delhi	Research India Publications

**PRINCIPAL**  
**METHODIST COLLEGE OF ENGG. & TECH.**  
 King Kofi Road, Abids, Hyderabad.

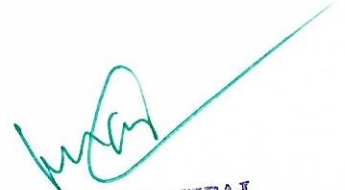
**Books/Book Chapters/Conference Papers 2014-15**

SI No.	Name of the Teacher	Title of the Paper/Books/Book Chapter	Title of the proceedings of the conference	Name of the conference	National/ International	Year of publication	ISBN/ISSN number of the proceeding	Affiliating Institute at the time of publication	Name of the Publisher
11	B. Naik, K.K.Khatua, Rahul Sahoo and Shiba Shankar Satapathy	Flow analysis for a converging compound channel	SITCEE – 2014	2nd International Conference On “Sustainable Innovative Techniques In Civil and Environmental Engineering	International	4-5 JANUARY 2014	ISSN 2278-3652	JNU, New Delhi	Research India Publications
12	Panigrahi, K., Khatua, K. K. and Naik, B	Effect of cylindrical staggered vegetation on roughness prediction in an open channel	Hydro- 2014 International	19th Conference on Hydraulics, Water resources & Environmental Engineering	International	December 18-20, 2014	ISSN : 2277-1581	Maulana Azad National Institute of Technology, Bhopal	International Journal of Scientific Engineering and Technology (ISSN : 2277-1581) Special Issue 3
13	B.Naik, K.K.Khatua and Shiba Shankar Satapathy	Boundary shear stress distribution along the converging floodplain of a non-prismatic compound channel flow	Hydro- 2014 International	19th Conference on Hydraulics, Water resources & Environmental Engineering	International	December 18-20, 2014	ISSN : 2277-1581	Maulana Azad National Institute of Technology, Bhopal	International Journal of Scientific Engineering and Technology (ISSN : 2277-1581) Special Issue 3
14	Lavanya Pamulaparty	A Novel Approach for avoiding overload in the Web Crawling	IEEE Sponsored 2014 International Conference on High Performance and Applications (ICHPCA-2014) published in IEEE Explore	IEEE Sponsored 2014 International Conference on High Performance and Applications (ICHPCA-2014) published in IEEE Explore	International	22-24 DECEMBER 2014	ISBN 978-1-4799-5958-7/14	CV Raman Engineering college, Bhuvaneshwar	IEEE
15	Lavanya Pamulaparty	XNNDF: Towards a framework for flexible Near-Duplicate Document detection using Supervised and Unsupervised Learning	proceedings of International Conference on Intelligent Computing, Communication and Convergence(ICCC-2014) 2. Published in ELSEIVER Procedia Computer Science	International Conference on Intelligent Computing, Communication and Convergence(ICCC-2014)	International	27-28 DECEMBER 2014	ISBN		Published in ELSEIVER Procedia Computer Science

**PRINCIPAL**  
 METHODIST COLLEGE OF ENGG. & TECH.  
 King Kotli Road, Abids, Hyderabad

**Books/Book Chapters/Conference Papers 2014-15**

SI No.	Name of the Teacher	Title of the Paper/Books/Book Chapter	Title of the proceedings of the conference	Name of the conference	National/ International	Year of publication	ISBN/ISSN number of the proceeding	Affiliating Institute at the time of publication	Name of the Publisher
16	T. Sravan Kumar and I. Srikanth	Multi Level Huffman Test Data Compression with Multiple Scan Chain method	Conference on Computing and Communication Technologies (ICCCT 2014)	Conference on Computing and Communication Technologies (ICCCT 2014)	International	26-28 september 2014			



**PRINCIPAL**  
METHODIST COLLEGE OF ENGG. & TECH.  
King Koti Road, Abids, Hyderabad



# Raja Rammohun Roy National Agency for ISBN

Department of Higher Education, Ministry of Human Resource Development

Government of India



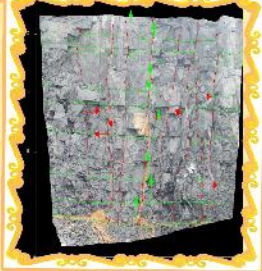
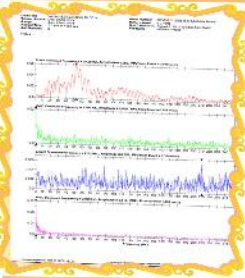
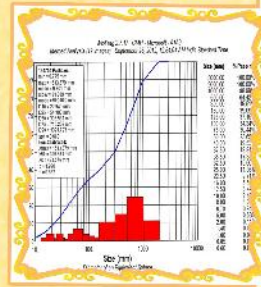
Date Time:25-04-2019|11:30:52

## Add Title Detail of the books for which ISBN IS required

[Add New Books](#)

Sl No.	Title	Author	Edition	Volume	pages	price	Year Of Allotment	Book Version	Book Description	Application Status	ISBN Number	Cover Page	Select <input type="checkbox"/>	Action	Language	Imprint
1	Rock Blasting	Dr. Raghu Chandra Garimella, Prof. V.R. Sastry	First	1	120	0	2019	PaperBack	THIS BOOK IS BASED ON THE REAL-TIME CASE STUDIES OF MINING INDUSTRY WITH CUTTING EDGE TECHNOLOGIES. IT IS A NON-COMMERCIAL BOOK PUBLISHED IN THE NATIONAL INSTITUTE OF TECHNOLOGY KARNATAKA FOR EDUCATING YOUNG MINING ENGINEERS.	Allotted	978-93-5361-241-2		<input type="checkbox"/>	Allotted	Allotted	English

No Safety  
Know Pain



Know Safety  
No Pain

# ROCK BLASTING



**Prof. V. R. SASTRY**

TEP  
Sept. 18-20, 2014

**TECHNOLOGY EXCHANGE PROGRAMME  
ON  
ROCK BLASTING**



*Organized by*  
**DEPARTMENT OF MINING ENGINEERING  
NATIONAL INSTITUTE OF TECHNOLOGY KARNATAKA  
SURATHKAL, MANGALORE**

*Editorial Board*  
**RAGHU CHANDRA GARIMELLA  
Prof. V.R. SASTRY  
Prof. D.V. REDDY  
E. MURALIDHAR  
M. VAISHNAVI**

TEP  
Sept. 18-20, 2014

# ROCK BLASTING



*Chief Editor*

**Prof. V.R. Sastry**

*Authors*

**Prof. V.R. SASTRY**

**RAGHU CHANDRA GARIMELLA**

*Other Contributors*

**Smt. Asha Khalwadekar**, Dy. Chief Controller of Explosives, PESO

**Dr. H.S. Venkatesh**, Scientist-V & HOD, NIRM

**P.V.S. Sarma**, General Manager - Technical Services, Gulf Oil Corporation Ltd.

**Dr. K. Ram Chandar**, NIT K-Surathkal

**Prof. D.Venkat Reddy**, NIT K-Surathkal

**M.M. Kamath**, Former Chief Engineer and INAE Distinguished Visiting Professor

## **GEOLOGICAL DISCONTINUITIES & INFLUENCE ON BLASTING**

**Dr. V.R. Sastry, Dr. D.Venkat Reddy & G. Raghu Chandra**  
Professor                      Professor                      Research Scholar  
NITK-Surathkal  
MANGALORE – 575025

### **ABSTRACT**

Fragmentation is the fundamental concern of rock blasting and it measures the effectiveness of blasting. Fragmentation is sensitive to not only the interrelationship among the design variables, but also is sensitive to local geology. Local geological conditions have a significant impact on the success of a blasting operation. The initial steps in these studies involved, determining the effect of rock properties on fragmentation via a literature search and the amount and quality of the geological data being utilized in blast pattern design at that time. The literature survey and then studies conducted clearly indicated that rock properties play a major role in determining both the fragmentation characteristics of a blast and the main blast pattern design parameters of burden, spacing, stemming and sub depth lengths if the same explosive and blasthole diameter is used.

### **INTRODUCTION**

Geological conditions in the given bench being blasted have a significant impact on the success of a blasting operation. Among various parameters, the single most important geological consideration is geological structure. Different structural discontinuities like joints, bedding planes and their orientation with respect to the bench face, and mud or soft seams can have a serious influence on the blasting process both from a performance and safety standpoint.

Soft seams, such as mud layers cause severe violence and poor fragmentation. Soft seams result in instantaneous release (escape) of the gaseous energy, since they often move as a hydraulic fluid. Soft seams can be thrown to significant distances with fly rock travelling with them. Also, bedding planes in non-homogeneous rock layers, depending on their location can cause potential for rock overhangs, unexpected muck pile height, toe problems, back breakage and differences in fragmentation in each rock layer. The beds layering also may have a considerable influence on burden movement.

The most effective method of optimizing mining costs is through efficient blasting as the degree of fragmentation affects the loading, hauling and crushing functions. Therefore, many mining operations are utilizing optimum blasting defined as that blasting practice which minimizes overall mining costs. Following are the four major variables influencing the blasting results:

- Explosive parameters - explosive density, VOD, gas volume, detonation pressure etc.
- Charge loading parameters - diameter and length of explosive, stemming length, sub depth, decoupling etc.
- Blast geometry - burden, blasthole spacing, shape and size of blast, initiation sequence, delay timing etc.
- Rock properties - density, compressive strength, tensile strength, Young's Modulus, Poisson's ratio, intensity of bedding, jointing and shearing, structure etc.

## JOINTING CHARACTERISTICS

*Jointing* is the occurrence of joint sets forming the system or pattern of joints as well as the amount or intensity of joints. The network of joints in the massifs between the weaknesses zones can according to Selmer-Olsen (1964) be characterized as 'the detailed jointing'.

### Joint Sets

Field studies of several workers have shown that rocks are invariably jointed in preferential directions and occur in joint sets. Two or three prominent sets and one or more minor sets often occur; in addition random joints may be present. Pollard and Aydin (1988) propose that each continuous joint set have been formed during a single deformation episode.

The conditions of the joints in the various sets can vary greatly depending on their mode of origin and the type of rocks in which they occur. Not only can the size and average spacing of joints vary, but also the other characteristics mentioned above. Variations in these properties cause that one joint set can have very different effect on the shear strength characteristics than another.

Although some characteristics are common for joints of different sets in a structural region, it does not, however, seem to be any general connection between all joint conditions in the different types of rock. Thus, for each of the joint sets, within a structural region with similar jointing characteristics, the various properties of each set must be considered individually.

In many cases one joints set is dominant, being both larger and/or more frequent than joints of other sets in the same locality. This set is often referred to as the main joint set (or by geologists as primary joints). Often, only one more joint set is developed (Price, 1969).

### Joint Spacing

Joint spacings varying from some millimetres to many metres may often seem arbitrary. There are, however, sometimes certain trends in the density of joints caused by spacings.

Nieto (1983) has observed variations in average spacing between joints from centimetres in highly tectonized rocks (folded, faulted, and intruded) of all types to more than 10 metres in massive, horizontally layered rocks. The regularity of joint spacing decreases with the amount of tectonic activity of the area.

Similarly, Pollard and Aydin (1988) mention that spacing of joints in some sets in intrusive igneous rocks is not uniform and that distances between joints range from less than 20 cm to more than 25 m, and that clusters of joints crop out sporadically.

Pollard and Aydin (1988) have further observed regular distribution of joints in sedimentary rocks and that the spacing of joints can scale with the thickness of the layer. Nieto (1983) mentions a general trend to a marked increase in the spacing or even the virtual disappearance of joints in flat-lying sedimentary sequences at depths of as little as 100m.

Pollard and Aydin (1988) suggest from field data that the following other factors also influence joint spacing:

- Two joint sets in the same lithological unit often have different spacings.
- Spacing of joints in different lithological units of comparable thickness can be different.
- Spacing can change as a joint set evolves. For example, columnar jointing - initiated at a flow base show an increase in spacing towards the interior - and the number of joints in a sedimentary unit decreases with distance from the initiation surface. The spacing of cooling joints that grow from the top of a lava flow is smaller than the spacing of those that grow up from the base. This has been attributed to a faster cooling rate at the flow top.

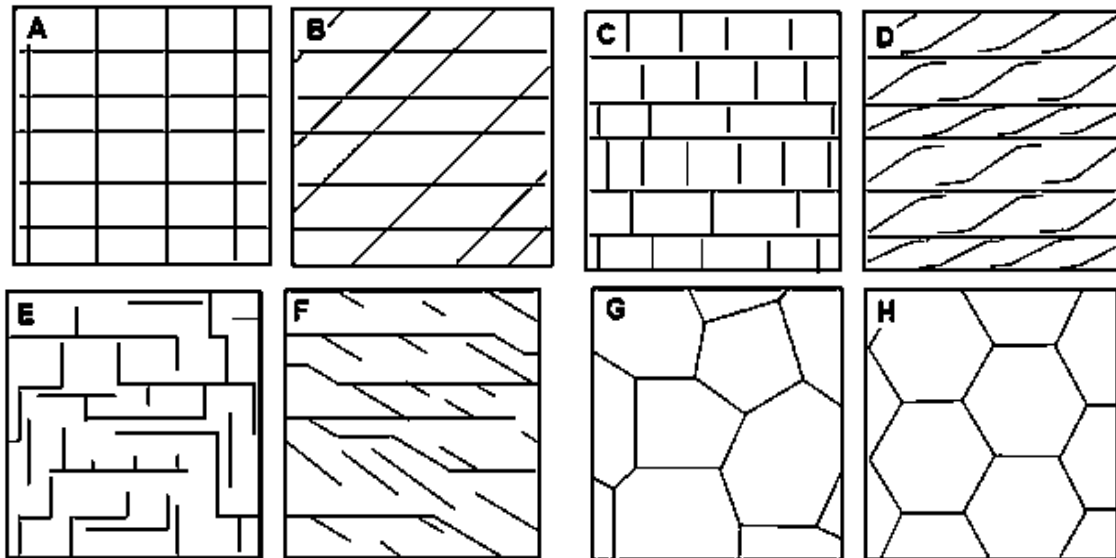
In addition two other trends should be mentioned:

- Rock masses that have undergone tectonic disturbance often present clusters of joints (joint zones).
- Often the joint Spacing is also influenced by weathering, as there often is an increase in jointing density within the zone of weathering, especially where mechanical disintegration has taken place.

### Jointing Pattern and Block Types

Joint *patterns* comprising of more than one set are common in nature. Piteau (1970) has observed that in instances where jointing is considered to have *random* distribution, it is usually the case that several joint sets occur simultaneously or are superimposed on earlier sets and the resulting complexity gives the appearance of randomness. Although there are many varieties of joint patterns in nature, there are few types of joint intersection geometries, which can be classified as *orthogonal* (+ intersections) and *non-orthogonal* (X intersections) (Fig. 1). Both types can be divided into three groups according to the persistence of the joints at intersections:

- All joints are persistent (crossing other joints)
- Some persistent, some non-persistent
- All joints are non-persistent



- A. Orthogonal pattern, with persistent sets (+ intersection)
- B. Non-orthogonal pattern, with persistent sets (X intersections)
- C. Orthogonal pattern, one set is persistent (T intersections)

- D. Non-orthogonal pattern, one set with persistent joints
- E. Orthogonal pattern, both sets have mainly discontinuous joints
- F. Non-orthogonal pattern, both sets have mainly discontinuous joints
- G. Triple intersections with all joints
- H. Triple intersections with 120° angles

FIG. 1 SCHEMATIC ILLUSTRATION OF MAIN JOINT PATTERNS  
(Pollard and Aydin, 1988)

Pollard and Aydin (1988) have observed that orthogonal joints often terminate against persistent joints. They mention, however, that there are many examples of joints that apparently cut across bedding interfaces and other joints. The + or X types of such intersections seem to contradict the notion that older discontinuities act as barriers to joint propagation, as implied by T intersections. The results from analyses carried out by Kikuchi et al. (1985) of joint connections in granitic rocks showed that most of the joints belonged to the X type, but also the T type and the + type were frequently observed. The joint termination type mainly belonged to the T type. Dershowitz and Einstein (1988) mention that 60% of joints in Stripa, Sweden terminate at T-type intersections; in other places 42% of this type has been recorded. According to Price (1969) joints frequently occur in relatively narrow zones, in which one joint is replaced *en echelon* by another joint, which is slightly off-set (Fig. 2).

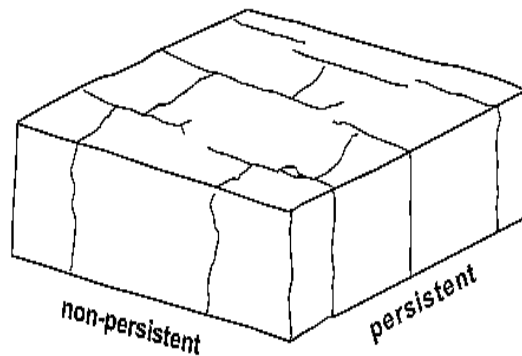
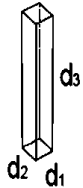
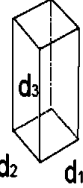
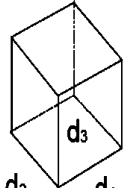
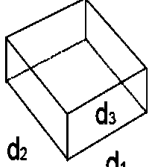
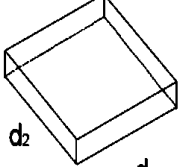


FIG. 2 JOINTS ARE SOMETIMES ARRANGED IN ZONES WITH REDUCED SPACING AND REPLACING EACH OTHER EN ECHELON (modified from Price, 1969)

### Block Types and Sizes

The joint sets and possible random joints divide the rock volumes into characteristic blocks. The jointing pattern and the difference in spacing between the joints within each joint set determine the shape of the resulting blocks, which can take the form of cubes, rhombohedrons, tetrahedrons, sheets etc. Müller et al. (1970) have made the division of block shapes as shown below in Table-2.

TABLE – 2 CLASSIFICATION OF BLOCK TYPES (Müller et al., 1970)

<b>Shape of rock block</b>					
<b>Joint spacing d (cm)</b>	$d_2$ $d_1$ $d_3$	$d_2$ $d_1$ $d_3$	$d_2$ $d_1$ $d_3$	$d_2$ $d_1$ $d_3$	$d_2$ $d_1$ $d_3$
<b>Ratio <math>d_1 / d_3 : d_2 / d_3</math></b>	$< 1 : 5$	$1 : 2$ to $1 : 5$	$\sim 1 : 1$	$2 : 1$ to $5 : 1$	$> 5 : 1$
<b><math>d_{max} &gt; 100</math></b>	column	big block parallelepiped	metric cube	slab	plate
<b><math>100 &gt; d_{max} &gt; 10</math></b>	small column	medium block parallelepiped	decimetric cube	medium slab	medium plate
<b><math>d_{max} &lt; 10</math></b>	pencil	small block parallelepiped	centimetric cube	small slab	small plate

Another characterization into *block types* has been presented by Dearman (1991), based on a description by Matula and Holzer (1978) as shown in Table-3 and Fig. 3.

TABLE - 3 BLOCK TYPES AND JOINTING CHARACTERISTICS (Dearman, 1991)

Type of block	Jointing characteristics
Polyhedral blocks	Irregular jointing without arrangement into distinct sets, and of small joints.
Tabular blocks	One dominant set of parallel joints, for example bedding planes, with other non-persistent joints; thickness of blocks much less than length or width.
Prismatic blocks	Two dominant sets of joints, approximately orthogonal and parallel, with a third irregular set; thickness of blocks much less than length or width.
Equidimensional blocks	Three dominant sets of joints, approximately orthogonal, with occasional irregular joints, giving equidimensional blocks.
	Three (or more) dominant mutually oblique sets of joints, giving oblique-shaped, equidimensional blocks.

Sen and Eissa (1991) has given the following, simpler characterization of block types:

- Prismatic block: The three dimensions of these blocks are individually significant in their definitions.
- Platy blocks : These are similar to slabs where two of the three dimensions are relatively larger than the third dimension.
- Bar blocks : Only one dimension is significant. This division has earlier also been applied by Burton (1965).

However, regular geometric shapes as given above are the exception rather than the rule since the joints in any one set are seldom consistently parallel (ISRM, 1978). Jointing in sedimentary and plutonic rocks usually produces the most regular block shapes. Block size delineated by the joint planes is a volumetric expression for jointing density. Block size is determined by the joint spacings and the number of joint sets - partly also by the joint length. Individual or random discontinuities may further influence the block size.

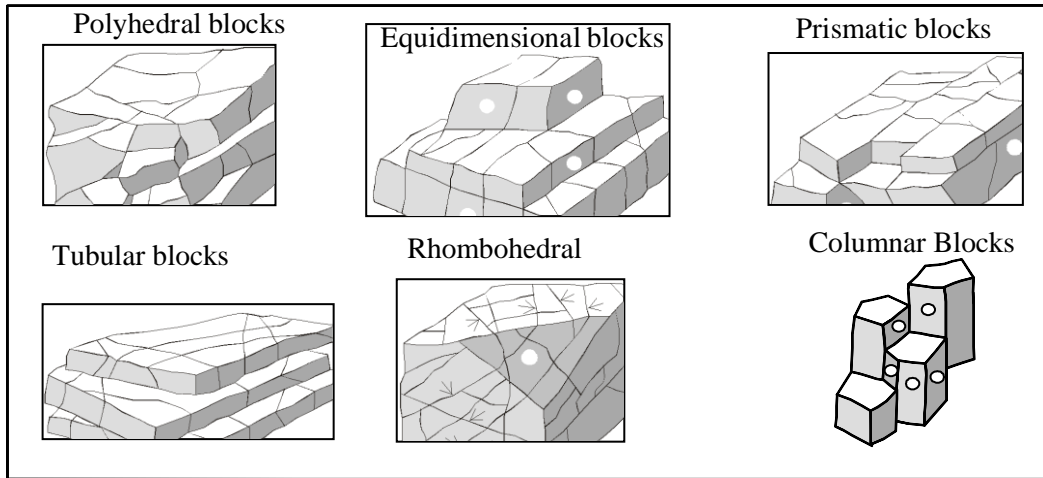


FIG. 3 VARIOUS TYPES OF JOINTING PATTERN EXPRESSED AS BLOCK SHAPE  
 (numbers refer to various joint sets)  
 (Dearman, 1991, based on data from Matula and Holzer, 1978)

**ANALYSIS OF BEDDED LAYER MODELS**

**Case I:** A shale layer is located between two layers of limestone, representing the condition in which a soft layer is present in a harder rock bench column (Fig. 4). This condition could cause severe violence and poor fragmentation, by almost instantaneous release of the explosive energy at the soft layer region. Therefore, the soft materials are thrown to a significant distance creating fly rock. Finite element analysis indicates the same behavior. In field practice, stemming across soft layers or mud seams is essential to obtain good blasting results.

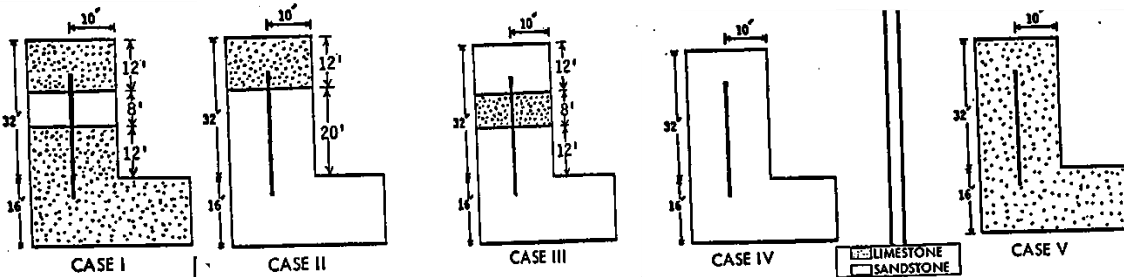


FIG. 4 DIFFERENT COMBINATIONS OF HARD & SOFT LAYERED STRATA

**Case II:** A limestone layer comprising the collar region of shale rock bench represents the condition of a hard layer (cap rock) at the collar region of soft bench column. In this condition there is potential for large boulders or for rock overhanging the face in the collar region. The loss of confinement and energy at the softer region of the bench column is the cause of the problem. In order to overcome the

problems in this condition, a re-distribution of explosive energy along the borehole wall is required. More energy at the bench collar region could be obtained by using satellite charges to break the rock at the collar, and a lower powder factor could be obtained along the softer layer by increasing the burden distance to provide adequate confinement to control air blast and fly rock.

**Case III:** A limestone layer is located between two shale layers representing the condition where a hard layer is present in a softer rock bench column. In order to correct the problem of coarse fragmentation in hard layers, boosters may be used to intensify the explosive reaction and input more energy into the hard layer.

**Case IV and V:** The bench columns consist of homogeneous layers of sandstone and limestone respectively. Since the limestone is a harder rock than sandstone, less rock movement is expected at the free face. The finite element model shows burden displacements of 6.7 feet for case V and 10.1 feet for case IV, as shown in the deformed geometry plots.

Five different three dimensional finite element models were used to analyse the effect of rock properties and bedding on burden displacement (Fig. 5). Three models had non-homogeneous burden columns and the other two were homogeneous. Burden displacement was shown to be larger at the soft layer regions as it was expected compared to hard rock regions.

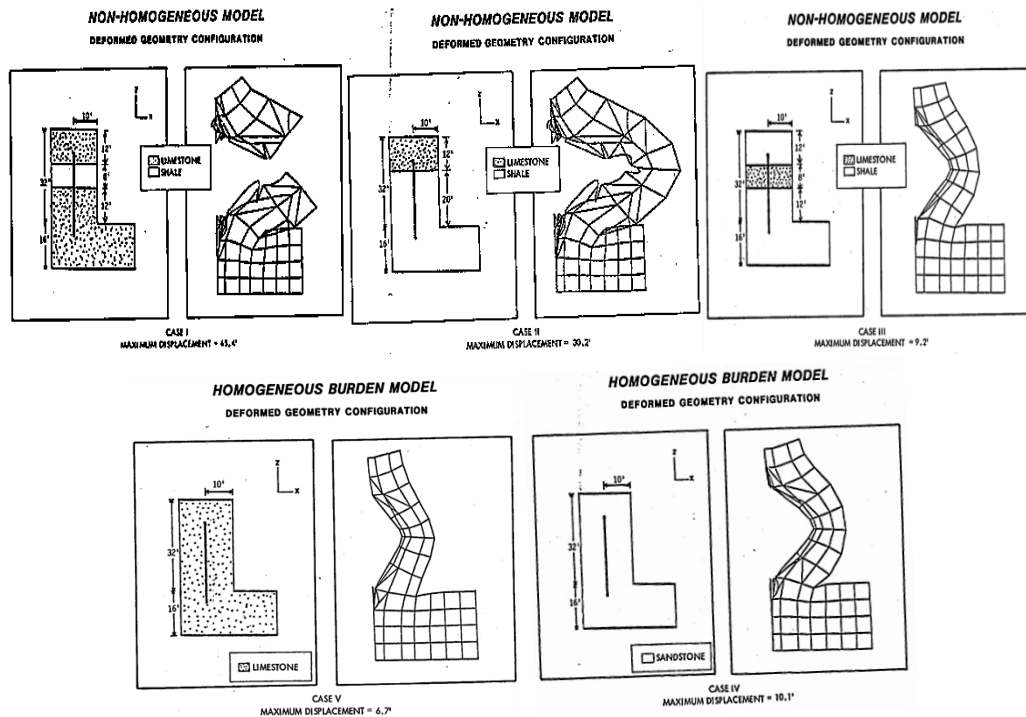
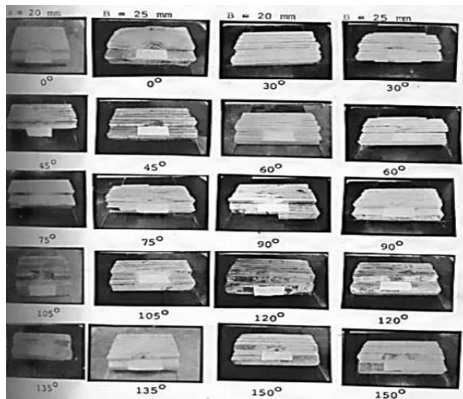


FIG. 5 BEHAVIOUR OF BENCH DUE TO BEAM BENDING MECHANISM IN THE PRESENCE OF SOFT BANDS IN BENCH

The results obtained from finite element modelling based on displacement compare well with field observation. The results confirm the hypothesis that rock breaks as a result of bending of the burden rock under stresses from the explosive gas pressure which is described by the flexural failure theory.

**INVESTIGATIONS**

The experiments for evaluating the influence of joint orientation were conducted in three stages with joints running parallel, perpendicular and angular to the face. In each set, studies were conducted with different joint orientation angles. Tests at each orientation angle were performed with two burdens, 20 mm and 25 mm in models with joints running parallel and perpendicular to face. Only 25 mm burden was used in models with joints running angular to the face. Forty eight models were blasted (Figs. 6, 7, 8 and 9).



**FIG. 6 MODELS WITH JOINTS RUNNING PARALLEL TO THE FACE AFTER BLASTING**

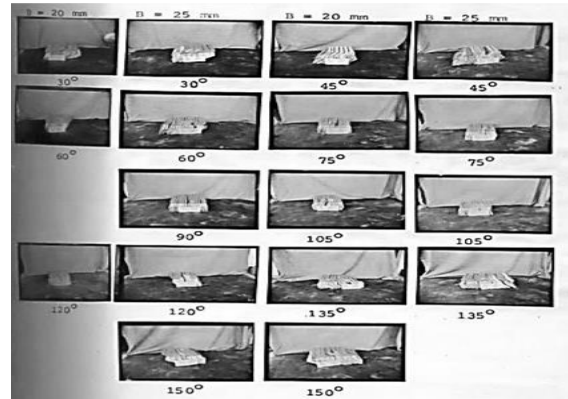


**FIG. 7 MODELS WITH JOINTS RUNNING PERPENDICULAR TO THE FACE AFTER BLASTING**

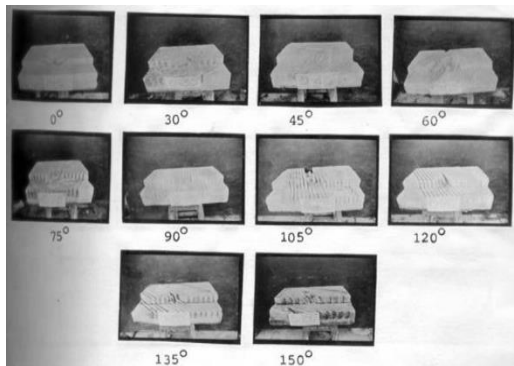


**FIG. 8 MODELS WITH JOINTS RUNNING ANGULAR TO THE FACE AFTER BLASTING**

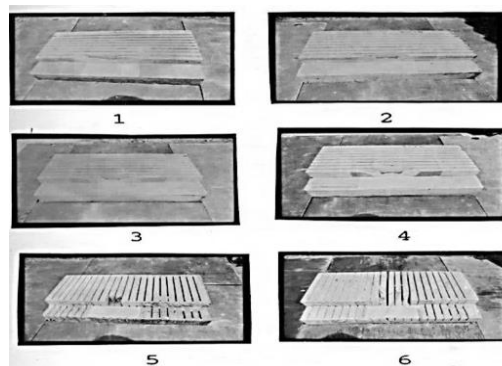


**FIG. 9 JOINTED MODELS WITH DOUBLE HOLES AFTER BLASTING**

Results of the blasts were analysed in terms of Average Fragment Size, Mass of fragments produced, New-Surface Area created and Mass Surface Area obtained from the blast. Significance tests were conducted to assess the influence of various parameters. It was concluded from studies that the joints were having highest influence on blast results.

**FIELD OBSERVATIONS**

The following conditions are quite common in the field in the presence of structural discontinuities (Fig. 10). Fig. 11 depicts the escape of gaseous energy through weak planes in the bench as shot by high speed video camera. Results are poor fragmentation, noise and fly rock.

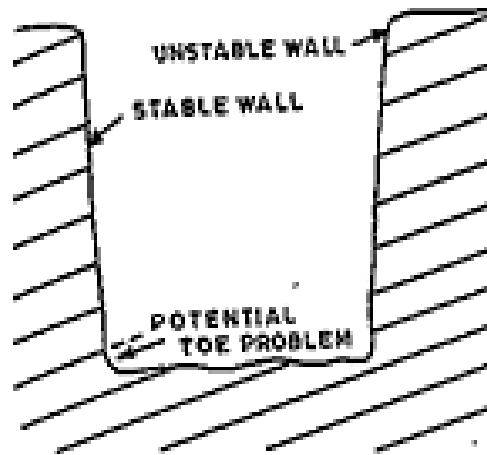
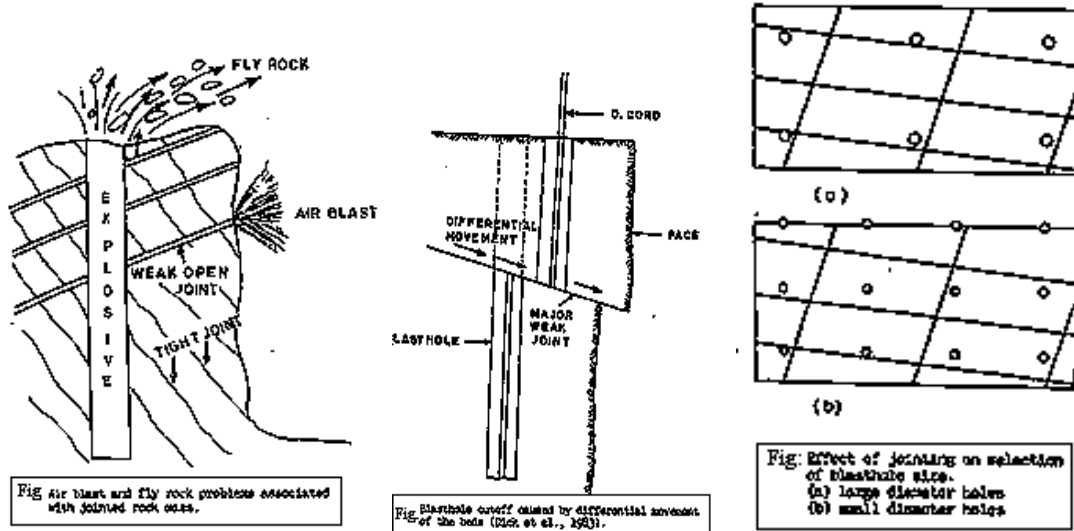


Fig. Effect of dip of jointing on blasting.

FIG. 10 EFFECT OF STRUCTURAL DISCONTINUITIES

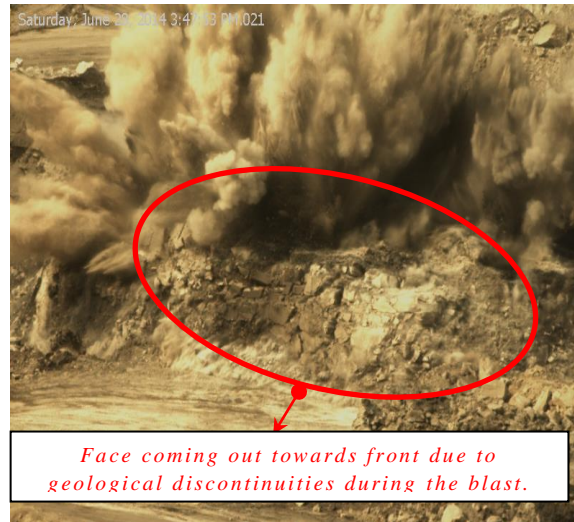


FIG. 11 ESCAPE OF GASEOUS ENERGY FROM THE BENCH LEADING TO POOR BLAST

## CASE STUDY

Field investigations were carried out in a limestone mine in Southern India. The limestone formation is a heavily jointed rock mass and the mine has been developed in benching method. Fig. 12 shows view of the limestone mine where the studies was carried out. Generally 115mm diameter blastholes are drilled for 8m height benches with 4m burden and 5m spacing. Each blasthole is charged with around 55kg of explosives and initiated with shock tube detonators. After the blast, muck pile images were taken for fragmentation analysis using WipFrag software (Fig. 13). In total, nine production blasts were monitored in the field which were conducted with different blast patterns and charge configuration. The same blasts were simulated using JKSim Blast software, to assess the energy distribution. The bench rock formation images were taken and analysed using SIROVISION™ to assess the characteristics of joint features.

The bench face was found to have a significant number of joints. The average joint spacing was determined for the benches where the blasts were conducted. The mean joint spacing is given in Table-4. The product of the vertical and horizontal joint spacing is called as meshing area. In practice, the meshing area is the area of a mesh formed due to the intersection of the horizontal and vertical joints much like a chequered square in a chess board, which influences fragmentation to a great extent.



FIG. 12 VIEW OF TADIPATRI LIMESTONE MINE



FIG. 13 CALIBRATOR FOR FRAGMENTATION ASSESSMENT USING WIPFRAG  
TABLE - 4 JOINT SPACING AND FRAGMENTATION INFORMATION FOR BLASTS

Blast	Vertical Discontinuity Spacing (m)	Horizontal Discontinuity Spacing (m)	Meshing Area (m <sup>2</sup> )	K <sub>25</sub> (mm)	K <sub>50</sub> (mm)	K <sub>75</sub> (mm)
1	0.499	0.401	0.200	39.001	143.308*	421.815
2	1.337	0.078	0.104	45.776	117.842	451.431
3	3.664	0.070	0.260	54.000	306.531	715.257
4	0.575	0.348	0.340	36.371	189.564*	429.952
5	2.002	0.075	0.151	30.304	131.266	395.607
6	2.484	0.075	0.187	32.061	181.157	650.531
7	2.643	0.073	0.193	39.11	277.584	501.443
8	0.778	0.081	0.063	20.313	92.112	377.302
9	2.774	0.071	0.197	40.774	292.495	625.153

\* These blasts were carried out using a charge per hole of 96 kg/hole unlike the other blasts which had 55 kg/hole, due to which they have not been considered for the regression analysis.

Figs. 14 to 17 detail the different SiroJoint outputs for a typical bench. Fig. 5 shows the traced lines denoting horizontal and vertical joints on the 3D image of a typical bench face. The horizontal joints have been marked by green traces while the vertical joints have been marked by red traces. Figs. 4 and 5 denote the histogram of the horizontal and vertical spacing respectively, giving the average discontinuity spacing and standard deviation on the top-centre of the graph. The x-axis shows the set spacing in metres and y-axis shows the number of joints. Fig. 6 gives the spatial orientation of the joint sets in a 3D frame of reference. This feature is made useful by the application of the Georeferencing option where the actual spatial coordinates in the form of latitude, longitude and reduced level can be added. It shows the use of the software in analysing the horizontal and vertical joint, which intersect to form a mesh, constituting the meshing area.

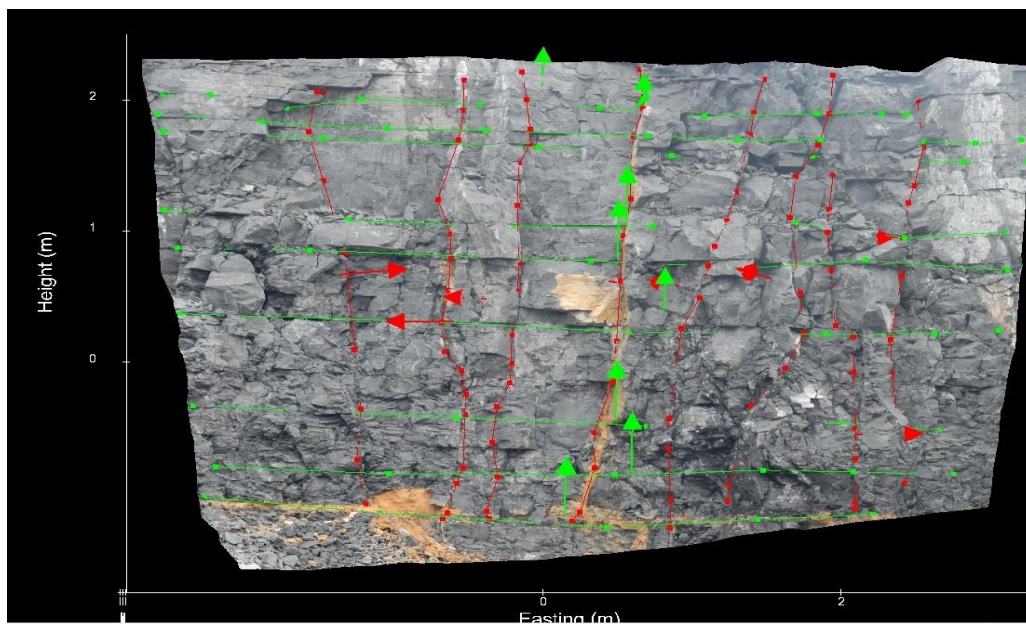


FIG. 14 HORIZONTAL (GREEN) AND VERTICAL (RED) TRACES OF JOINTS ON 3D IMAGE OF BENCH 1

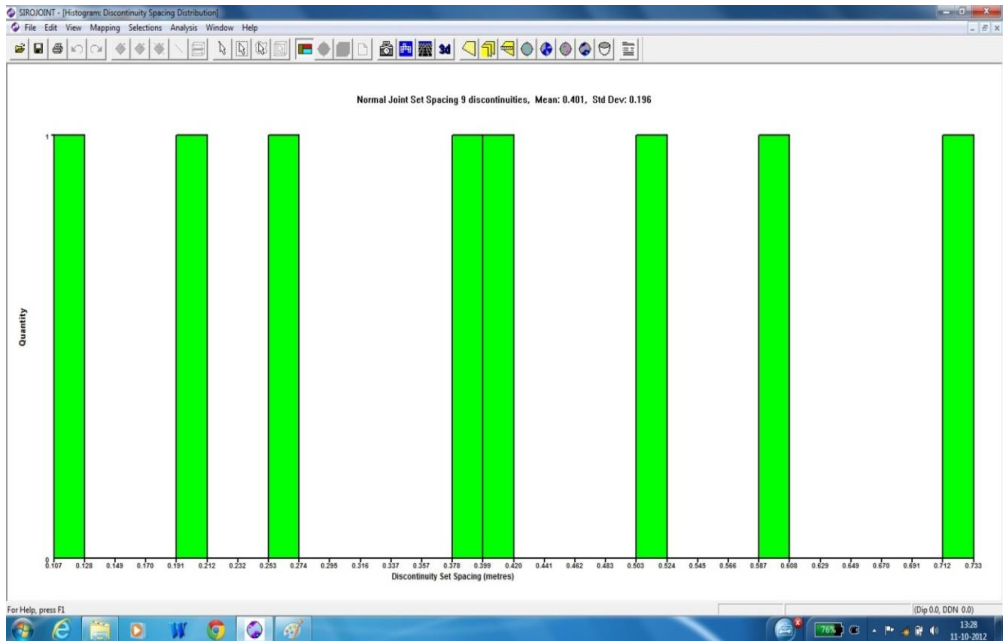


FIG. 15 HORIZONTAL JOINT SPACING GENERATED BY SIROJOINT FOR BENCH 1

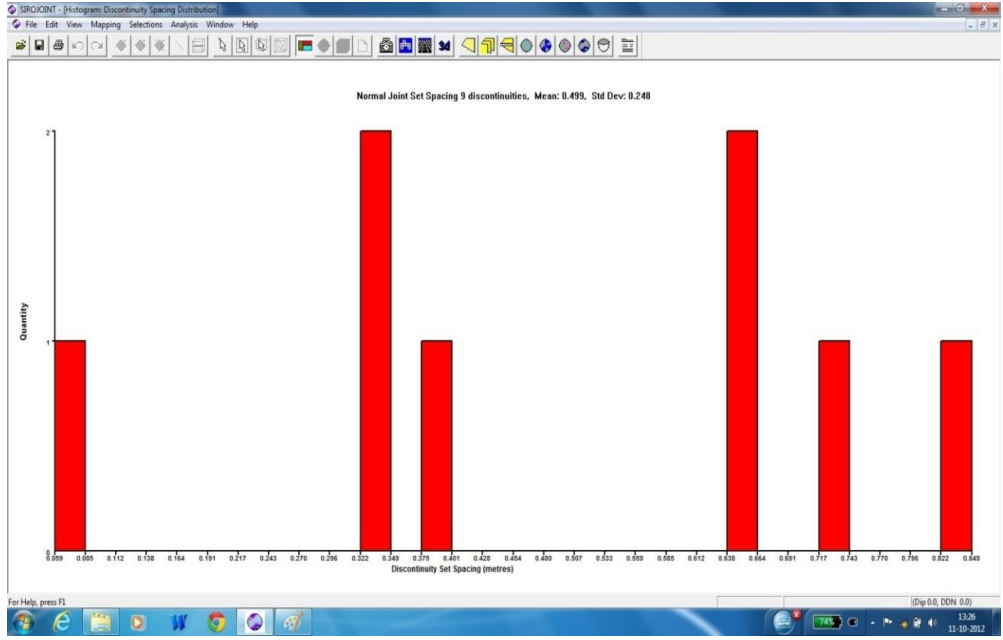


FIG. 16 VERTICAL JOINT SPACING GENERATED BY SIROJOINT FOR BENCH 1

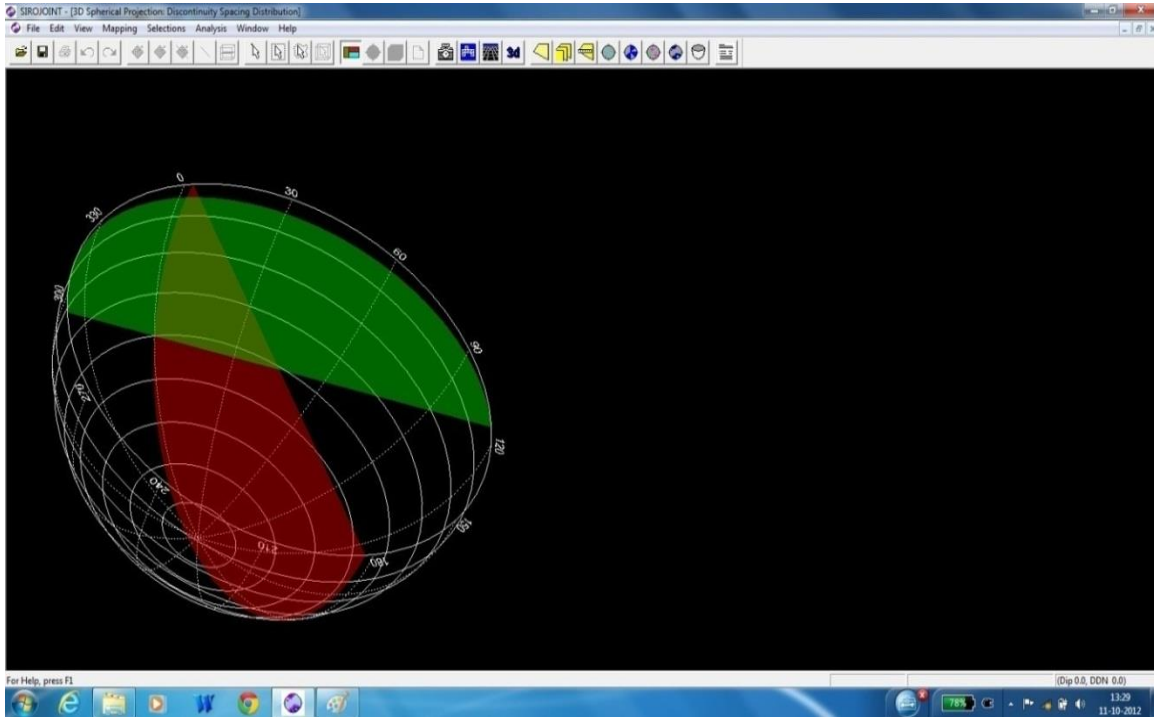


FIG. 17 3D PLOT OF JOINTS IN BENCH 1

The meshing area has been used to correlate the joint spacing to the fragmentation of the blasts. The images of fragmentation of all the blasts were assessed systematically, layer by layer as the muck pile was cleared by the shovel. Table-4 summarizes the average fragment size ( $K_{50}$ ) values of the blasts and Fig. 18 shows the result of the regression between meshing area and mean fragment size.

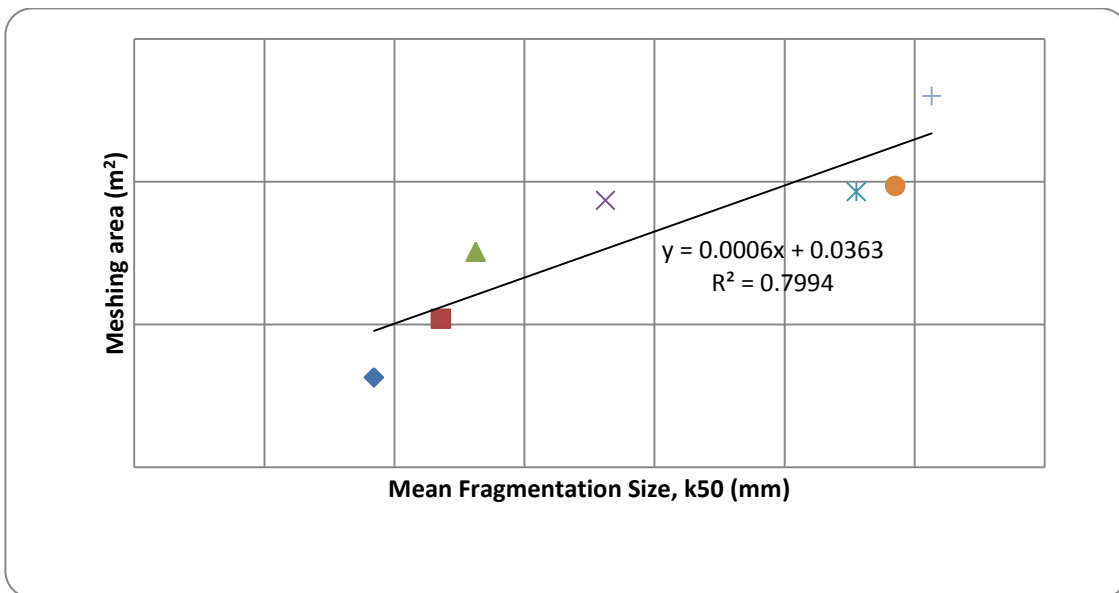


FIG. 18 MESHING AREA VS MEAN FRAGMENTATION

JKSim Blast software used to simulate the blast with actual field parameters and simulate the blast to obtain energy distribution around the blastholes. Figs. 19 through 24 show the output where JKSim Blast was used for the estimation of the energy contours. The contours were produced in vertical slices from the surface (0 m) to a depth of 10 m. Fig. 25 is a screenshot of the legends used for the colours of the energy contours. In Fig. 19 shows the simulation of the blast at 0m depth i.e. the surface of the blast, which is marginal as compared to energy at deeper levels of the blast due to the stemming. Similarly the Figs. 20, to 24 represent the energy emanated by the blast at lower depths along the blast at every 2m intervals respectively. At each depth, a representative area of the given demarked simulated area and a quantitative number which denotes the amount of area which lies in a given range is obtained. Since the range can be specified by the user, the software can depict the energy released. Now this result will give a pristine idea about the use and release of energy due to the blast. it can be seen that at a depth of -10 m, the blast releases about 5MJ/m<sup>3</sup> in blast 1 for 2.81% of the total area simulated. In this manner, a fair idea of the energy released by the blast can be concluded based on the use of this blast simulation. Table-5 shows a comparison of energy distribution at 8m and 10m depth of blastholes.



FIG. 19 BLAST ENERGY DISTRIBUTION AT 0m (Surface)

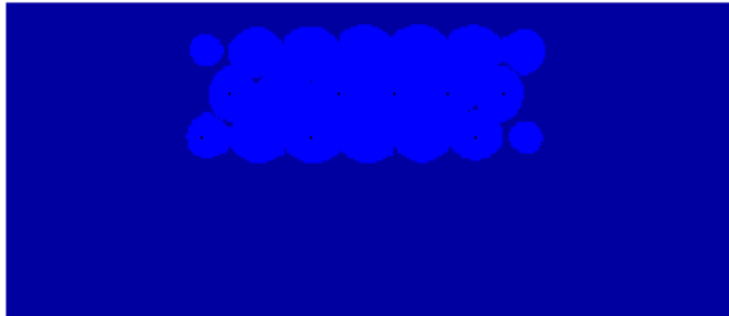


FIG. 20 BLAST ENERGY DISTRIBUTION AT 2m

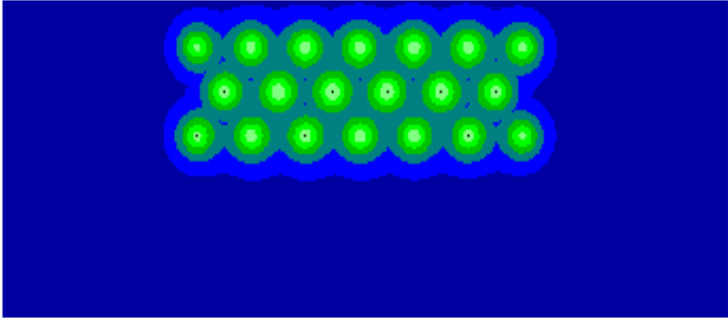


FIG. 21 BLAST ENERGY DISTRIBUTION AT 4m

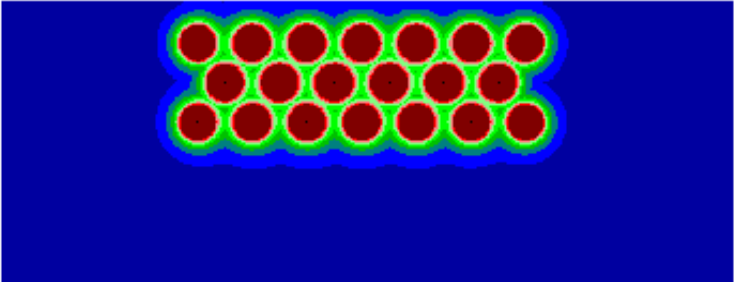


FIG. 22 BLAST ENERGY DISTRIBUTION AT 6m

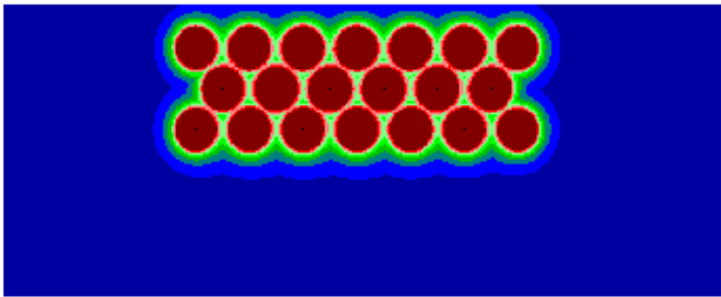


FIG. 23 BLAST ENERGY DISTRIBUTION AT 8m

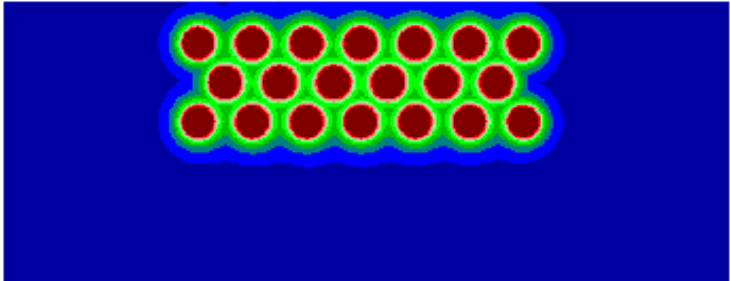


FIG. 24 BLAST ENERGY DISTRIBUTION AT 10m (Hole Bottom)

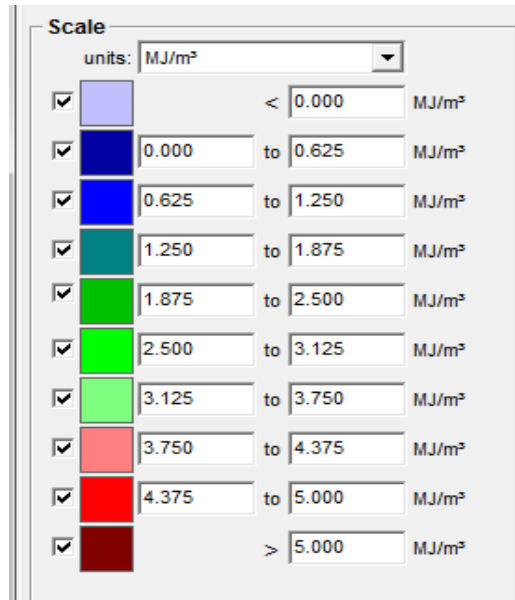


FIG. 25 SCREENSHOT OF SCALE USED IN JKSIM BLAST

Table-5 gives an indication of the use of the software JKSim Blast and the importance of energy assessment in blast design. The table represent the amount of area shown in the figures 10 through 15, that this range of energy covers, i.e. a value of 2.3 will mean that at a depth of 10 meters below the blast hole, the energy in the range of 4.375 to 5 MJ/m<sup>3</sup>, is present or represents 2.3 % of the total area of simulation of the blast. Hence more the percentage of covered area more is the energy of the blast in that particular energy range. The information for the 10m slice and 8 m slice have been presented. The blast has to be analysed in sections; therefore the energy of the blast will have to be analysed in sections of the blast, i.e. 10m below the surface or 8m below the surface of the blast. Fig. 26 shows the correlation between the energy of the blastholes with the K<sub>50</sub> value. It can be seen that there is a very good correlation exists between the energy and the fragmentation, as the percentage of area increases the K<sub>50</sub> value decreases. Aberrations are seen in blast 1 and 4 since the charge per hole is almost double as compared to the other blasts. Hence they have not been considered for making the regression analysis.

TABLE – 5 ENERGY DISTRIBUTION AT DIFFERENT DEPTH OF BLASTHOLES ESTIMATED USING JKSIM BLAST

Blast No.	% Area in 8m slice		% Area in 10m slice		K <sub>50</sub> (mm)	Charge per hole (kg)
	Energy between 4.375 - 5 (MJ/m <sup>3</sup> )	Energy > 5 (MJ/m <sup>3</sup> )	Energy between 4.375 - 5 (MJ/m <sup>3</sup> )	Energy > 5 (MJ/m <sup>3</sup> )		
1	2.71	14.77	2.11	8.68	143.3	95
2	8.34	14.62	2.38	9.07	117.842	55
3	2.1	0.23	0	0	306.53	55
4	2.56	14.36	3.11	9.54	189.56	96

5	6.34	12.34	1.71	9.25	131.26	55
6	2.58	11.67	1.15	6.29	181.15	55
7	2.71	8.62	0.17	2.16	277.58	55
8	4.64	17.51	6.8	12.4	92.11	55
9	2.60	8.12	0.15	1.23	292.495	55

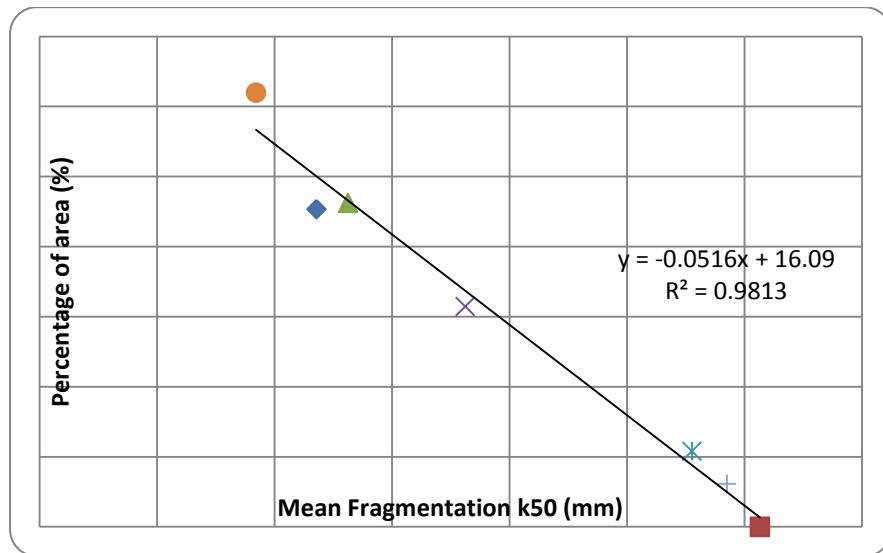


FIG. 26 PERCENTAGE OF AREA WITH ENERGY GREATER THAN 5 MJ/m<sup>3</sup> VS.

### MEAN FRAGMENT SIZE

The results intensify the use of the given methods in blast assessment. The use of JKSim Blast software gives an output of the energy of a given blast at specific points. The software however does not include the inclusion of joints or other structural discontinuities into the software which will shorten the bridge between the simulation and the actual blast results. Hence the use of Sirovision in this venture will turn out to be more useful. Along with the energy produced in a given blast, the mapping of the joints will provide the blasting engineer with an idea of the bench and the parameters to vary to increase the efficiency of the blast.

Sirovision will give a comprehensive view of the vertical and horizontal spacing of the joints. This can be combined to form the meshing area which will have a significant effect on the blast as they compose the planes of weaknesses. The product of the given horizontal and vertical joints will give us the meshing area, and higher area will result in higher  $K_{50}$  value as shown in Table-4.

### CONCLUSIONS

- Geology plays a very important role in blasting process.
- Rock fragmentation mechanisms get altered, due to inhibition of radial cracking and reflection breakage mechanisms.
- Presence of weak planes leads to escape of gaseous energy resulting in noise, fly rock coupled with poor fragmentation.
- Survey of the benches is very essential for the blast design.

- There is very good correlation between number of joint sets and their frequency and the fragmentation resulting from the blasts.
- Tools like SIROVISION, JKSimBlast and fragmentation assessment softwares become quite useful in predicting and assessing the blast results.

## REFERENCES

- Anon, 1995. *A Rock Mass Characterization System for Rock Engineering Purposes*. PhD thesis, Oslo University, Norway, 1995, 400 p.
- B. L. Lindsey, Jr. and David A. Smith, 1979. The Influence of Variable Geology on the Blasting of Arkansas Bauxite, 5<sup>th</sup> SEE Proceedings, St. Louis, Missouri, Feb. 7-9, 1979.
- Haghighi, R. G. and C. J. Konya, 1986 . Effect of geology on burden displacement, Proc. of the Second Mini-Symp. on Explosives and Blasting Research, SEE, Ohio, pp. 92-102.
- Haghighi, R.G. and Konya, C.J., 1985. The Effect of Bench Movement With Changing Blasthole Length, Proceedings of the First Mini-Symposium on Explosives and Blasting Research, pp. 95-105, S.E.E. Annual Conference in Atlanta, Georgia, January 1985.
- Peter Bellairs, The Application of Geological and Downhole Geophysical Data to Blast Pattern Design”, Proceedings Second International Symposium on Rock Fragmentation.
- Sastry, V.R., 1989. Unpublished Ph.D. Thesis, Department of Mining Engineering, IIT-Banaras Hindu University.

# Design, Simulation and Analysis Of Automatic Multifastener Device

R Moses Krupavaram  
Assistant Professor, Mechanical  
Engineering  
MCET  
Hyderabad, India  
moseskrupavaram@gmail.com

Y M.Maheswara Reddy  
Assistant Professor, Mechanical  
Engineering  
MCET  
Hyderabad, India  
mmr315@gmail.com

M Amresh Reddy  
Assistant Professor, Mechanical  
Engineering  
MCET  
Hyderabad, India  
mudiam.amresh@gmail.com

**Abstract**— This paper deals with the design, simulation and analysis of automatic multifastener device. This device is designed by considering M22 standard metric bolt for a four wheeler tire assembly system. Assembly technology is an essential component of modern industrial production, and threaded joints are among the most common and widely used types of fasteners. Current industry demands the tools that offer One hand operation, Extended service life, Operator Comfort, Ease of serviceability to minimize the downtime, High value verses low cost. These demands can be met by the use of automatic devices. Now days the use of these type of automatic devices has gained an important role in the automobile industries, Laboratories and also in all mechanical industries Main components used in this device are motor, base stand, nut fitting and removing plate and a keypad for on/ off switches and some mechanical parts are used for driving operation. This device is operated by a DC motor. Selection of DC. Here Spur gears are used for transmitting the power. Proposed design and mechanism has been done in Pro-wild fire. Structural analysis of the device is carried out in Ansys at different loads.

**Keywords**- fastener; Device, bolt tightner, Gear assembly, DTDP Switch, Battery, structural analysis.

## I. INTRODUCTION

Assembly technology is an essential component of modern industrial production, and threaded joints are among the most common and widely used types of fasteners. The broad spectrum of assembly equipment ranges from state of the art robotics to work stations using hand-held tools. The criteria of these assembly tasks are just as varied, depending upon the application needs, the production method, quantity and the accuracy requirements.

Conventional fastening requires tools like a wrench or an electric or pneumatic tool. Industrial assembly or joining technology increasingly requires meeting long-term safety-oriented, and function oriented solutions. Historically there have been disadvantages associated with the use of conventional tools such as inaccurate tightening, high tool wear and requires more time for fastening.

Current industry demands the tools that offer One hand operation, Extended service life, Operator Comfort, Ease

of serviceability to minimize the downtime, High value verses low cost. These demands can be met by the use of automatic devices. Now days the use of automatic devices has gained an important role in the automobile industries, Laboratories and also in all mechanical industries Bolted assemblies are the most commonly used connecting systems in mechanics. And although they appear to be quite simple, bolted assemblies do pose several challenges at many levels: design department, assembly workshop, on-site, and maintenance. In an assembly that contains threaded fasteners, the nut or bolt needs to be physically tightened to a specific torque. A bolted assembly quite simply means the putting together of at least two parts using one or several bolts. The design and implementation of a bolted assembly requires a very strict methodological approach, for errors can lead to costly and often disastrous failures. Several studies have shown that incidents encountered on bolted assemblies are most often due to improper design of the assembly or poor implementation like tightening method, tooling, and inspection.

Today it is known that of all the various causes of failure like overloading, design flaws, manufacturing defects, and others the most frequent is improper assembly. Tightening problems, whether insufficient tightening, excessive tightening or heterogeneous tightening, alone account for over 30% of all bolted assembly failures. More specifically, 45% of all fatigue failures are estimated to be due to improper assembly. Therefore, the importance of the design of the bolted assembly and the means used to tighten it are of utmost importance.

V.K. Zamyatin manufactured a device ie-3115a and ie 3112 electrical manual impact (chum) nut tightner for the assembly and dismantling of threaded connections at industrial firms. They used IE-3115A tightener for the calibrating the tightening of bolts size M18-M30, strength class 3.6-6.6, and bolts size M12-M20, strength class 6.8- 14.9. It consists of an electric motor, a planetary reducing gear, an impact mechanism, a handle with switch, the current-supply cable, and they found that this device is used for the elimination of radio interferences. They used IE-3112 nut tightener for the calibration of tightening of high-strength bolt of different sizes (M22-M30) or medium-strength bolts (35 steel) with diameters up to M42 ram. This tightener is a reversible tool and is equipped with a protective switch-off device. The IE-

3115A nut tightener is manufactured by the "Elektroinstrument" Production Association at Rostov-on-Don and the IE-3112 tightener by the "Elektroinstrument" Plant at Vyborg[1].

The "Uralkhimmash" Production Association produced a dual-spindle nut tightener intended for the tightening of the plates of plate heat exchangers during hydraulic testing and final assembly. This tightener has an upper and lower head, a gear box, telescopic head links, a suspension support, and a control panel. By suspension from a crane the tightener is placed on the nuts of the plate heat exchanger. The electric motor of the tightener sets the spindles into rotation through the gear box and worm reducers of the upper and lower heads. The spindles have ball inserts with an internal hexagon. The nuts of the heat exchanger bolts are located in the hexagons of the inserts. The telescopic Link compensates deviations from the distance between the bolts and nuts of the heat exchanger. The outer spherical surface of the inserts compensates the face slackness of the nuts of the heat exchanger during tightening. As the spindles rotate, the tightener travels together with the nuts in the direction of tightening until the required tightening stress is reached. This is followed by hydraulic testing of the heat exchanger[2].

SKF industries designed a standard Hydro cam tensioner. A standard Hydro cam tensioner has a hydraulic body which, using a hydraulic fluid, exerts a strong tension load on the bolt through the brace screwed on that bolt. In some tensioner types (HTC R), the body is screwed directly on the bolt to be tightened. The body also rests on the skirt in order to apply the reaction force on the assembly to be tightened. Prior to screwing the body-brace-skirt unit on the protruding end of the bolt, a socket has to be placed on the nut of the bolt. This nut can then be "turned down" (screwed until the lower surface of the nut comes into contact with the assembly bearing surface), by a tommy bar, while the tensioner applies the tension load. The turndown socket is placed over the nut and the hydraulic tensioner grasps the bolt. The brace/retraction unit is screwed onto the protruding end of the bolt. After the hydraulic connections, the tensioner is pressurized and applies the required tractive force on the bolt. While the pressure is maintained, the nut is turned down without loading, using the socket and the tommy bar. Their pressure is released and the piston is pushed back. The tightening load is now exerted through bolt tension. The tensioner and the socket can be removed[3].

A segment bolt tightener is developed by New shield machine technology. This segment bolt tightener automatically tightens fastening nuts and bolts of the primary lining segments assembled in an excavated tunnel. A movable cart equipped with tighteners is provided separate from the shield machine, so adverse affects due to shield machine backlash and vibration are eliminated, and tightening work can be performed more effectively from behind the shield. The bolt and nut tighteners are each mounted at the end of a multi-articulated manipulator, so the system can handle bolts and nuts mounted at any angle. The multi-articulated manipulators can handle segments with different inner diameters and

shapes. Two tighteners are provided one on the left and one on the right, and these fasten bolts simultaneously, thereby achieving automation and labor-savings[4]. Automation Industries developed a self-contained tensioner. A self-contained tensioner and tightener device is provided in accordance with this invention for a threaded stud projecting from a hole in a foundation surface. It comprises an expandable tensioning device which itself comprises a tensioning nut threadable onto the stud in spaced relation to the foundation surface and telescoping annular piston and cylinder elements defining a pressure chamber and loosely encircling the stud between the tensioning nut and the foundation surface. The expandable tensioning device also includes pressuring means communicating with the chamber for forcing the piston and cylinder elements and thus the tensioning nut and foundation surface apart to tension the stud. The invention also includes a spacer sleeve adapted to encircle the stud end portion and tensioning nut in abutting relation with the foundation surface. A locking nut is threadable onto the stud against the spacer sleeve to be tightened on the tensioned stud so that the pressuring means can be deactivated and the tensioning nut loosened. A take-up finger is fixed in relation to the tensioning device coaxial with and spaced closely adjacent the end of the stud and is threaded correspondingly to the stud so that the tensioning nut, the spacer sleeve and the locking nut necessarily move onto and are retained by the finger when removed off the end of the stud[5].

Cooper Industries, Inc. Houston, TX has designed a device called Impulse or torque screw or bolt tighteners. Impulse or torque screw or bolt tighteners which are used for a number of different screwing and tightening processes are fitted with a valve with which the bolt or screw tightener is switched on and off. The valve is located along the compressed-air supply line that leads to the screw or bolt tightener. This valve can be actuated manually by the operating personnel or by an electronic measuring and control device. Prior art screw or bolt tighteners, when switched on, operate at a constant pressure throughout the screwing and tightening process. As a result, the same kinetic energy is used to fasten both an M10 screw and an M8 screw. This is undesirable. In certain cases, this constant kinetic energy that is delivered to the screw or bolt tightener may induce the tool to penetrate the material to which the screw or bolt is to be applied and cause a rupture. This may result in damage to the screwed connection. With self-tapping screws, for example, the resistance is higher at the beginning of the screwing process; however, after the sheet metal has been perforated, this resistance drops to nearly zero. Yet, the prior art bolt or screw tightener uses the same high force, and the screw is struck at full force, which may cause the screw or the screw thread to rupture[6].

Kozo Wakiyama of Osaka Sangyo University in there investigations on earthquake damage have identified that there was there was a little damage of the high strength bolted joints when compared with the welding joints of the steel frames. With this investigation they came to a conclusion that adoption of the high strength bolt joints contributes to the

improvement of the safety of the steel frame buildings. adoption of the high strength bolt joints contributes to the improvement of the safety of the steel frame buildings. . If a bolt is made more high strength, the bolt number of the joint decreases. But the risk of the delayed fracture is entailed for higher strength of the high strength bolts. The development of the super high strength bolt which delay fracture doesn't occur in was begun by the research proposal of Kozo Wakiyama in Nippon Steel Corp. in 1989[7].

A.U. de Koning, T.K. Henriksen, National Aerospace Laboratory NLR, Amsterdam, The Netherlands have identified some problems on fastener joints and suggested FEA Solution for the problems. one of the most challenging problems in fracture mechanics is related to its application to fastener and joints. By nature, not only the quality such as material, manufacturing and mounting processes, of the fasteners are playing a role, but also the stiffness, surface conditions and geometry of the parts are to be considered. Moreover, a fastener cannot be considered exclusively as an individual item, but has to be seen also as a link in a multi load path design. For a reliable integrity analysis of fasteners to be performed it is of paramount importance that accurate knowledge about load distribution and stress intensity factors is available. In their study the load transfer (tension and bending) as well as stress intensity factor solutions for various crack locations and sizes have been derived by advanced 3D FE analyses including threaded bolt and nut[8].

II. SELECTION OF MOTOR, DESIGN OF PARTS AND MATERIAL SELECTION

a. Selection Of Motor

Main components used in this device are motor, base stand, nut fitting and removing plate and a keypad for on/ off switches and some mechanical parts are used for driving operation. This device is operated by a DC motor. Selection of DC motor depends upon the total torque required to fit/remove the bolt. This DC motor works on the simple principle of electromagnetism. Here Spur gears are used for transmitting the power. Proposed design and mechanism has been done in Pro-e wild fire. Structural analysis of the device is carried out in Ansys at different loads.

An equation for estimating initial fastening load in a bolt, based on experiments is approximately

$$P = 284 * d \text{ kg} \text{-----(1)}$$

Where d is the nominal diameter of the bolt in mm

In order to find mean torque value needed for fastening it is essential to find out the maximum torque and minimum torque required. If one uses a torque which is greater than the maximum torque required for fastening, due to excessive torque there will be a chance of application of over load on the bolt which damages the treads.

An empirical formula for finding the tightening torque is given by

$$T_{max} = C * d * p / 1000 \text{-----(2)}$$

Where C is a constant, depends upon lubricating condition.

Minimum torque required based on experiment

$$T_{min} = 120 \text{ N-m}$$

Mean torque is given by

$$T_{mean} = T_{max} / T_{min} \text{-----(3)}$$

Then

$$\begin{aligned} \text{Work done for tightening for one bolt } w &= \int_{\theta_1}^{\theta_2} T_{mean} d\theta \\ &= T_{mean} \int_{\theta_1}^{\theta_2} d\theta \text{----(4)} \end{aligned}$$

Total Work done for tightening four bolts  $W = 4 * w$  N-m  
Based on W value motor has been selected.

Table 1 Standard metric bolt dimensions

Size Design - nation	Nominal (Major) Diameter $D_n$	Minor Diameter $D_m$	Nominal Shank Area, $A_n$	Pitch (mm per thread) $p$	Pitch Diameter, $d_p$	Minor Diameter Area, $A_s$
M22	22	18.93	380.13	2.5	20.39	270.51

b. Design Of Gear

Spur gears have been used in this device and the material used for the manufacturing of the gears is alloy steel. The teeth project radically, and with these "straight-cut gears", the leading edges of the teeth are aligned parallel to the axis of rotation. These gears can only mesh correctly if they are fitted to parallel axes.

Dynamic load is calculated by

$$F_d = F_t + \frac{21 v (bc + Ft)}{21 v + \sqrt{(bc + Ft)}} \text{-----(5)}$$

where  $F_t$  is Tangential load in N

$v$  Pitch line velocity in m/s

$b$  face width in mm

$c$  Deformation factor

and beam strength is calculated by

$$F_s = \pi * m * b * \sigma_b * y \text{-----(6)}$$

where,  $\sigma_b$  bending stress in  $N/mm^2$

$m$  module in mm

$y$  is a Form factor

As the Dynamic load is less than the beam strength the gear tooth has adequate beam strength and it will not fail by breakage.

Table 2 Alloy steel properties

Properties	Units
Tensile Strength, psi	97,000
Brinell Hardness	201
Yield, psi	57,000
Elongation	25%
Machinability	66%

### III . CONSTRUCTION AND WORKING OF AUTOMATIC MULTIFASTER DEVICE.

The proposed device is bolt/nut fitting & removing without human help for driving. This device is designed to fit and remove bolt/nut of M22 size. Mechanical parts are used here for driving operation. Here spur gears are used for the driving operation. The different components of the device are Motor ,Battery, Gear system, DPDT switch.

Initially, make alignment of the device nut holder with the nut which we want to tight or remove. Keypad has a switch to drive the nut holder. This switch is called as DPDT Switch which stands for Double pole double through switch. Her we used the positive potential and negative potential of the motor. If we push the DPDT switch in forward direction, it helps to fix the bolt/nut, or if we push the DPDT switch in reverse direction, the given polarity will be changed oppositely and it helps to remove the bolt/nut. The efficient function of the motor has own driver unit which enables by small power.

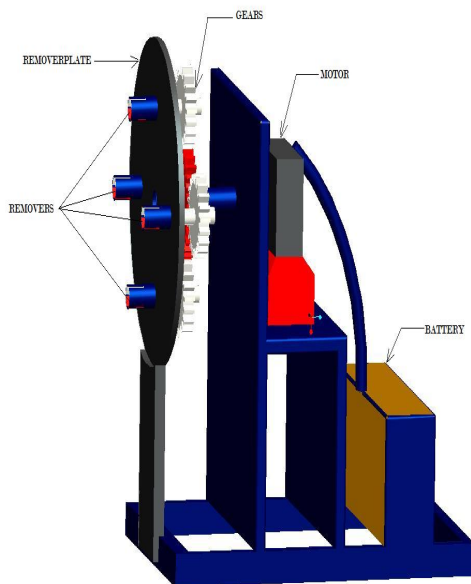


Fig 1.Design of Automatic Multi fastener Device

In this proposed device an DC electric motor of 2.5kw is used. Electric motor, operation is based on simple electromagnetism. A current-carrying conductor generates a magnetic field; when this is then placed in an external magnetic field, it will experience a force proportional to the current in the conductor, and to the strength of the external magnetic field. The internal configuration of a DC motor is designed to harness the magnetic interaction between a current-carrying conductor and an external magnetic field to generate rotational motion. DC motor has six basic parts they are axle, rotor (armature), stator, commutator, field magnet(s), and brushes. In most common DC motors, the external magnetic field is produced by high-strength permanent magnets. The stator is the stationary part of the motor this includes the motor casing, as well as two or more permanent magnet pole pieces. The rotor (together with the axle and attached commutator) rotate with respect to the stator. The rotor consists of windings generally on a core, the windings being electrically connected to the commutator.

In this device we used secondary type battery. A battery is one or more electrochemical cells, which store chemical energy and make it available as electric current. There are two types of batteries, primary batteries and secondary batteries, both of which convert chemical energy to electrical energy. Primary batteries are also called as disposable batteries. Secondary batteries are also called as rechargeable batteries. Primary batteries can only be used once because they use up their chemicals in an irreversible reaction. Secondary batteries can be recharged because the chemical reactions they use are reversible; they are recharged by running a charging current through the battery, but in the opposite direction of the discharge current. Secondary, also called rechargeable batteries can be charged and discharged many times before wearing out.

In this Automatic Multi fastener Device spur gears are used for the driving operation. Design of the spur gears has been done according to the design conditions. Dynamic load and beam strength has been calculated, As the Dynamic load is less than the beam strength it has been concluded that gear tooth has adequate beam strength and it will not fail by breakage. Therefore the design is satisfactory. Spur gears have teeth parallel to the axis of rotation are used to transmit motion from one shaft to another shaft. Spur gears are the simplest and most common type of gear. Their general form is a cylinder or disk. The teeth project radially, and with these "straight-cut gears", the leading edges of the teeth are aligned parallel to the axis of rotation. These gears can only mesh correctly if they are fitted to parallel axles. Modeling and assembly of the gears is done in ProE software. Simulation of the Automatic Multi fastener Device is performed in Pro E software .One driver gear with four driven gears will form a gear assembly unit this is shown in fig 2. This entire gear assembly unit is attached to the base plate of the Automatic Multi fastener Device. Fig 3 describes the design of a bas plate. Power to drive the driver gears will be given from the batter. When driver gear completes one rotation, driven gears completes two rotations and the gear ratio is 2.

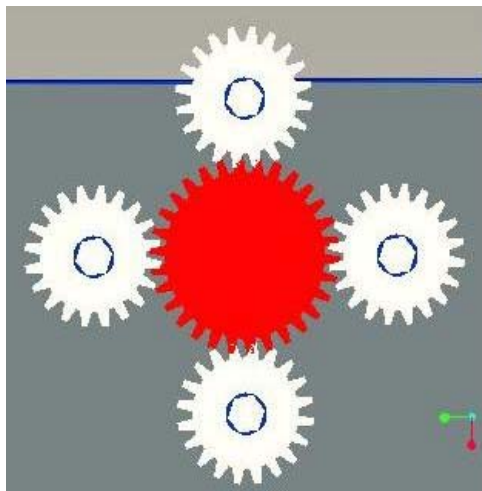


Fig 2.Gears Assembly

In order to have clock wise and anti clock wise rotation of the removers a DTDP switch is used. DPDT Switch stands for Double Pole Double Through Switch. In electronics, a switch is an electrical component which can break an electrical circuit , interrupting the current or diverting it from one conductor to another. The most familiar form of switch is a manually operated electromechanical device with one or more sets of electrical contacts. Each set of contacts can be in one of two states: either 'closed' meaning the contacts are touching and electricity can flow between them, or 'open', meaning the contacts are separated and nonconducting.

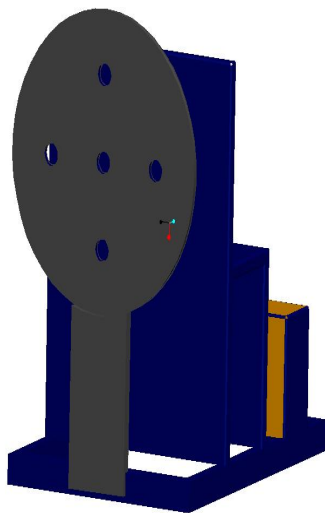


Fig .3 Base Stand

#### IV ANALYSIS AND RESULTS

structural analysis of the Automatic multi fastener device is done in Ansys. Automatic multi fastener device is modeled in Proe. This model is saved in IGS format and it is exported to Ansys for performing analysis. Analysis is performed at three different load conditions. In the preprocessing element type, material properties, meshing and loads have been defined. In the post processing deformed shapes and the displacements have been identified.

structural analysis of the Automatic multi fastener device is carried out at different load conditions. Three different loads have been considered L1 as 800 N,L2 as 1600 N and L3 as 2400 N.

Table 3 Structrual Analasys

Load( N)	Deformation(mm)	Max VonMises(N/mm <sup>2</sup> )
(L1) 800	.390e-4	.134143
(L2) 1600	.489e-4	.330091
(L3) 2400	.702e-4	.726869

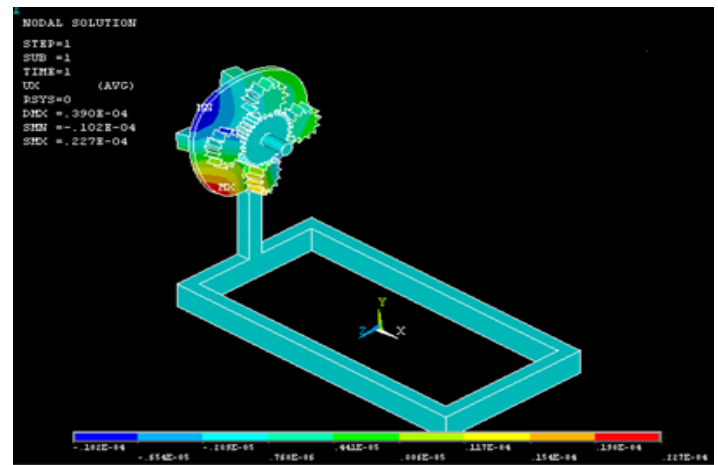


Fig 4 Nodal solution dof x with load L1

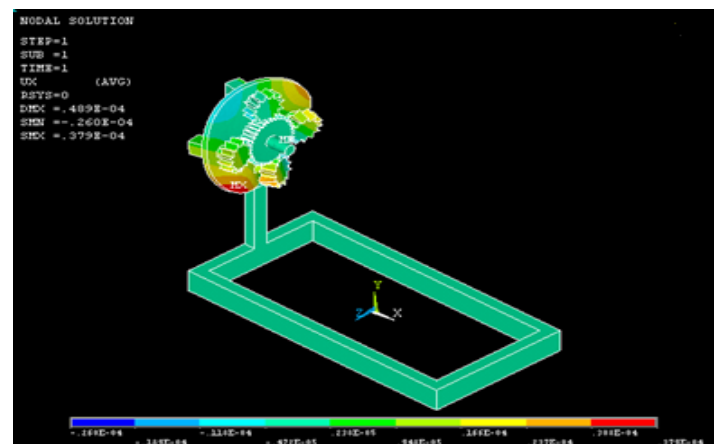


Fig 5 Nodal solution dof x with load L2



Fig 6 Nodal solution dof x with load L3

Nodal solutions for the different loads is given in Fig4, Fig 5, Fig 6. From the structural analysis of the Automatic multi fastener device it is found that the structure will fail if the applied load is beyond the designed value.

#### REFERENCES

- [1] V. K. ZAMYATIN, NOVEMBER, 1979, "ELECTRICAL MANUAL IMPACT NUT TIGHTNER". AT THE EXHIBITION OF ACHIEVEMENTS OF THE NATIONAL ECONOMY, USSR, PP. 36- 38
- [2] V. K. Zamyatin, November, 1979, "dual-spindle nut tightener". At the exhibition of achievements of the national economy, USSR
- [3] SKF Linear motion and precision technologies manual:
- [4] New shield machine technology from Hitachi Zosen manual
- [5] Automation Industries, Inc. manual:
- [6] Cooper Industries, Inc. Houston, TX.
- [7] Kozo Wakiyama Osaka Sangyo University, Osaka, Japan, Keiji Hirai Nishi Nippon Inst. of Tech, Fukuoka, Japan Nobuyoshi Uno Nippon Steel Corp., Tokyo, Japan
- [8] A.U. de Koning, T.K. Henriksen, National Aerospace Laboratory NLR, Amsterdam, The Netherlands
- [9] CURRENT RESEARCH IN PRODUCT DESIGN FOR AUTOMATED ASSEMBLY by Mark Jakiela Graduate Student Report No. UM-MEAM-83-16 Research Funded by International Business Machines Corp. Participating Faculty: P. Papalambros A.G. Ulsoy R.A. Volz T.C. Woo Ann Arbor September 1983
- [10] ACF Components Specifications Hand Book

## Prediction of energy loss along the non-prismatic reach of a compound channel using ANN

B. Naik, Kamel Miri & K.K. Khatua

*Department of Civil Engineering, National Institute of Technology, Rourkela, India*

**ABSTRACT:** Flooded Rivers usually generate transition reaches making the width of floodplain varies. Additional energy loss occurs during interaction between main channel and floodplain as well as due to non-uniformity of flow occurring during movement through non-prismatic reach. The calculation of energy loss in a non-prismatic compound channel is more complex as compared to a non-prismatic simple channel and prismatic compound channel. Hence an easily implementable technique the ANN can be used for predicting the energy loss at different sections of a converging compound channel for different geometry and flow conditions. At first experimental investigations have been performed to study the dependency of flow variables to predict the energy loss, then the ANN technique is applied. The model performed quite satisfactory results. The model can also be used for estimating energy loss on-line but the accuracy of the model depends upon the proper training and selection of data points.

### 1 INTRODUCTION

Distribution of energy in a compound channel is an important aspect in river hydraulics which needs to be addressed properly. It is seen that, the river generally exhibit a two stage geometry (deeper main channel and shallow floodplain called compound section) having either prismatic or non-prismatic geometry (geometry changes longitudinally). Due to flow interaction between the main channel and flood plain, the flow in a compound section consumes more energy than a channel with simple section carrying the same flow and having the same type of channel surface. Due to continuous settlement of people near the river bank and due to other natural causes, the channel with floodplain cross sections behaves as converging/diverging compound channel. An improper estimation of floods in these regions, will lead to an increase in the loss of life, and properties. The modelling of such flows is of primary importance when seeking to identify flooded areas and for flood risk management studies etc. There is always a strong interaction exist between the deep main channel and shallow floodplain even for a prismatic compound channel. In non-prismatic compound channels with converging/diverging floodplains, due to continuous change in floodplain geometry along the flow path, the resulting interactions and momentum exchanges is further increased (Bousmar et al. 2004; Proust et al. 2006; Rezaei 2011). This extra momentum exchange is very important parameter and should be taken into

account in the overall flow modelling of a spatially varied river flow. The flow interaction between the main channel and a prismatic flood plain have been investigated intensively by many investigators such as Knight and Demetriou (1983), Shiono and Knight (1991), Khatua and patra (2008), Khatua et al. (2012) etc. They showed that there are three main sources of energy losses occurring in a compound channel flow assuming in uniform flow conditions those are bed friction, momentum flux due to both turbulent exchange and secondary current across the total cross section. But in a non-prismatic compound channel where the flow is highly non-uniform causing remarkable additional contraction loss of energy making prediction of all flow variables more complex. In the past, numerous studies on channel contractions have been presented by different investigators. Hager (1987) investigated local head losses in different zones along the contraction and their effects on the discharge characteristics. Molinas and Marcus (1998) proposed a discharge equation that considered the energy losses due to contractions. But their study were limited to short, abrupt channel contractions. Conventional approaches lack in providing high accuracy for the prediction of the energy losses in channels due to neglecting the factors causing non-uniformity of flow. That's why a new and accurate technique is highly demandable. The present research investigates some experimental findings of converging compound channels of different geometry and converging angles. The effect of geometry and converging angle on flow prediction

of such channels are studied and finally an efficient approach is proposed to estimate the energy losses with the help of Artificial Neural Network (ANN) which is a promising computational tool. Some of the important past studies in this direction are Neuro-Fuzzy model to simulate Coolbrook-White equation by Walid and Shyam (1998), prediction of friction factor in smooth open channel flow using ANN by Bigil and Altum (2008) and Yuhong and Wenxin (2009), and prediction of discharge in straight compound open channel flow by Mrutyunjaya Khatua and S.S. Mahapatra (2011). New experiments have been conducted to analyse the behaviour of water surface profile and energy losses caused by floodplain contractions. An evaluation for the energy losses in different converging section of a compound channel reach for different hydraulic and geometric conditions are done and the dependency of energy loss for such channels are analysed. An attempt is also made to develop a mathematical model based on ANN to predict the energy losses due to contraction for several converging compound channels and the results are finally compared with the experimental data.

## 2 ANALYSIS OF ENERGY LOSSES AND INFLUENCING PARAMETERS

The resistance to flow of a channel can be significantly increased by the presence of contractions of floodplain. Various methods exist for accounting the additional resistance which are generally for simple channels or meandering channels. It has been confirmed that ignoring contraction losses due to converging cross-section can introduce significant error in channel conveyance estimation.

Consider a prismatic compound channel which has total width =  $B$  and main channel width of  $b$ . Let the floodplain has been contracted from width  $B$  at section 1 to the width of  $b$  at section 5 as shown in Figure 1. Here the total converging part of the channel has been divided into 5 arbitrary sections where the corresponding average flow depths occurring are let  $Y_1, Y_2, Y_3, Y_4$  and  $Y_5$  respectively. The energy loss between two consecutive sections can be calculated from the equation of conservation of energy between those sections. For calculating the energy, let the datum may be taken as bottom of extreme downstream end of the converging part of the channel. i.e. here the channel bottom at section 5. The total energy with non-uniform flow can be considered as the sum of macroscopic kinetic energy, potential energy of the gravity force and of the internal energy Proust et al. (2010). The change in internal energy between two consecutive sections is very less as compared to the corresponding potential and kinetic energies.

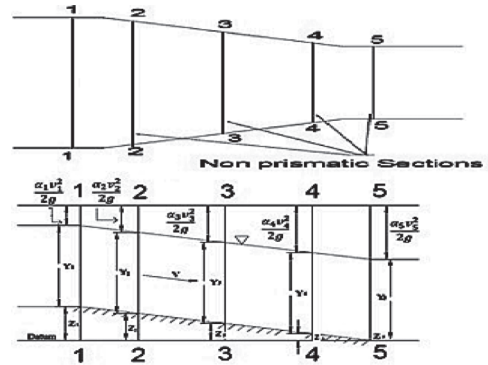


Figure 1. Sketch of energy profile for converging channels at NITRKL.

Therefore the contribution of internal energy here is not considered while applying the conservation of energy principle for any two sections i.e. section 1 and section 2.

$$E_1 = Z_1 + Y_1 + \frac{V_1^2 \alpha_1}{2g} \quad (1)$$

$$E_2 = Z_2 + Y_2 + \frac{V_2^2 \alpha_2}{2g} \quad (2)$$

where  $E$  = total energy head at any section,  $Z$  the bottom elevation of the respective section above the datum,  $Y$  the flow depth,  $V$  the mean velocity at that section and  $\alpha_1$  and  $\alpha_2$  are the velocity head correction factor at that consecutive sections. Considering  $h_l$  the total energy loss between those two sections, we can write.

$$Z_1 + Y_1 + \frac{V_1^2 \alpha_1}{2g} = Z_2 + Y_2 + \frac{V_2^2 \alpha_2}{2g} + h_l \quad (3)$$

It may be noted that the energy loss ( $h_l$ ) may not be linearly varying between sections to sections. It mainly depends on the channel geometry, converging angle, and surface and flow conditions (Naik and Khatua, Rezaei).

Knowing the energy loss between two sections, the energy slope between those sections can be calculated by

$$S_f = h_l / l = (E_1 - E_2) / l \quad (4)$$

where  $h_l = E_1 - E_2 / l$ , and  $l$  is distance between two consecutive sections. Calculation of this energy slope is helpful for correct estimation of flow or average velocity in any part of the non-prismatic sections. This is further helpful for drawing the

energy gradient and the energy slope. The energy losses between sections to section of the present experimental converging compound channels and channels of Rezaei (2006) for different converging floodplain angles and geometries are calculated using equation (4). Here the entry of the converging of the section is taken as reference for calculating the length of the reach. As the estimation of energy loss depends on prediction of total energy at any section which is a difficult task because of dependency on different hydraulic and geometric variability that exist in such compound channels. It is very difficult to establish the nonlinear relation of geometrical and hydraulic input parameters with energy loss. Apart from these loss factors, there are other two remarkable energy loss factors such as interaction between the main channel and floodplain and the second factor is due to contraction of floodplain. This complex phenomenon existing in a non-prismatic compound channel makes prediction of flow more complex. Looking to this an ANN techniques can be easily applied to predict the energy loss, the calculation of which has directly or indirectly have significant effect on predicting important variables such as stage-discharge relationship, shear stress distribution, energy slope prediction, flow distribution etc. Therefore an attempt is made here to predict the Energy Loss of a non-prismatic compound channel using Artificial Neural Network (ANN).

### 2.1 Selection of hydraulic parameters

Flow hydraulics and momentum exchange in converging compound channels are significantly influenced by both geometrical and hydraulic variables. The computation of flow variables in a converging compound channel is more complex than that for simple compound channel. The geometrical and flow factors responsible for the estimation of energy losses at different reaches of a converging compound channel are

- i. Relative flow depth ( $\beta$ ) =  $(H-h)/H$ . where  $H$  = height of water at a particular section and,  $h$  = height of water in main channel
- ii. Converging angle denoted ( $\theta$ )
- iii. Width ratio ( $\alpha$ ) i.e. ratio of width of floodplain ( $B$ ) to width of main channel ( $b$ )
- iv. Aspect ratio ( $\sigma$ ) of main channel i.e. ratio of width of main channel to depth of main channel
- v. Relative distance ( $Zr$ ) from a reference or origin i.e. The distance of the arbitrary reach or section in longitudinal direction of the channel/ total length of the non-prismatic channel. Total five flow variables were chosen as input parameters and energy loss as output parameter.

## 3 EXPERIMENTAL PROCEDURE AND RESULTS

Experiments had been conducted at the Hydraulics and Fluid mechanics Laboratory of National Institute of Technology, Rourkela, India. Two sets of non-prismatic compound channels with varying cross sections were built inside a concrete flume measuring 15 m long  $\times$  0.90 m width  $\times$  0.55 m depth and flume with perspex sheet of same dimensions. The width ratio of the channel was  $\alpha = 1.8$  and the aspect ratio was  $\sigma = 5$ . Keeping the geometry constant, the converging angles of the channels were varied as  $12.38^\circ$  and  $5^\circ$  respectively. Converging length of the channels fabricated were found to be 0.84 m and 2.28 m respectively. Water was supplied through a series of Centrifugal pumps (each 15 hp capacity) discharging into a large RCC overhead tank. In the downstream end there was a measuring tank followed by a sump which feed the water to the overhead tank through pumping. This arrangement completes the recirculation system of water for the experimental channels. The plan view of experimental channels is shown in Figure 2a. Typical grid showing the arrangement of velocity measurement points along horizontal and vertical direction at the test section is shown in Figure 2b. At the downstream end another adjustable tail gate was provided to control the flow depth and maintain a uniform flow in the channel. A movable bridge was provided across the flume for both span wise and stream wise movements over the channel area so that each location on the plan of

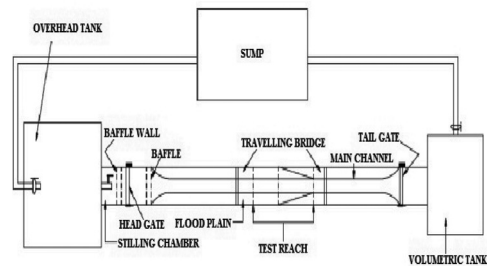


Figure 2a. Plan view of experimental setup.

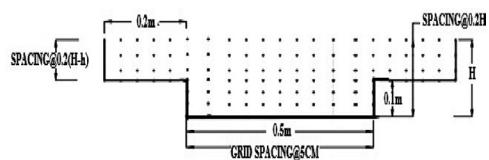


Figure 2b. Typical grid showing the arrangement of velocity measurement points at the test section.

compound converging channel could be accessed for taking measurements. Point velocities were measured along verticals spread across the main channel and flood plain so as to cover the width of entire cross section. Measurements were also taken from mid-point of main channel to the left edge of floodplain at a number of horizontal layers in each vertical point. The lateral spacing of grid points over which measurements were taken was kept 5 cm inside the main channel and the flood plain. Velocity measurements were taken by Pitot static tube (outside diameter 4.77 mm) and two piezometers fitted inside a transparent fibre block fixed to a wooden board and hung vertically at the edge of flume the ends of which were open to atmosphere at one end and connected to total pressure hole and static hole of Pitot tube by long transparent PVC tubes at other ends. The angle of limb of Pitot tube with longitudinal direction of the channel was noted by circular scale and pointer arrangement attached to the flow direction meter. Pitot tube was physically rotated with respect to the main stream direction till it records the maximum deflection of the manometer reading. A flow direction finder was used to get the direction of maximum velocity with respect to the longitudinal flow direction. Steady uniform discharge was maintained in every runs of the experiments and several runs were conducted for overbank flow with relative depth varying between 0.15–0.51. Table 1 shows the hydraulic parameters of different channels used in this paper. For the present analysis, we have also used the data of Rezai (2006). Rezai (2006) conducted experiment on different converging angles. As said before, total converging part of the channels has been divided into 5 arbitrary sections. Now we have evaluated the energy losses in the flow due to convergence of floodplain at different sections of the converging portions.

From the experimental results on converging compound channels, it is seen that the energy loss between two sections at the beginning is higher than that in later sections. These value gradually decreases and reaches minimum just before the mid of converging section. After reaching minimum, there is a gradual increase trend is observed. This may be due to that at the entry section there is a huge loss of energy because of sudden contraction from prismatic part to non-prismatic part. After that the flow gets a transition reducing the loss and it is believed that the transition is complete before mid-section. In the lower width ratio converging experimental channels energy loss is higher at initial overbank flow depths then the loss decreases and reaches minimum at the end of non-prismatic section. This is because the present lower width floodplain converging compound channels have a shorter reach as compared to other higher

Table 1. Hydraulic parameters for the experimental channel data set collected from literature experiments.

Verified test channel	Types of channel	Angle of convergent (°)	Longitudinal slope (S)	Cross sectional geometry	Total channel width (B)		Main channel width (b)		Main channel depth (h)		Ranges of energy loss in two consecutive sections	
					Meter	Meter	Meter	Meter	Meter	B/b	Joule	
Rezai (2006)	Convergent (CV2)	11.31°	0.002	Rectangular	1.2	0.398	0.398	0.05	3	0.0004–0.0015		
Rezai (2006)	Convergent (CV6)	3.81°	0.002	Rectangular	1.2	0.398	0.398	0.05	3	0.004–0.0028		
Rezai (2006)	Convergent (CV6)	1.91°	0.002	Rectangular	1.2	0.398	0.398	0.05	3	0.0011–0.0137		
N.I.T. Rkl	Convergent	5°	0.0011	Rectangular	0.9	0.5	0.5	0.1	1.8	0.0000015–0.0044		
N.I.T. Rkl	Convergent	12.38°	0.0017	Rectangular	0.9	0.5	0.5	0.1	1.8	0.0000032–0.0016		

width ratio channels. The results show that the energy loss is non-linearly depending on those non-dimensional parameters. Therefore an attempt has been taken to model the prediction of energy loss by applying an efficient ANN tool which are described below.

#### 4 ARTIFICIAL NEURAL NETWORK

ANN is a new and rapidly growing computational technique. In recent years it has been broadly used in hydraulic engineering and water resources. It is a highly self-organised, self-adapted and self-trainable approximator with high associative memory and nonlinear mapping. ANNs can be seen to be a simplified model of human nervous system; it can simulate complex and nonlinear problems by employing a different number of nonlinear processing elements i.e. the nodes or neurons. Nodes are connected by links or weights. ANNs may consist of multiple layers of nodes interconnected with other nodes in the same or different layers. Various layers are referred to as the input layer, the hidden layer and the output layer. Input layer receives information from the external source and passes this information to the network for processing. Hidden layer receives information from the input layer and does all the information processing, and output layer receives processed information from the network and sends the results out to an external receptor. The input signals are modified by interconnection weight, known as weight factor  $W_{ij}$  which represents the interconnection of  $i$ th node of the first layer to the  $j$ th node of the second layer. The sum of modified signals (total activation) is then modified by a sigmoidal transfer function ( $f$ ). Similarly output signals of hidden layer are modified by interconnection weight ( $W_{ji}$ ) of  $k$ th node of output layer to the  $j$ th node of the hidden layer. The sum of the modified signal is then modified by a pure linear transfer function ( $f$ ) and output is collected at output layer.

Let  $I_p = (I_{p1}, I_{p2}, \dots, I_{pn})$ ,  $p = 1, 2, \dots, N$  be the  $p$ th pattern among  $N$  input patterns.  $W_{ji}$  and  $W_{kj}$  are connection weights between  $i$ th input neuron to  $j$ th hidden neuron and  $j$ th hidden neuron to  $k$ th output neuron respectively.

Output from a neuron in the input layer is

$$O_{pi} = I_{pi}, i = 1, 2, \dots, 1 \quad (5)$$

Output from a neuron in the hidden layer is

$$O_{pj} = f(NET_{pj}) \\ = f\left(\sum_{i=0}^l W_{ji} O_{pi}\right), j = 1, 2, m \quad (6)$$

Output from a neuron in the hidden layer is

$$O_{pk} = f(NET_{pk}) \\ = f\left(\sum_{i=0}^l W_{kj} O_{pj}\right), k = 1, 2, n \quad (7)$$

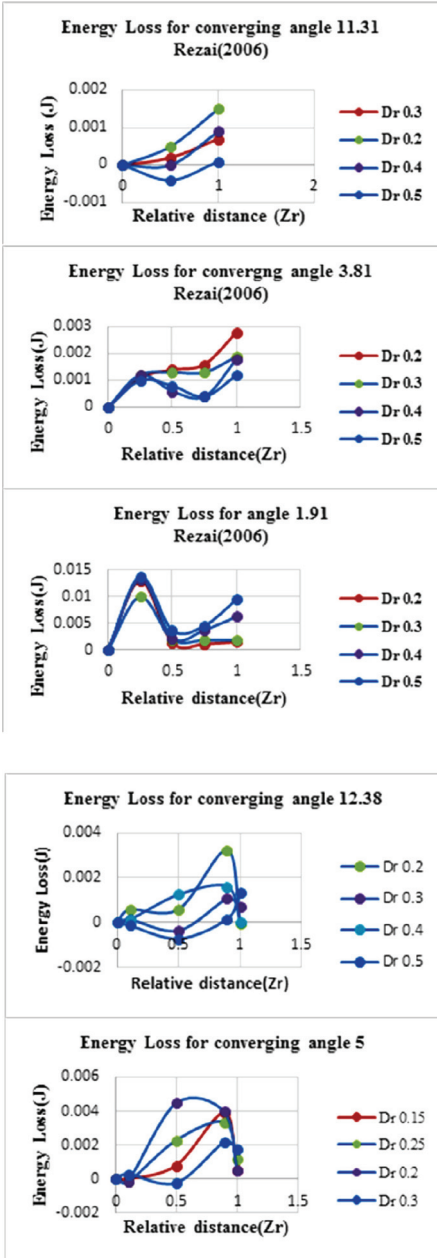


Figure 3. Energy losses vs relative distance for different converging angles.

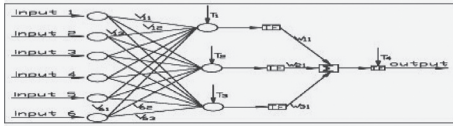


Figure 4. The architecture of back propagation neural network model.

#### 4.1 Sigmoidal function

A bounded, monotonic, non-decreasing, S Shaped function provides a graded non-linear response. It includes the logistic sigmoid function

$$F(x) = \frac{1}{1 + e^{-x}} \quad (8)$$

where  $x$  = input parameters taken.

The architecture of back propagation neural network model. That is the  $l$ - $m$ - $n$  ( $l$  input neurons,  $m$  hidden neurons, and  $n$  output neurons) is shown in the Figure 4.

#### 4.2 Learning or training in back propagation neural network

Batch mode type of supervised learning has been used in the present case in which interconnection weights are adjusted using delta rule algorithm after sending the entire training sample to the network. During training the predicted output is compared with the desired output and the mean square error is calculated. If the mean square error is more, then a prescribed limiting value, it is back propagated from output to input and weights are further modified till the error or number of iteration is within a prescribed limit.

Mean Squared Error,  $Ep$  for pattern  $p$  is defined as

$$EP = \sum_{i=1}^n \frac{1}{2} (Dpi - Opi)^2 \quad (9)$$

where  $Dpi$  is the target output,  $Opi$  is the computed output for the  $i$ th pattern.

Weight changes at any time  $t$ , is given by

$$\Delta W(t) = -nEp(t) + \alpha \times \Delta W(t-1) \quad (10)$$

$n$  = learning rate i.e.  $0 < n < 1$

$\alpha$  = momentum coefficient i.e.  $0 < \alpha < 1$

## 5 RESULTS AND DISCUSSIONS

### 5.1 Testing of back propagation neural network

From the entire experimental data sets, 70% of them were used for training for the ANN model

and remaining 30% used for testing of the ANN model for both the Energy and Energy loss calculation. Train and test sets were selected randomly to find a optimum structure of ANN model.

For Energy Calculations 679 data were used among which 476 were training data and 203 were taken as testing data. Similarly for Energy loss modelling, 532 data set were used among which 373 data were taken as training data and the remaining 159 were taken as testing data. The number of layers and neurons in the hidden layer were fixed through exhaustive experimentation when mean square error was minimised for training data set. It was observed that minimum error obtained for 5-7-1 architecture. So the Back Propagation Neural Network (BPNN) used in this work has three layered feed forward architecture. The model was run on MATLAB commercial software dealing with trial and error procedure.

A regression curve is plotted between actual and predicted Energy and Energy Loss which are shown in Figures 5 and 6. It can be observed that data for both cases are well fitted because a high degree of coefficient of determination  $R^2$  of 0.993 is obtained for the Energy Calculations and  $R^2$  of 0.977 is obtained for the Energy Loss Analysis between the sections.

The residual analysis are carried out by calculating the residuals from the actual energy loss and

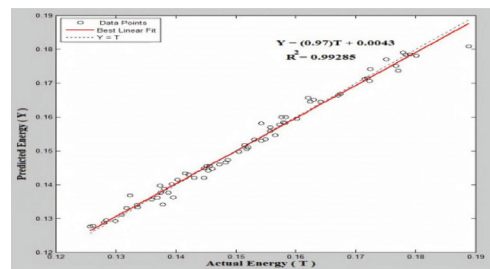


Figure 5. Correlation plot of actual energy and predicted energy.

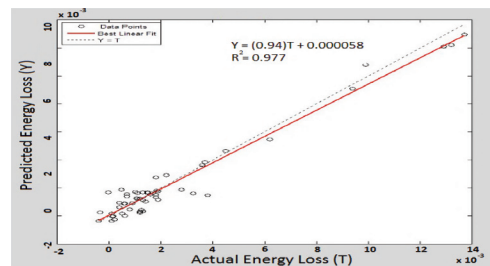


Figure 6. Correlation plot of actual energy loss and predicted energy loss.

predicted energy loss data. The residual testing and training data are plotted against the sample number as shown in Figures 7 and 8, which shows that the residuals are distributed evenly along the centreline of the plot. From this it can be said that the data are well trained.

The actual energy data and predicted energy data sets against the sample numbers are shown in Figure 9. Similarly the actual energy loss and predicted energy loss data against the sample number is shown in Figure 10. As the predicted data pattern follows actual data with little or no exception, it means the models predict the pattern of the data distribution with adequate accuracy.

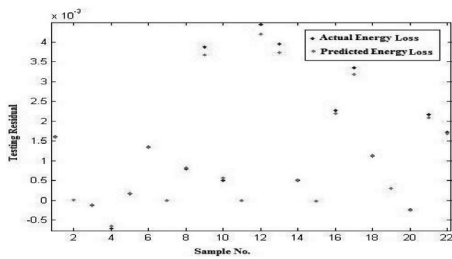


Figure 7. Residual distribution of testing data of energy loss.

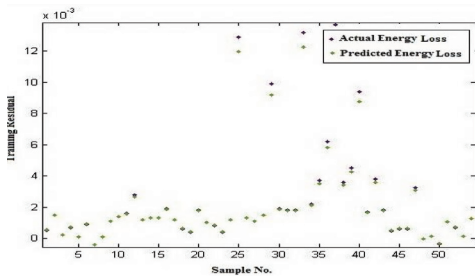


Figure 8. Residual distribution of training data of energy loss.

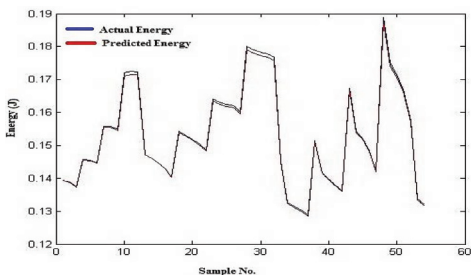


Figure 9. Comparison of actual and predicted energy training data.

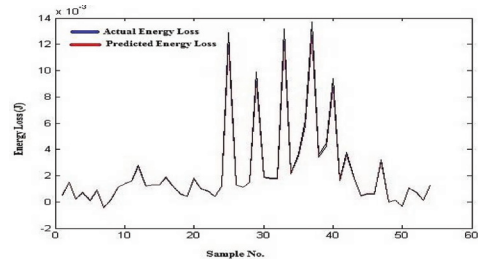


Figure 10. Comparison of actual and predicted energy loss (training data).

Table 2. Statistical results of empirical equation in predicting energy and energy loss.

Error calculations	Energy	Energy loss
MSE	0.00000045	0.00000006
RMSE	0.0006673	0.000238211
MAE	0.0004949	0.000107582
MAPE	0.3	4.49

## 6 CONCLUSIONS

1. From the experimental results on converging compound channels, it is seen that the energy loss between two sections at the beggins is higher than that in later sections. These value gradually decreases and reaches minimum just before the mid of converging section. After reaching minimum, there is a gradual increase trend is observed. This may be due to that at the entry section there is a huge loss of energy because of sudden contraction from prismatic part to non-prismatic part. After that the flow gets a transition reducing the loss and it is believed that the transition is complete before mid-section.
2. In the lower width ratio converging experimental channels, energy loss is higher at initial over-bank flow depths then the loss decreases and reaches minimum at the end of non-prismatic section. This is because the present lower width floodplain converging compound channels have a shorter reach as compared to other higher width ratio channels.
3. Selection of energy loss of converging compound channels are found to depends upon a numbers of non-dimensional hydraulic and geometric parameters out of which aspect ratio, depth ratio, width ratio, relative distance, converging angle and relative depth are the most influencing parameters.
4. An ANN model is proposed for accurate estimation of energy loss of converging compound

channels. The trend and pattern of experimental data matches with predicted energy loss. The basic reason of high degree of prediction accuracy lies in the fact of capability of nonlinear mapping of inputs and outputs in a Neural Network system. The nonlinear relation of geometrical and hydraulic input parameters with energy loss is difficult to establish with traditional energy loss prediction methodology. In addition, the conventional techniques cannot be taken into account the real life factors operating in the system it can be inferred that this model is more adaptive to the prediction of energy loss under different conditions.

- ANN model holds the energy loss prediction with minimal error i.e. MSE as 0.00000006 RMSE as 0.000238211 MAE as 0.000107582 and MAPE 4.49 which less than 10%. Similarly for energy MSE as 0.00000045 RMSE as 0.0006673 MAE as 0.0004949 and MAPE 0.3. So the present ANN model is more convincing model.

## ACKNOWLEDGEMENT

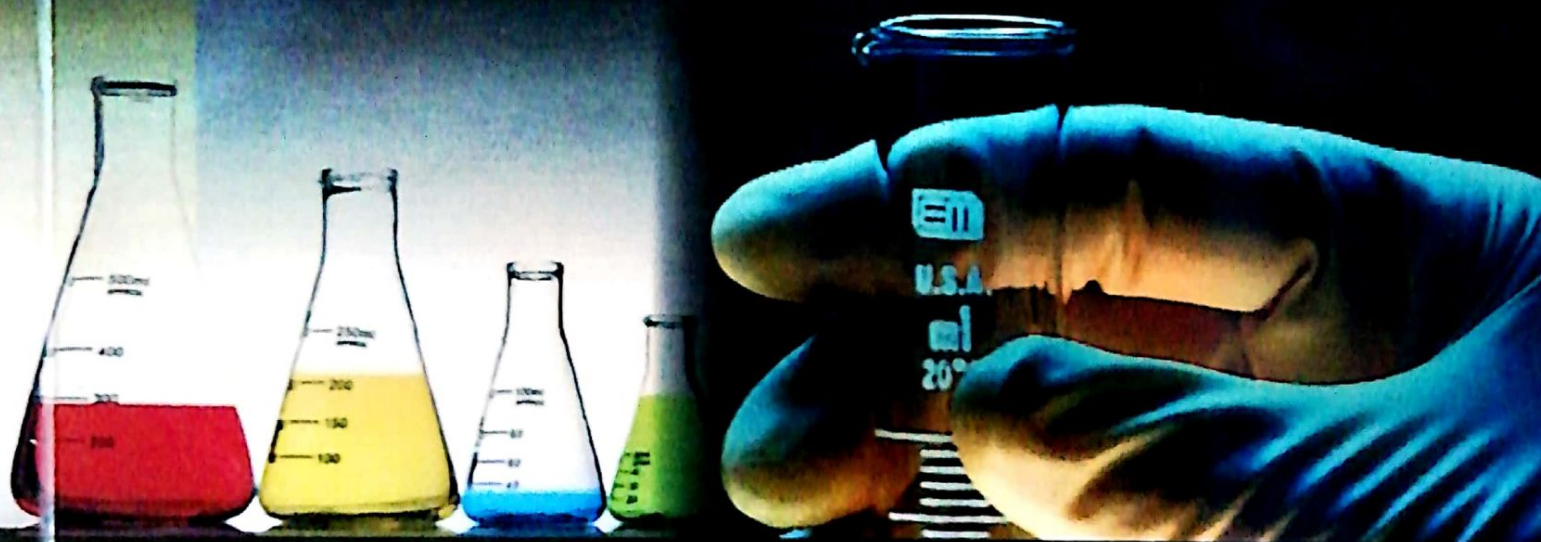
The support from the Institute and the Research project (UKIERI) by the second authors for carrying out the research work in the Hydraulics laboratory at National Institute of Technology, Rourkela is thankfully acknowledged.

## REFERENCES

- Bigil, A. & Altun., H. 2008. Investigation of flow resistance in smooth open channels using artificial neuralnetwork, *Flow Measurement and Instrumentation*, vol.19, 404–408.
- Bousmar, D. & Zech, Y. 2002. Discussion of two-dimensional solution for straight and meandering overbank flows. *J. Hydraul. Eng.* 128(5), 550–551.
- Bousmar, D. and Zech, Y. 1999. Momentum transfer for practical flow computation in compound channel. *J. Hydraul. Eng.*, 125(7), 696–706.
- Bousmar, D., Wilkin, N., Jacquemart, J.H. and Zech, Y. 2004. Overbank flow in symmetrically narrowing floodplains. *J. Hydraul. Eng., ASCE*, 130(4), 305–312.
- Chow VT. 1959. Open-channel hydraulics. *New York: Mc Graw-Hill Book Co.* *Hydraul. Eng.*, 137(8), 815–824.
- Field, W.G., Lambert, M.F. and Williams, B.J. 1998. Energy and momentum in one dimensional open channel flow. *J. Hydr. Res., IAHR*, 36(1), 29–42.
- Hager, W.H. 1987. Discharge characteristics of a local, discontinuous contraction (Part II). *J. Hydraul. Res., IAHR*, 25(2), 197–214.
- Knight, D.W. & Detriou, J.D. 1983. Floodplain and main channel flow interaction. *Journal of the Hydr. Eng., ASCE, Vol.109, No.HY*, 1073–1092.
- Knight, D.W. & Shiono, K. 1990. Turbulence measurements in a shear layer region of a compound channel. *J. Hydr. Res., IAHR*, 28(2), 175–196.
- Khatua, K.K. 2005. Energy losses in Two Stage Meandering and straight Compound Channels. *Hydro Conference (2005)*, Dec 2005, Tumkur, Karnatak, India.
- Khatua, K.K., Patra K.C. and Mohanty, P.K. 2012. Stage Discharge Prediction for Straight and Smooth Compound Channels with Wide Floodplains. *Journal of Hydraulic Engineering, ASCE, Vol. 138*, 93–99.
- Molinas, A. & Marcus, K.B. 1998. Choking in water supply structures and open channels. *J. Hydraul. Res., IAHR*, 36(4), 675–694.
- Proust, S. & Bousmar, D. et al. 2010. Energy losses in compound open channels. *Journal of Advance in Water Resources, Elsevier. Vol-33*, 1–16.
- Proust, S., Rivière, N., Bousmar, D., Paquier, A. and Zech, Y. 2006. Flow in compound channel with abrupt floodplain contraction. *J. Hydraul. Eng.*, 132(9), 958–970.
- Rezaei, B. 2006. Overbank flow in compound channels with prismatic and non-prismatic floodplains. *PhD Thesis*, Univ. of Birmingham, UK.
- Rezaei, B. & Knight, D.W. 2011. Overbank flow in compound channels with non-prismatic floodplains. *J. Hydraul. Research*.
- Sahu, M., Khatua, K.K. and Mahapatra, S.S. 2011. A neural network approach for prediction of discharge in straight compound open channel flow. *Flow Measurements and Instrumentations* 22, 438–446.
- Sahu, M., Singh, P., Mahapatra, S.S. and Khatua, K.K. 2012. Prediction of entrance length for low reynolds number flow in pipes using neuro fuzzy interference system. *Flow Measurements and Instrumentations* 39, 4545–4557.
- Wormleaton & Hadjipanous, P. 1985. Flow Distribution in Compound Channels. *Journal of the Hydr. Engg., ASCE, Vol.111, No.7*, 1099–1104.
- Walid, H.S. & Shyam, S.S. 1998. An artificial neural network for non-iterative calculation of the friction factor in pipeline flow. *Comput Electron Agric*, 21:219–228.
- Yuhong, Z. & Wenxin, H. 2009. Application of artificial neural network to predict the friction factor of open channel. *Commun Nonlinear Sci Numer Simul* 2009;14:2373–2378. 0.038.

ISBN: 978-93-83083-88-6

# Innovations & Research in Physico-Chemical Sciences-A Step towards Sustainability



*Editors*

**Dr. B.B. Singh**

**Prof. (Dr.) Govind Chandra Mishra**

*Published by*

**Excellent Publishing House, New Delhi**

*Online Link:*

**[www.krishisanskriti.org/books.html](http://www.krishisanskriti.org/books.html)**

# Contents

Preface

i

## SECTION- A PHYSICAL SCIENCE RESEARCH PAPERS

1. **Structural and Dielectric Studies of Nickel Substituted Lithium Nano Ferrites by Low Temperature Combustion Method**  
*G. Aravind, G. Koteshwari, Abdul Gafoor, D. Ravinder* 3
2. **Deposition Technique**  
*Divya Aggarwal* 13
3. **Dynamics of Coupled FN Neuron Model**  
*Neharika Chebrol, Supreeti Das, Arshia Ruina* 20
4. **IR Spectra and Molecular Structure of Melatonin: A Computational Study**  
*Santosh K. Srivastava, Vipin B. Singh* 30
5. **X-ray Crystal Structure Determination of  $C_{10}H_{11}N_3O_3S$**   
*Bharti Mishra, R.K.Tiwari* 41
6. **Parametric Coupling of Crossed Laser Beams in Plasma under Raman Backscatter Instability**  
*Vijay Singh, Cephas J. Lyobha* 51
7. **Nuclear Structure of the Neutron-deficient  $^{132}Ce$**   
*Parveen Kumari, Harish Mohan Mittal* 63

## ABSTRACTS

1. **Nuclear Structure of  $N = 90$  Isotones in the Framework of Asymmetric Rotor Model and Energy Staggering** 68  
*Amit Bindra, H.M. Mittal*
2. **Systematic Study of SWCNT for Antenna Efficiency** 69  
*Shruti, Amit*
3. **Parameterization of Finite Rotations** 70  
*Pesaru Vigneswar Reddy, Pavan Kumar Parvathaneni*

# Structural and Dielectric Studies of Nickel Substituted Lithium Nano Ferrites by Low Temperature Combustion Method

G. Aravind<sup>1</sup>, G. Koteswari<sup>2</sup>, Abdul Gafoor<sup>3</sup>, D. Ravinder<sup>4</sup>  
<sup>1,2,3,4</sup>Dept of Physics, Osmania University, Hyderabad-500007, Telangana-India

## ABSTRACT

Nano crystalline spinel ferrites having compositional formula  $\text{Li}_{0.5-0.5x}\text{Ni}_x\text{Fe}_{2.5-0.5x}\text{O}_4$  (where  $x=0.0$  to  $1.0$  with step of  $0.2$ ) have been prepared by non conventional low temperature citrate gel auto combustion method. The synthesized ferrite powders were sintered at  $500^\circ\text{C}$  for 4 hours. The single phase cubic structure of the prepared samples was confirmed by X-ray diffraction analysis. By increasing in the Ni doping in the Li-Ni ferrites, the variations in the structural parameters like lattice parameter, crystallite size and X-ray density etc, were observed. The dielectric parameters like dielectric constant, dielectric loss tangent ( $\tan\delta$ ) and A.C. Conductivity of the prepared samples were measured by using Agilent E4980A precession LCR meter at room temperature in the frequency range 20-2MHz. The dielectric constant ( $\epsilon'$ ), dielectric loss tangent ( $\tan\delta$ ) and A.C. Conductivity of the prepared samples shows a normal dielectric behaviour of ferrites with frequency which indicates the dielectric dispersion is due to the hopping of electrons between the  $\text{Fe}^{+2}$  and  $\text{Fe}^{+3}$  ions. A qualitative explanation was given for composition and frequency dependent dielectrical properties of the prepared Li-Ni ferrite samples.

**Keywords:** Ferrites, Citrate gel method, X-ray diffraction and dielectric properties

## 1. INTRODUCTION

Ferrosinels have interesting structural, electrical and magnetic properties and widely used in many important applications such as microwave devices like circulators, phase shifters, memory cores, magnetic recording media, transformers, choke coils, high frequency instruments, data storage, noise filters and recording heads, owing to their high magnetic permeabilities and low magnetic losses [1,2]. The properties of spinel ferrites depend upon the method of preparation substitution of suitable cations, heat-treatment, annealing conditions and pH value etc.[3].

Ferrite materials are insulating iron oxides. Unlike most materials, they possess high permeability and moderate permittivity operating at different frequencies. Due to their small eddy current losses, there exist no other materials with such wide ranging value to the electronic applications in terms

## ABSTRACT

### Waste cooking oil as feedstock to produce biodiesel & Saponification reaction as by product

<sup>1</sup>**Md. Fakhruddin H.N /**

<sup>2</sup>**Srinivas Ragahavan**

<sup>1</sup>Associate Professor / <sup>2</sup>Assistant Professor  
Methodist College of Engg. & Technology  
Aftd. to Osmania University Hyderabad,  
mfhnn@yahoo.com

<sup>3</sup>**Dr. Mohammed Yousuf Ali /**

<sup>4</sup>**Dr. Manzoor Hussain**

<sup>3</sup>Professor & Principal  
Nawab Shah Alam Khan College of Engg. & Tec.  
<sup>4</sup>Professor & Principal  
JNTUH College of Engg. Sultanpur Hyderabad,

Biodiesel produced cost from virgin vegetable oil is higher than that of fossil fuel, because of high raw material cost. To minimize the bio-fuel cost, the alternate is found to be waste cooking oil used as feedstock. Food against fuel conflict will not arise if this is used for biodiesel production. Catalysts used in WCO bio-fuel are usually acids, base, and lipase. But lipase catalysts are more expensive, the usage of lipase in biodiesel production is limited. In most cases, NaOH is used as alkaline catalyst, because of its low cost and higher reaction rate. In the case of waste cooking oil containing high percentage of free fatty acid, alkaline catalyst reacts with free fatty acid and forms soap by saponification reaction. Also, it reduces the biodiesel conversions. In order to reduce the level of fatty acid content, waste cooking oil is pretreated with acid catalyst to undergo esterification reaction, which also requires high operating conditions. In this review paper, various parameters influencing the process of biofuel production such as reaction rate, catalyst concentration, temperature, stirrer speed, catalyst type, alcohol used, alcohol to oil ratio, free fatty acid content, and water content have been summarized.

Keywords: Waste cooking oil, lipase, saponification, esterification & catalyst

#### ***Introduction***

Fuels, generated from biological feed stocks, are termed as “*biofuels*.” In general, biofuels can be broadly classified into first-generation fuels and second-generation fuels. First generation fuels or conventional biofuels are generally derived from sugar, starch, and vegetable oil source. Whereas, second-generation biofuels are generated from sustainable feedstocks. The major classification of biofuels is shown in Figure 1. Because of high viscous nature, direct application of vegetable oil as a fuel in compression ignition engines has been limited [1]. It is possible to reduce its viscosity by converting vegetable oil into alkyl esters using transesterification reaction [2–4]. Nowadays, biodiesel production has been increased enormously to compete with fossil fuels. The production of biodiesel in recent years around the world is shown in Figure 2. Biofuels are mostly derived from edible oil, non edible oil, fats, waste cooking oil, and algae. Advantage

of using virgin vegetable oil (edible oil) as raw material for production of biodiesel is their low free fatty acid content [5]. Similarly, the main advantage of biodiesel synthesis over non edible oil source is due to their high free fatty acid content [6]. Instead of using virgin vegetable oil, waste cooking oil can be used as raw material for biodiesel production [8]. In most of hotels, restaurants, and in other food industries, the waste cooking oil is either simply discharged into the river or dumped into the land. In spite of this, the waste cooking oil can be used effectively for the biodiesel synthesis.

Biodiesel production from waste cooking oil is found to be economically feasible method [9]. Different sources of raw material used for the production of biodiesel are shown in Figure 3. The property of biodiesel depends on the type of fresh cooking oil used [10]. Biodiesel can also be blended with mineral oil [11].

Even the wastes (byproducts) generated from biodiesel production can be used for power production [12].

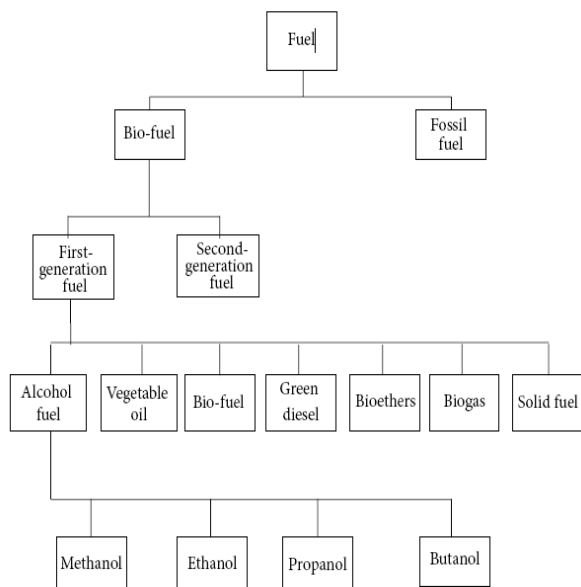


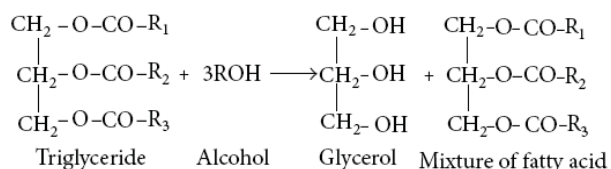
FIGURE 1: Classification of biofuels.

### Transesterification

The major component of vegetable oil is triglycerides. When the triglycerides react with alcohol in the presence of base catalyst, this is called “transesterification.” In this reaction, triglycerides are converted to diglyceride, monoglyceride, and finally converted to glycerol. The reaction mechanism is shown in Scheme 1.

### Side Reaction 1(Saponification Reaction)

If vegetable oil contains free fatty acid, it will react with homogenous base catalyst to form soap and water. The saponification reaction is represented as shown in Scheme 2.



SCHEME 1

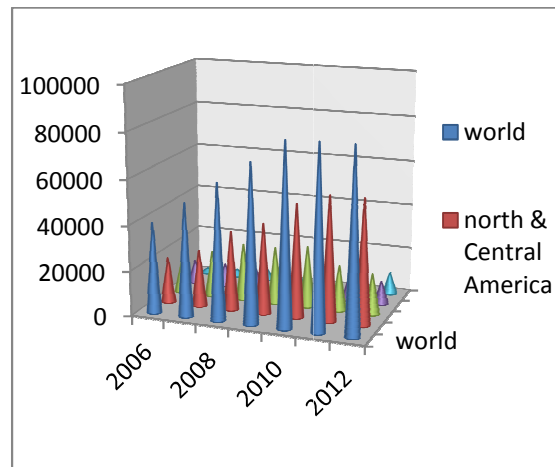


Figure 2: Production of biodiesel in recent years [7].

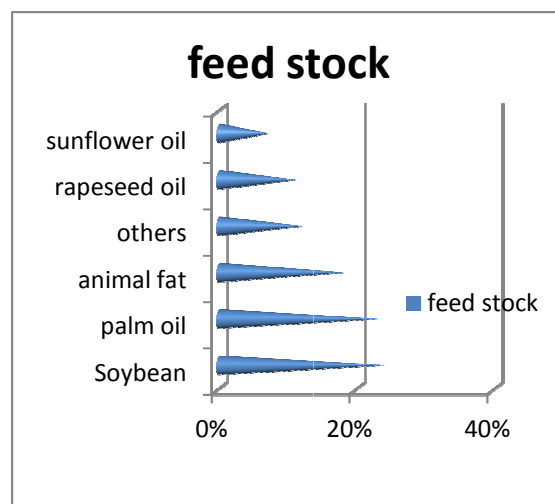
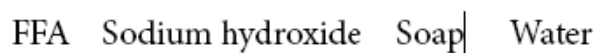
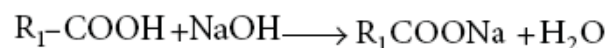


Figure 3: Production of biodiesel from different feed stock [13].

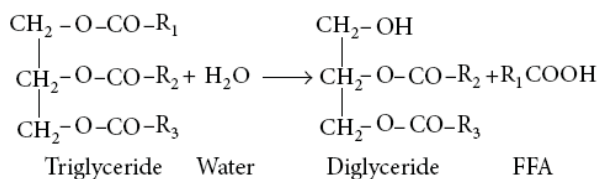


SCHEME 2

The main drawback in this reaction is the consumption of catalyst and increased difficulty in separation process, which leads to high production cost. In addition to that, formation of water in the product will also inhibit the reaction.

### Side Reaction 2(Hydrolysis Reaction)

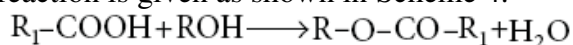
Water generated either from vegetable oil or formed during *saponification* reaction will hydrolyze triglyceride to form more free fatty acid. The hydrolysis reaction is given as shown in Scheme 3.



SCHEME 3

### ***Esterification***

In order to eliminate saponification reaction (formation of soap when FFA reacts with homogenous base catalyst) vegetable oil can be pretreated with acid catalyst, which esterifies free fatty acid to form esters of free fatty acid (biodiesel). This reaction is very much useful when raw material contains high percentage of free fatty acid (esterification of free fatty acid to form free acid esters). But this reaction is slower than base catalyzed transesterification reaction. The esterification reaction is given as shown in Scheme 4.



FFA (alcohol) Fatty acid ester (water)

SCHEME 4

### **Factors affecting the production of biodiesel from waste cooking oil**

#### ***Water Content***

Water content in waste cooking oil will accelerate the hydrolysis reaction and simultaneously reduce the amount of ester formation [14]. Water content should not always exceed 0.5% to obtain 90% yield of biodiesel.

#### ***Free Fatty Acid***

Waste cooking oil contains high free fatty acid content than the fresh cooking oils [15]. Hence, it is known that higher free fatty acid contents will lead to formation of soap and water. Similarly, if free fatty acid content exceeds 3%, transesterification reaction will not proceed even with homogenous base catalyst [16]. Hence this problem could be solved by using heterogeneous catalyst [12, 17, and 18] and also on pretreatment with acid homogenous catalyst [19, 20–22] or heterogeneous catalyst [11] to esterify the free fatty acid to form free fatty acid ester. Usually, the acid-catalyzed reaction rate is low and high reaction conditions are required [10]. Soaps formed while neutralizing free fatty

acid using homogenous base catalyst can be converted back to free fatty acid by adding phosphoric acid to decanted glycerol and soap mixture obtained from final product [6].

#### ***Type of Alcohol***

In most cases, methanol is used for the production of biodiesel, because recovery of methanol from the final product is much easier. Yield of biodiesel obtained from waste cooking oil using methanol is higher than other alcohols (ethanol, butanol) [24] and viscosity of biodiesel obtained using methanol is lesser than that of biofuel obtained from other alcohols [24].

#### ***Alcohol to Oil Ratio***

To produce three moles of alkyl esters, three moles of alcohol and one mole of triglyceride are required [25]. Alcohol to oil ratio always has positive effect on biofuel conversion.

#### ***Catalyst Type***

In recent years, various catalysts (homogenous, heterogeneous, and enzyme catalyst) had been tested for the production of alkyl esters. Vicente et al. [26] studied using various base catalysts for production of alkyl esters and concluded that NaOH is the fastest catalyst among the catalysts used (NaOH, KOH, sodium methoxide, the potassium methoxide). Refaat et al. [27] reported that KOH gives the highest yield for feedstock he had used. Some of the researchers used concentrated sulfuric acid as acid, but it requires high reaction time and high reaction condition. Even 1% (mole) can give up to 99% conversion.

#### ***Catalyst Concentration***

In the absence of catalyst, conversion of waste cooking oil into biofuel requires high temperature conditions [28].

#### ***Stirrer Speed***

The mixing of reactants is very important to achieve completion of transesterification reaction and also it increases the yield of product [29].

#### ***Temperature***

Temperature has significant influence on transesterification reaction [30]. If the reaction temperature is increased, then the rate of

reaction and yield of product will also tend to increase.

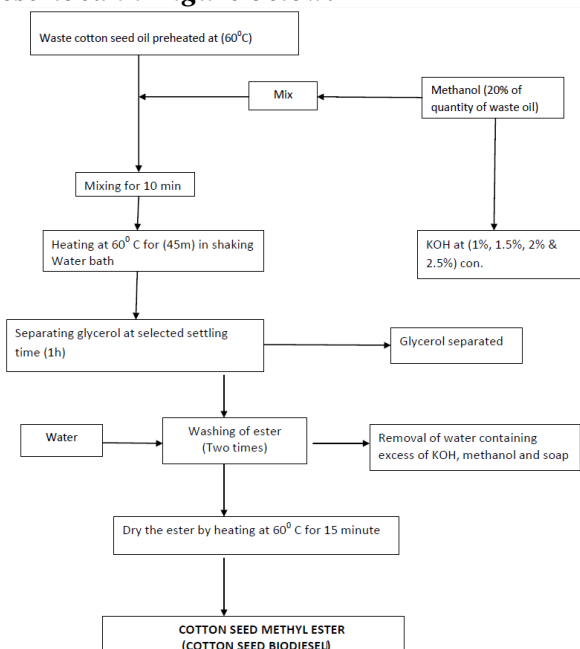
### **Reaction Time**

When the reaction was carried out for a longer time, even 99% of yield could be obtained, but it depends on the availability of reactants in the reaction mixture. If the reaction parameters are not properly adjusted, there are possibilities for the backward reaction, which will decrease the yield of product [24, 30]. For lipase-catalyzed reaction, time required varies over a range of 7–48 hours [31].

### **pH**

pH is not a major factor, when base/acid catalyst are used in the reaction. When lipase was used as catalyst, pH needs to be considered, because at lower or higher pH value, enzymes may decompose. Devanesan et al. [32] studied biodiesel production from *Jatropha* oil using immobilized *Pseudomonas fluorescens* and studied the effect of pH and concluded that pH value of 7 is optimum for production for biodiesel.

**The methyl transesterification of waste cotton seed were carried out as per the steps described in Figure below.**



### **Conclusions**

The recovery of esters by transesterification of waste cotton seed oil with methanol is affected by varying the composition of catalyst.

- The blends B10, B15, B20 of cotton seed have higher flash and fire point as compare to diesel.
- The blends B10, B15, B20 of cotton seed have higher cloud and pour point as compare to diesel.
- Ash content increases as we increase the amount of biodiesel in petro diesel. The blends B10, B15 and B20 of cotton seed have higher ash content as compared to diesel.
- The esters of cotton seed are found to have carbon residue content lower than that of diesel which is better for engine performance and it also prevents carbon deposition inside the combustion chamber.
- The calorific values of diesel and cotton seed methyl ester were found as 43,000 & 40,000KJ/Kg respectively.
- Use of 10% blend of CSME as partial diesel substitutes can go a long way in conservation measure, boosting economy, reducing uncertainty of fuel availability and making more self-reliant.

### **References**

- [1] P. K. Gupta, R. Kumar, B. S. Panesar, and V. K. Thapar, "Parametric studies on bio-diesel prepared from rice bran oil," *CIGR E-Journal*, vol. 9, EE 06-007, 2007.
- [2] O. J. Alamu, T. A. Akintola, C. C. Enweremadu, and A. E. Adeleke, "Characterization of palm-kernel oil biodiesel produced through NaOH-catalysed transesterification process," *Scientific Research and Essays*, vol. 3, no. 7, pp. 308–311, 2008.
- [3] S. Fariku, A. E. Ndongya, and P. Y. Bitrus, "Biofuel characteristics of beniseed (*Sesamum indicum*) oil," *African Journal of Biotechnology*, vol. 6, no. 21, pp. 2442–2443, 2007.
- [4] J. Connemann and J. Fischer, "Biodiesel processing technologies," in *Proceedings of the International Liquid Biofuels Congress*, July 1998.
- [5] F. Ullah, A. Nosheen, I. Hussain, and A. Bano, "Base catalyzed transesterification of wild apricot kernel oil for biodiesel production," *African Journal of Biotechnology*, vol. 8, no. 14, pp. 3289–3293, 2009.
- [6] G. E. Diwani, N. K. Attia, and S. I. Hawash, "Development and evaluation of biodiesel fuel and by-products from *Jatropha* oil," *International Journal of Environmental Science and Technology*, vol. 6, no. 2, pp. 219–224, 2009.
- [7] F. O. Licht, "The Global Renewable Fuels Alliance is a non-profit organization dedicated to promoting biofuel friendly policies internationally," *Global Renewable Fuels Alliance*, 2011.

- [8] M. Canakci, "The potential of restaurant waste lipids as biodiesel feedstocks," *Bioresource Technology*, vol. 98, no. 1, pp. 183–190, 2007.
- [9] B. Supple, R. Howard-Hildige, E. Gonzalez-Gomez, and J. J. Leahy, "The effect of steam treating waste cooking oil on the yield of methyl ester," *Journal of the American Oil Chemists' Society*, vol. 79, no. 2, pp. 175–178, 2002.
- [10] D. Y. C. Leung, X. Wu, and M. K. H. Leung, "A review on biodiesel production using catalyzed transesterification," *Applied Energy*, vol. 87, no. 4, pp. 1083–1095, 2010.
- [11] B. Rice, A. Fröhlich, and R. Leonard, "Bio-diesel production from camelina oil, waste cooking oil and tallow," *The Science of Farming and Food*, 1998.
- [12] Y. Feng, Q. Yang, X. Wang, Y. Liu, H. Lee, and N. Ren, "Treatment of biodiesel production wastes with simultaneous electricity generation using a single-chamber microbial fuel cell," *Bioresource Technology*, vol. 102, no. 1, pp. 411–415, 2011.
- [13] The Endress+Hauser Group, <http://www.au.endress.com/>.
- [14] N. Arun, M. Sampath, S. Siddharth, and R. A. Prasaanth, "Experimental Studies of base catalyzed transesterification of karanja oil," *Journal of Energy and Environment*, vol. 2, no. 2, pp. 351–356, 2011.
- [15] A. B. Chhetri, K. C. Watts, and M. R. Islam, "Waste cooking oil as an alternate feedstock for biodiesel production," *Energies*, vol. 1, no. 1, pp. 3–18, 2008.
- [16] M. Ahmad, S. Ahmed, F. U. Hassan et al., "Base catalyzed transesterification of sunflower oil biodiesel," *African Journal of Biotechnology*, vol. 9, no. 50, pp. 8630–8635, 2010.
- [17] J. Zhang, S. Chen, R. Yang, and Y. Yan, "Biodiesel production from vegetable oil using heterogenous acid and alkali catalyst," *Fuel*, vol. 89, no. 10, pp. 2939–2944, 2010.
- [18] S. T. Jiang, F. J. Zhang, and L. J. Pan, "Sodium phosphate as a solid catalyst for biodiesel preparation," *Brazilian Journal of Chemical Engineering*, vol. 27, no. 1, pp. 137–144, 2010.
- [19] S. Liu, T. McDonald, and Y. Wang, "Producing biodiesel from high free fatty acids waste cooking oil assisted by radio frequency heating," *Biotechnology Advances*, vol. 28, no. 4, pp. 500–518, 2010.
- [20] S. A. El Sherbiny, A. A. Refaat, and S. T. El Sheltawy, "Production of biodiesel using the microwave technique," *Journal of Advanced Research*, vol. 1, no. 4, pp. 309–314, 2010.
- [21] J. Van Gerpen, "Biodiesel processing and production," *Fuel Processing Technology*, vol. 86, no. 10, pp. 1097–1107, 2005.
- [22] G. Knothe and K. R. Steidley, "A comparison of used cooking oils: a very heterogeneous feedstock for biodiesel," *Bioresource Technology*, vol. 100, no. 23, pp. 5796–5801, 2009.
- [23] J. M. Dias, C. A. Ferraz, and M. F. Almeida, "Using mixtures of waste frying oil and pork lard to produce biodiesel," *World Academy of Science, Engineering and Technology*, vol. 44, 2008.
- [24] A. B. M. S. Hossain, A. N. Boyce, A. Salleh, and S. Chandran, "Impacts of alcohol type, ratio and stirring time on the biodiesel production from waste canola oil," *African Journal of Agricultural Research*, vol. 5, no. 14, pp. 1851–1859, 2010.
- [25] B. K. Highina, I. M. Bugaje, and B. Umar, "Biodiesel production from *Jatropha caucis* oil in a batch reactor using zinc oxide as catalyst," *Journal of Petroleum Technology and Alternative Fuels*, vol. 2, no. 9, pp. 146–149, 2011.
- [26] G. Vicente, M. Martinez, and J. Araci, "Integrated biodiesel production: a comparison of different homogeneous catalysts systems," *Bioresource Technology*, vol. 92, pp. 297–305, 2004.
- [27] A. A. Refaat, N. K. Attia, H. A. Sibak, S. T. El Sheltawy, and G. I. ElDiwani, "Production optimization and quality assessment of biodiesel from waste vegetable oil," *International Journal of Environmental Science and Technology*, vol. 5, no. 1, pp. 75–82, 2008.
- [28] K. T. Tan, K. T. Lee, and A. R. Mohamed, "Potential of waste palm cooking oil for catalyst-free biodiesel production," *Energy*, vol. 36, no. 4, pp. 2085–2088, 2011.
- [29] M. Canakci and J. Van Gerpen, "A pilot plant to produce biodiesel from high free fatty acid feedstocks," *Transactions of the American Society of Agricultural Engineers*, vol. 46, no. 4, pp. 945–954, 2003.
- [30] D. Darnoko and M. Cheryan, "Kinetics of palm oil transesterification in a batch reactor," *Journal of the American Oil Chemists' Society*, vol. 77, no. 12, pp. 1263–1267, 2000.
- [31] D. Royon, M. Daz, G. Ellenrieder, and S. Locatelli, "Enzymatic production of biodiesel from cotton seed oil using t-butanol as a solvent," *Bioresource Technology*, vol. 98, no. 3, pp. 648–653, 2007.
- [32] M. G. Devanesan, T. Viruthagiri, and N. Sugumar, "Transesterification of *Jatropha* oil using immobilized *Pseudomonas fluorescens*," *African Journal of Biotechnology*, vol. 6, no. 21, pp. 2497–2501, 2007.
- [33] A. Gnanaprakasam, V. M. Sivakumar, A. Surendhar, M. Thirumarimurugan, and T. Kannadasan, Hindawi Publishing Corporation *Journal of Energy* Volume 2013, Article ID 926392, 10 pages <http://dx.doi.org/10.1155/2013/926392>

# ★iCARTE'15

INTERNATIONAL CONFERENCE ON ADVANCE  
RESEARCH IN TECHNOLOGY AND ENGINEERING

31<sup>st</sup> March, 2015



ORGANIZED BY  
INTERNATIONAL JOURNAL FOR TRENDS IN  
ENGINEERING AND TECHNOLOGY

in Association with



**SRI RANGANATHAR**

INSTITUTE OF ENGINEERING AND TECHNOLOGY  
Approved by AICTE, New Delhi and Affiliated by Anna University, Chennai  
Athipalayam, Coimbatore-641 110



## QoS Oriented Relay Selection and Converge casting in Wireless Sensor Networks

**R.RAMYAA<sup>1</sup>**

PG scholar, Department of ECE, Sri Krishna College of Engineering and Technology  
ramyaec6@gmail.com

**R.NIVEDHA<sup>2</sup>**

Assistant Professor, Department of ECE, Sri Krishna College of Engineering and Technology  
nivedhar@skcet.ac.in

**Abstract**— In this paper, a method called Enhanced Relay Selection based on QoS-factors (ERS-QoS) is proposed for relay selection in wireless sensor networks. The selection of relays is accomplished by computing the factors like energy level, throughput, and delay of the nodes, and based on the weight value of relay nodes; they are selected to transfer data from source to the sink. This is used to improve the QoS in the existing method. In the existing system ALBA-R, a protocol for convergcasting in wireless sensor network is used. ALBA-R combines geographic routing, handling of dead ends, MAC, awake-asleep scheduling, and back-to-back data packet transmission for achieving an energy-efficient data gathering mechanism. The drawbacks of this method is , it provides less quality-of-service in terms of throughput, packet delivery ratio and end-to-end delay .Through ns2 based simulation results we show that the proposed method achieves high quality-of-service when compared to the existing method.

**Index Terms**— Convergecasting, Geographic routing, Relay Selection, Wireless sensor networks, Quality of service

## Modified CI Engine Performance by Varying Injection Timing

**MD. FAKHRUDDIN H.N<sup>1</sup>**

Associate Professor, Methodist College of Engineering & Technology  
mfhnn@yahoo.com

**DR. MOHAMMED YOUSUF ALI<sup>2</sup>**

Professor & Principal,  
Nawab Shah Alam Khan College of Engineering & Technology

**Abstract**— The ever increasing consumption of fossil fuel and petroleum products has been a matter of great concern for India. The huge outflow of foreign exchange on one hand and the increase in the price of crude oil on the other hand have affected the development of the country in contest of energy security.

The consumption of diesel fuel is six times higher than that of gasoline in India and even a minute percentage of efficiency improvement for diesel fuel will save a considerable amount of foreign exchange. The energy consumption can be minimized by improving the efficiency of equipment i.e. CI engine.

The present work where the modification of CI engine has been done, so as to induce turbulence for enhancing the vaporization characteristics of fuel in a combustible mixture by providing a rotating blade in the crown (bowl) of the reciprocating piston located in the main combustion chamber. The oscillation of the connecting rod causes the blade to rotate by an angle of 60°. This arrangement induces the turbulence in a combustible mixture during engine operation, there by facilitating a better combustion performance.

The effects of operating parameters by in turbulence, varying injection pressure and injection timing on performance characteristics of diesel fuelled a compression ignition engine are to be investigated.

**Index Terms** — Android App security, Antimalware, Transformation attacks

# Performance of CI engine with and without swirl in crown of piston with varying injection timing

Md. Fakhruddin H.N / K.Srinivasa Ragahavan  
Associate Professor/Assistant Professor  
Methodist College of Engineering & Technology  
Affiliated to Osmania University Hyderabad, India  
mfhnn@yahoo.com

Dr. Mohammed Yousuf Ali / Dr.Manzoor Hussain  
Professor & Principal  
Nawab Shah Alam Khan College of Engineering & Technology  
JNTUH College of Engineering Sultanpur  
Hyderabad, India

**Abstract**— The ever increasing consumption of fossil fuel and petroleum products has been a matter of great concern for India. The huge outflow of foreign exchange on one hand and the increase in the price of crude oil on the other hand have affected the development of the country in contest of energy security.

The consumption of diesel fuel is six times higher than that of gasoline in India and even a minute percentage of efficiency improvement for diesel fuel will save a considerable amount of foreign exchange. The energy consumption can be minimized by improving the efficiency of equipment i.e. CI engine.

The present work where the modification of C I engine has been done, so as to induce turbulence for enhancing the vaporization characteristics of fuel in combustible mixture by providing a rotating blade in the crown (bowl) of the reciprocating piston located in the main combustion chamber. The oscillation of the connecting rod causes the blade to rotate by an angle of  $60^\circ$ . This arrangement induces the turbulence in combustible mixture during engine operation, there by facilitating a better combustion performance.

The effects of operating parameters by induced turbulence, varying injection pressure and injection timing on performance characteristics of diesel fuelled compression ignition engine are to be investigated.

**Keywords**— C I Engine, Piston Crown, Swirl, Injection Pressure, Injection Timing and Performance.

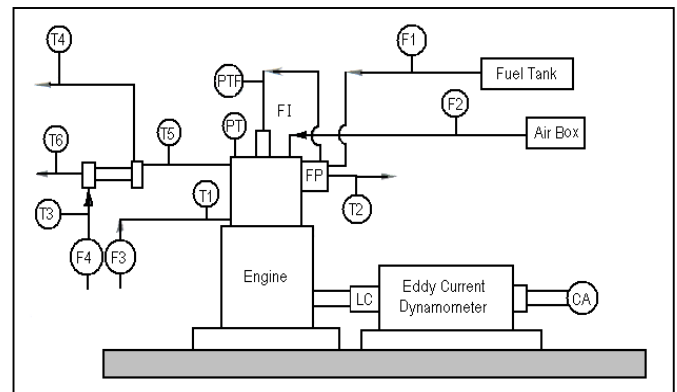
## I. INTRODUCTION

First standard engine is fully instrumented and connected to the dynamometer. The experiments are conducted at constant speed and at four different loads levels viz., 20%, 40%, 60% and 80% of full load. The required engine load percentage is adjusted by using the eddy current dynamometer.

Fig.1 shows the schematic diagram of a complete experimental setup for determining the effects of squish and tumble effect on the performance parameters of compression ignition engine. It consists of a single cylinder four stroke water cooled compression ignition engine connected to an eddy current dynamometer. It is provided with temperature sensors for the measurement of jacket water, calorimeter water, and calorimeter exhaust gas inlet and outlet temperature. It is also provided with pressure sensors for the measurement of combustion gas pressure and fuel injection pressure. An encoder is fixed for crank angle record. The signals from these

sensors are interfaced with a computer to an engine indicator to display P- $\theta$ , P-V and fuel injection pressure versus crank angle plots. The provision is also made for the measurement of volumetric fuel flow. The built-in program in the system calculates indicated power, brake power, thermal efficiency, volumetric efficiency and heat balance. The software package is fully configurable and averaged P- $\theta$  diagram, P-V plot and liquid fuel injection pressure diagram can be obtained for various operating conditions.

Fig.1



## II. ENGINE MODIFICATION

Figure 2 and 3 shows the base line piston and modified piston respectively. Base piston is having simple bowl shaped structure on the crown of it. But the modified piston is made with three chambers at  $120^\circ$  to each other. Same aluminum alloy material is used in fabrication of chamber. 2mm thick small strips are used to make the chambers.



Fig3



Fig2

### III. EXPERIMENTAL DETAILS

Experiments are conducted on an IV-stroke 1 cylinder 3.68Kw Kirlosker water cooled Diesel engine at the rated speed of 1500 rpm. From the experiments observed that combustibility of the fuel is very important in order get a good power output and good thermal efficiencies. The turbulence was played an important role here. In the present work it can be obtained by arranging the rotating blades inside the piston bowl of the engine.

### IV. METHODOLOGY

The engine has a compression ratio of 20.1 and a normal speed of 1500 rpm controlled by the governor. An injection pressure of 250bar, 300bar is used. The engine is first run with neat diesel at loading conditions such as 20%, 40%, 60% and 80%. Between two load trials the engine is allowed to become stable by running it for 3 minutes before taking the readings. At each loading conditions, performance parameters namely speed, exhaust gas temperature, brake power, peak pressure are measured under steady state conditions. The experiments are repeated for various pressures and injection timing. With the above experimental results, the parameters such as total fuel consumption, brake specific fuel consumption, brake specific energy consumption, brake thermal efficiency are calculated. And finally break specific fuel consumption, brake thermal efficiency is plotted with respect to loading conditions for diesel and each diesel oxygenate blend. From these plots, performance characteristics of the engine are determined.

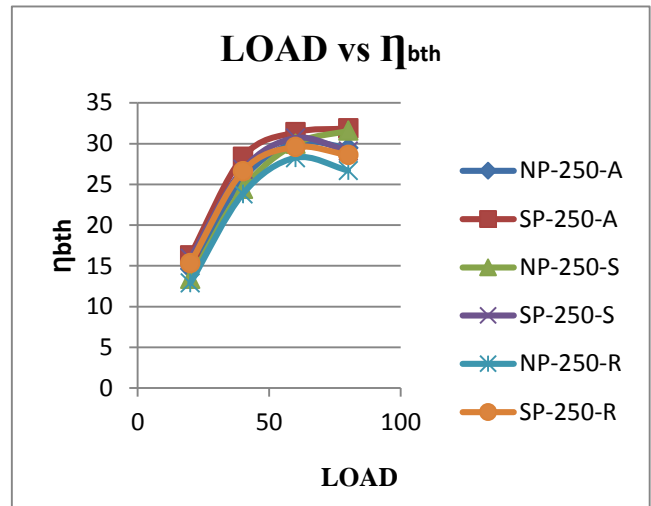
### V BRAKE THERMAL EFFICIENCY

The variation of break thermal efficiency with respect to load applied 20.1 compression ratio and advanced, standard and retard injection timings for normal and modified pistons are shown in graph 1. Turbulence is caused by modified piston. Turbulence enhances mixing and probably produces a leaning effect. The turbulence in the combustion chamber makes the charge into homogeneous and increases the combustibility of fuel. So brake thermal efficiency of modified piston is 2% more than the normal piston. Brake thermal efficiency is increasing with load applied. Compared to normal piston the efficiency increased by 2.2% for modified piston with 20.1 compression ratio. Thus we can get better improvement in brake thermal efficiency. Brake thermal efficiency is maximum for the advanced injection timing compared to standard and retard timings. So that the brake thermal efficiency can be increased by more than 2% for modified piston of 20.1 compression ratio and advanced injection timing.

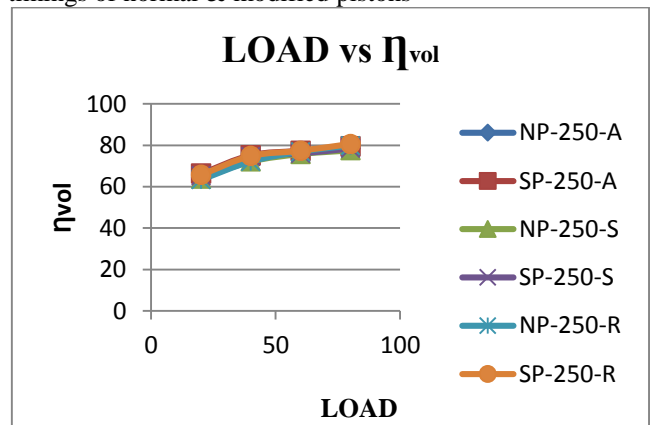
### VI VOLUMETRIC EFFICIENCY

The variation of volumetric efficiency with respect to load applied for 20.1 compression ratios and advanced, standard and retard injection timings for normal and modified pistons are shown in graph 2. Volumetric efficiency depends up on the intake air into the combustion chamber. As the intake air into cylinder is more then we get better volumetric efficiency. By Turbulence we get better results. The volumetric efficiency of modified piston is 2-3 % more than the normal piston compared

to normal piston the efficiency increased by 2.6% for modified piston with 20.1 compression ratio. For 20.1 compression ratio it is 250 bar pressure and advance timing, so that the brake thermal efficiency can be increased by more than 2%.



Graph1.comparison of brake thermal efficiencies with load applied for 20.1 Compression ratio and different injection timings of normal & modified pistons

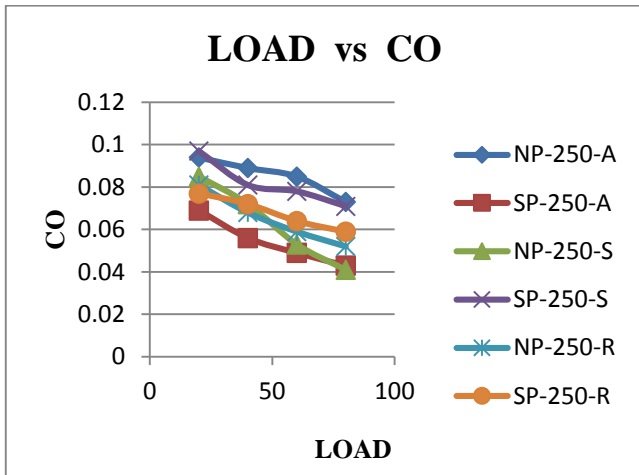


Graph 2.comparison of volumetric efficiencies with load applied for 20.1 compression ratio and different injection timings of normal & modified pistons.

### VII CARBON MONOXIDE (CO) EMISSIONS

Amount of Carbon monoxide (CO) emissions present in the exhaust with respect to load applied for 20.1 compression ratios and advanced, standard and retard injection timings for normal and modified pistons are shown in graph 3. As more amount of oxygen is available in cylinder results the reduction in CO emissions. Due to the turbulence there will be a good amount of oxygen supply to cylinder. Turbulence is caused by modified piston. So that carbon monoxide emissions are reduced by 15% vol with modified piston. Carbon monoxide emissions are reduced with load applied. For 20.1 compression ratio the

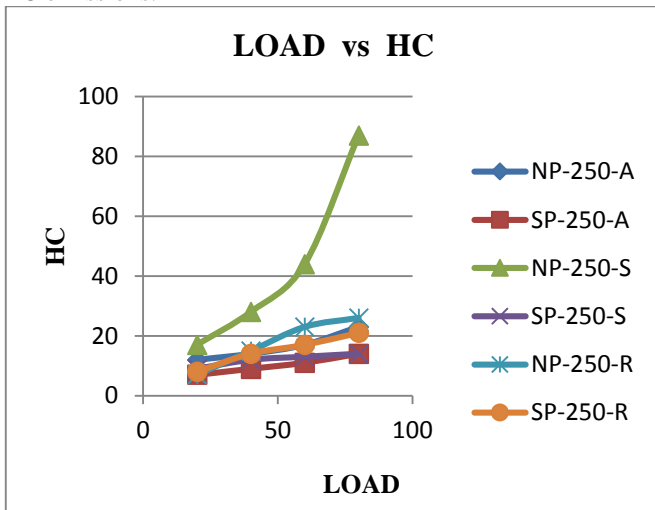
reduction in CO emissions is 17% vol for modified piston. At 250 bar pressure and the standard injection timing for 20.1 compression ratio CO emissions are reduced by 15 % with modified piston



Graph 3.comparison of carbon monoxide emissions with load applied for 20.1 compression ratio and different injection timings of normal & modified pistons.

#### VII HYDRO CARBON (HC) EMISSIONS

The HC emission for normal piston is 6 ppm and 4 ppm for swirl piston. This is shown in graph 4. Hence with the use of swirl piston there has been a considerable decrease of 2 ppm in HC emissions.



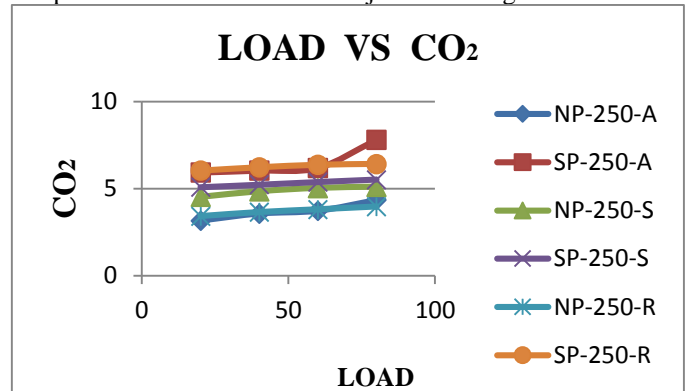
Graph 4.comparison of Hydro carbon emissions with load applied for 20.1 compression ratio and different injection timings of normal & modified pistons.

#### VIII CARBON DIOXIDE EMISSION

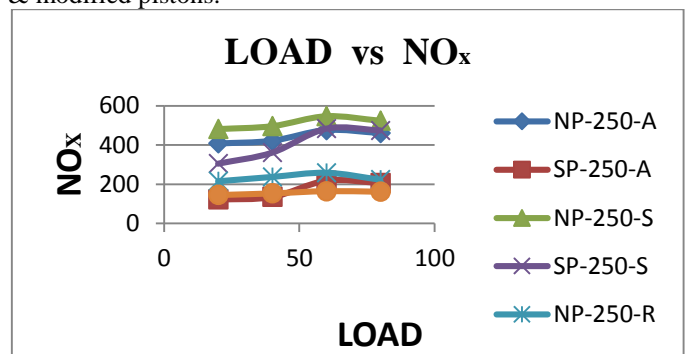
The CO<sub>2</sub> emissions are 2.43 %vol for swirl piston and 3.54 %vol for normal piston. This is shown in graph 5. There by there is an increase of 1-2 % in CO<sub>2</sub> emissions.

#### IX OXIDES OF NITROGEN

The amount of Oxides of Nitrogen (NO<sub>x</sub>) emissions present in the exhaust with respect to load applied for 20.1 compression ratios and advanced, standard and retard injection timings for normal and modified pistons is shown in graph 6. NO<sub>x</sub> is created mostly from nitrogen in the air. NO<sub>x</sub> is a very undesirable emission, and regulations that restrict the allowable amount continue to become more stringent. Released NO<sub>x</sub> reacts in the atmosphere to form ozone and is one of the major causes of photochemical smog. Most of this will be nitrogen oxide (NO), with a small amount of nitrogen dioxide (NO<sub>2</sub>), and traces of other nitrogen-oxygen combinations. NO<sub>x</sub> emissions are reduced by 7% with modified piston. For 20.1 compression ratio the reduction in NO<sub>x</sub> emissions is 8% for modified piston. Thus we can get good reduction in NO<sub>x</sub> emissions at 20.1 compression ratio and standard injection timing.



Graph 5.comparison of Carbon dioxide with load applied for 20.1compression ratio and different injection timings of normal & modified pistons.



Graph 6.comparison of Oxides of Nitrogen with load applied for 20.1compression ratio and different injection timings of normal & modified pistons.

#### VI CONCLUSIONS

Fuel economy is most important factor for any I.C. engine. But environmental protection is much more important than fuel economy. It is necessary that modification in the engine may be incorporated so as to minimize the exhaust emissions which are of topmost priority. In this connection, the geometry of the piston is modified by accommodating rotating blades in the piston crown to induce turbulence by means of swirl motion of charge.

- With the rotating blades inside the piston, turbulence is generated inside the combustion chamber. This further increases the combustibility of the mixture.
- The homogeneous mixture inside the combustion chamber increases the break thermal efficiency of modified piston by 2% compared to normal piston.
- The turbulence in the combustion chamber provides the homogeneous mixture; this increases the volumetric efficiency by 2% with modified piston.
- The turbulence in the combustion chamber increases the oxygen present in it. With this emissions are drastically reduced.
- The NO<sub>x</sub> emissions are increased due to the high temperatures in the combustion chamber caused by the turbulence.

### **References**

1. Katasuhika Moyamito Yoshiyuki Hosiba, Kiyotaka Hosono, Syunichi Hirao "Enhancement of Combustion by Means of Squish Pistons" MITSUBISHI MOTORS technical review 2006, NO 18.
2. B. Murali Krishna and J. M. Mallikarjuna "Tumble Flow Analysis in an Unfired Engine Using Particle Image velocimetry" World Academy of Science, Engineering and Technology 5-4- 2009.
3. John B. Heywood "Internal combustion Engine fundamentals". McGraw-Hill International Edition, Automotive technology series. year 1998.
4. S. Baghdar Hosseini, K. Bashirnezhad, A.R. Moghiman, Y. Khazraii, N. and Nikoofal, "Experimental Comparison of Combustion Characteristic and Pollutant Emission of Gas oiland Biodiesel," International Journal of Mechanical and Materials Engineering 1:1 2010.
5. Lu Xingcai \*, Hou Yuchun, Zu Linlin, Huang Zhen "Experimental Study on The Auto-Ignition and Combustion Characteristics in the Homogeneous Charge Compression Ignition (HCCI) Combustion Operation with Ethanol/n-heptanes Blend Fuels," by Port Injection School of Mechanic and Power Engineering, Shanghai Jiaotong University, Shanghai, People's Republic of China. Received 2 August 2005; received in revised form 23 April 2006.
6. Z.H.Huang, .W.Wang, H.Y.Chen,L.B.Zhou & D.M.Jiang"Study of combustion characteristics of a compression ignition engine fuelled with dimethyl ether," Xi'an Jiao tong University Institute of Internal Combustion Engines, School of Energy and Power Engineering Xi'an, People's Republic of China.
7. M. Pugazhivadivul and S. Rajagopan Dept. of Mechanical Engineering, "Investigations on a Diesel Engine Fuelled with Biodiesel Blends and Diethyl Ether as an additive," Dept. of Chemistry, Pondicherry Engineering College, Pondicherry, India- 605 014 ,Vol.2 No 5 (May 2009) ISSN: 0974- 6846.
8. Yi Ren, Zuohua Huang , Deming Jiang, Liangxin Liu, Ke Zeng, Bing Liu, Xibin Wang, "Combustion Characteristics of a Compression-Ignition Engine Fuelled with Diesel-di-Methoxy Methane Blends Under Various Fuel Injection Advance Angles," State Key Laboratory of Multiphase Flow in Power

Engineering, Xi'an Jiaotong University, Xi'an 710049, People's Republic of China.

9. Kidoguchi Yoshiyuki (univ. Of Tokushima) Miwa Kei (univ. Of Tokushima) Yang.C (zexel corp., jpn) kato ryoji (Isuzu Motor Ltd.)"Effect of High Squish Combustion Chamber on Smoke and NO<sub>x</sub> Emissions of a Direct-Injection Diesel Engine" ISSN: VOL.2000; NO.Vol.4; PAGE.335- 336(2000).



Md.Fakhruddin H.N. has pursued engineering in the year 1996 meritoriously from K.B.N. College of Engineering affiliated to Gulbarga University, Karnataka state. He completed masters in distinction from Jawaharlal Nehru Technological University\_Anantapur campus in the year 2006 in the field of Refrigeration & Air-Conditioning. Currently he is pursuing his Doctorate from Jawaharlal Nehru Technological University\_Hyderabad, kukatpally in the field of thermal engineering with domain of Internal Combustion Engine using nonconventional fuels.

He is having nineteen years of hands on experience, of which fourteen years in teaching and five years in Industry of Electro-Mechanical services, comprising H.V.A.C, Firefighting M.E.P He has published research papers in two International refereed journals & presented the three papers in International Conferences on various topics in thermal domain. Two of his papers were also presented in National Conferences.

He Organized 2-days two National level workshop/Symposium in the core subjects like Internal Combustion Engine and Refrigeration & Air-Conditioning.

He guided tens of students in the project for the post graduate and innumerable students in the projects for undergraduate level. Under his guidance various projects model were made, to name few are Go-Kart, Suitcase Car, Compressed Air Engine, LPG-Refrigeration, Mist-free Desert Air –Cooler, Pin –fin analyzer. He also guide out going students in the field of building services design jobs like M.E.P, H.V.A.C, Firefighting, Plumbing & Electrical.



K.SRINIVASA RAGHAVAN has pursued engineering in the year 2011 meritoriously from P.B.R viswodaya institute of technology and science, Kavali, Andhrapradesh. He completed masters in distinction from Jawaharlal Nehru Technological University\_Anantapur campus in the year 2013 in the field of Internal combustion engines.

He is having Two years of hands on experience in teaching. He has published research papers in one International refereed journals & presented the one papers in International Conferences on various topics in thermal domain. He Organized 2-days two National level workshop/Symposium in the core subjects like Internal Combustion Engine.



- Dr. Mohammed Yousuf Ali is the Principal of the College and Professor in Mechanical Engineering. He has done B.E. (Mech.) from Osmania University and M.E. (Thermal Power Engineering) from Amravati University. He has completed Ph.D., in the topic Performance Evaluation of biodiesel and Hydrogen dual Fuel in a VCR C.I. Engine (Simulation, CFD and experimental analysis). He was ratified as Principal by JNTU in 2010.
- He has twenty three years of teaching experience and industrial experience of one year. He is working as Principal for last five years.
- He has published 20 papers in international Journals, National Journals and Conferences. He has authored two text books for Engineering students of B.Tech. & M. Tech. Courses. He has evaluated many Ph. D. thesis and has been the examiner for a number of Ph. D. and M. Tech. Viva voce exams.
- Four students are doing research work under him. He is a reviewer of two International Journals.

- He is a life member of Indian Society for Technical Education and also of Solar Energy Society of India.
- He has taught many subjects like Heat Transfer Engineering, Graphics Engineering, Thermodynamics, Thermal Engineering -1, Non-conventional Energy sources, Refrigeration Air-conditioning etc. He has delivered guest lectures in many Engineering Institutions.



#### **Dr. M. Manzoor Hussain**

**Chairman, Board of Studies, Automobile Engineering and Mechatronics Engineering JNT University Hyderabad.**

#### **Educational Qualifications:**

- Ph D - Performance Evaluation of Vertical Axis Wind Turbine Rotor, Experimental and CFD Analysis, Mechanical Engineering Department J N T University Hyderabad
- M.Tech (Production Engineering) First Division, J N T U Hyderabad
- B.Tech (Mechanical Engineering), First class with distinction, Osmania University, Hyderabad 1986
- L.A.E. (Automobile Engineering) First class with distinction, Govt. Polytechnic, Masabtank, Hyderabad.1982

#### **Academic Experience:**

Total working experience: 25 Years presently Principal, JNTUH College of Engineering Sultanpur, Medak Dist. From 06-06-2012 till.today

#### **Academic Activities:**

- ▶ Research guide/Supervising Ph.D students. 8 students registered.
- ▶ Project Guide for M.Tech Students. Guided above 40 projects.
- ▶ Project guide for B.Tech Mechanical Engineering Students.
- ▶ Coordinator, four day workshop on Engineering Design using Unigraphics, Under Center of Excellence in CADE, 24-27 Nov.2010.
- ▶ Organizing Secretary Two day National Seminar on Precision Engineering, July 10 and 11, 2009. Jointly by Mechanical Engineering Department , JNTUH College of Engineering Hyderabad and PRRM Engineering College.

#### **Countries Visited:**

- ▶ Ethiopia, Academic assignment at Defence Engineering College Debrizeit. Dec.1998- Dec.2000.

- ▶ Kuwait, International Conference. 2002.
- ▶ Australia, Industrial Training on Pneumatic and Hydraulic in manufacturing automation.
- ▶ Germany, International study mission, 2-6 Dec 2013.

**Journal publications:**

- ▶ National - 23, International - 31

**Conferences attended:**

- ▶ National – 12, International - 15

**Membership in Professional Organizations:**

- ▶ I S T E
- ▶ Combustion Institute (Indian section).
- ▶ International Association of Engineers



INTERNATIONAL CONFERENCE ON WATER RESOURCES, COASTAL AND OCEAN  
ENGINEERING (ICWRCOE 2015)

## Water Surface Profile Computation In Nonprismatic Compound Channels

B. Naik<sup>a</sup>, K.K.Khatua<sup>a\*</sup>

<sup>a</sup>*Department of Civil Engineering , N.I.T. Rourkela, INDIA.*

---

### Abstract

A river generally exhibits a two stage geometry i.e. deeper main channel and shallow floodplain called compound section. In most of the compound channels, the floodplain geometry is found to be varying along the length of the flow called non-prismatic compound channel. The modelling of such flows is of primary importance when seeking to identify flooded areas and for flood risk management studies etc. The water surface profile is a series of transition curve from the normal depth line in one sub reach to the normal depth line in the adjacent sub reach. Water surface modeling help for the study of flood waves, water level calculation during flood, stage discharge relation, design of water work structures. All non-prismatic open channel flows are found to be unsteady and non-uniform. So these flows are difficult to analyse. In this paper experiments have been conducted to compute the water surface profile of non-prismatic compound channel for different converging angle and an attempt has been made to formulate mathematical models for predicting water surface profile by using the new experimental data of N.I.T, Rourkela and other standard data sets for different converging compound channels.

© 2015 Published by Elsevier B.V. This is an open access article under the CC BY-NC-ND license (<http://creativecommons.org/licenses/by-nc-nd/4.0/>).

Peer-review under responsibility of organizing committee of ICWRCOE 2015

*Keywords:* water surface profile, compound channel, converging angle, flow depth

---

### 1. INTRODUCTION

A compound channel consists of a main channel and floodplains. The main river channel carries low flows and the flood plains transport overbank flows during flooding. The storage provided by floodplains in overbank flow reduces river channel that carries low flows flood stages. The interaction between the main channel and floodplain

---

\* Corresponding author. Tel.:09861068249

E-mail address: [kkkhatua@yahoo.co.in](mailto:kkkhatua@yahoo.co.in)

flow is a complex one because of the momentum transfer at the interface. This phenomenon is more complex in non-prismatic compound channels with converging floodplains due to change in geometry. In converging compound channel the flow is forced to leave the flood plains and enter the main channel resulting in increased interactions and momentum exchange (Bousemer and Zech (1999), Bousemer et al. (2004), Proust et al. (2006), Rezai (2006)). This extra momentum exchange should also be taken into account in the flow modelling. Today more than half of the world's population live within 65km of a sea cost, and most of the major cities are also located on main river systems. So whenever flood occurs, this has lead to increase in the loss of life and economic cost (Knight and Shamseldin 2005). Water surface profile prediction is a vital issue in flood risk management and also in assessing ecological effects of bridge construction or changing the cross section geometry of channels. The effect of contraction on the water depth in a compound channel with converging compound channel is now investigated. In present work based on the experimental data of N.I.T Rourkela data and Rezai (2006) data an attempt has been made to develop a mathematical model for water surface calculation in converging compound channels. The method can be applied to the converging compound channels of different configurations and flow conditions.

### Nomenclature

$\alpha$	width ratio
$\delta$	aspect ratio
$\beta$	relative depth
$X_r$	relative distance
$\theta$	converging angle

## 2. EXPERIMENTAL WORK

### 2.1. Experimental Setup

Experiments had been conducted at the Hydraulics and Fluid mechanics Laboratory of Civil Engineering Department of National Institute of Technology, Rourkela, India. Three sets of non-prismatic compound channels with varying cross sections were built inside a concrete flume measuring 15m long  $\times$  0.90m width  $\times$  0.55m depth and flume with Perspex sheet of same dimensions. The width ratio of the channel was  $\alpha = 1.8$  and the aspect ratio was  $\delta = 5$ . Keeping the geometry constant, the converging angles of the channels were varied as  $12.38^\circ$ ,  $9^\circ$  and  $50^\circ$  respectively. Converging length of the channels fabricated were found to be 0.84m, 1.26m and 2.28m respectively. Longitudinal bed slope of the channel was 0.0011. Roughness of the floodplain and main channel were identical and the Manning's n was determined as 0.011 from the experimental runs in the channel. A re-circulating system of water supply was established with pumping of water from an underground sump to an overhead tank from where water flows under gravity to the experimental channel. Adjustable vertical gates along with flow strengtheners are provided in upstream section sufficiently ahead of rectangular notch to reduce turbulence and velocity of approach in the flow near the notch section. An adjustable tailgate at the downstream end of the flume helps to maintain uniform flow over the test reach. Water from the channel was collected in a volumetric tank that helps to measure the discharge rate. From the volumetric tank water runs back to the underground sump. Figure 1(a) shows the plan view of experimental setup. Figure 1(b) shows the plan view of experimental sections.

A movable bridge was provided across the flume for both span wise and stream wise movements over the channel area so that each location on the plan of compound channel could be accessed for taking measurements. The broad parameters of this channel are aspect ratio of main channel ( $\delta$ ), width-ratio ( $\alpha$ ).

A micro-Pitot tube of 4.77 mm external diameter in conjunction with suitable inclined manometer is used to measure velocity at these points of the flow-grid. The Pitot tube is physically rotated with respect to the main stream direction till it gives maximum deflection of the manometer reading. A flow direction finder having a least count of  $0.1^\circ$  is used to get the direction of maximum velocity with respect to the longitudinal flow direction. The angle of limb of Pitot tube with longitudinal direction of the channel is noted by the circular scale and pointer arrangement attached to the flow direction meter. The overall discharge obtained from integrating the longitudinal velocity plot

and from volumetric tank collection is found to be within  $\pm 3\%$  of the observed values.

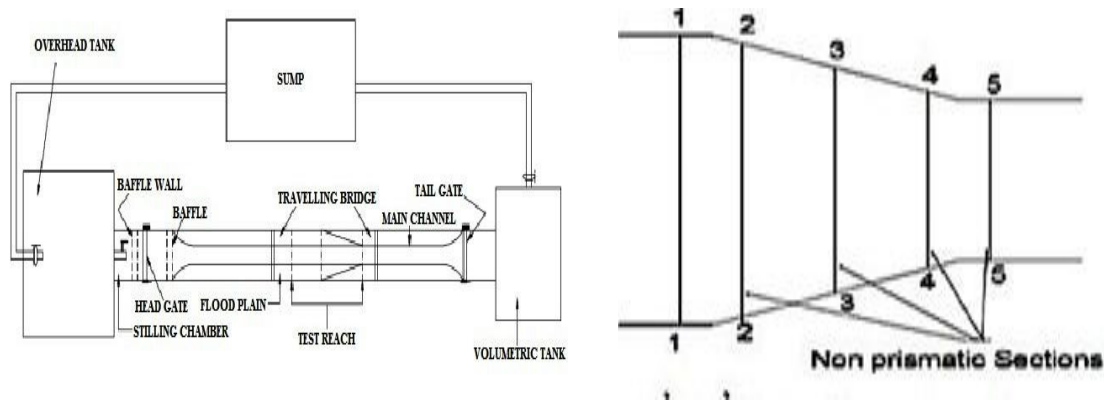


Fig.1 (a). Plan view of experimental Setup (b). Plan view of experimental Section

Table1. Hydraulic parameters for the experimental channel data set collected from literature experiments

Verified test channel	Types of channel	Angle of convergent ( $\Theta$ )	Longitudinal slope (S)	Cross sectional geometry	Total channel width (B)	Main channel width (b)	Main channel depth (h)	Width ratio (sec-1) B/b ( $\alpha$ )	Converging length (Xr)	Aspect Ratio b/h ( $\delta$ )
					Meter	Meter	Meter		Meter	
Rezai (2006)	Convergent (CV2)	11.31°	0.002	Rectangular	1.2	0.398	0.05	3	2	7.96
Rezai (2006)	Convergent (CV6)	3.81°	0.002	Rectangular	1.2	0.398	0.05	3	6	7.96
Rezai (2006)	Convergent (CV6)	1.91°	0.002	Rectangular	1.2	0.398	0.05	3	6	7.96
N.I.T. Rkl	Convergent	5°	0.0011	Rectangular	0.9	0.5	0.1	1.8	2.28	5
N.I.T. Rkl	Convergent	9°	0.0011	Rectangular	0.9	0.5	0.1	1.8	1.26	5
N.I.T. Rkl	Convergent	12.38°	0.0011	Rectangular	0.9	0.5	0.1	1.8	0.84	5

### 3. EXPERIMENTAL RESULTS

The stage discharge relationship of different sections for the converging compound channel of angle 12.38° from in bank to over-bank flow conditions are shown in Fig.2 (a) and Fig.2 (b). A total 13 stage-discharge runs for are observed at the test reach.

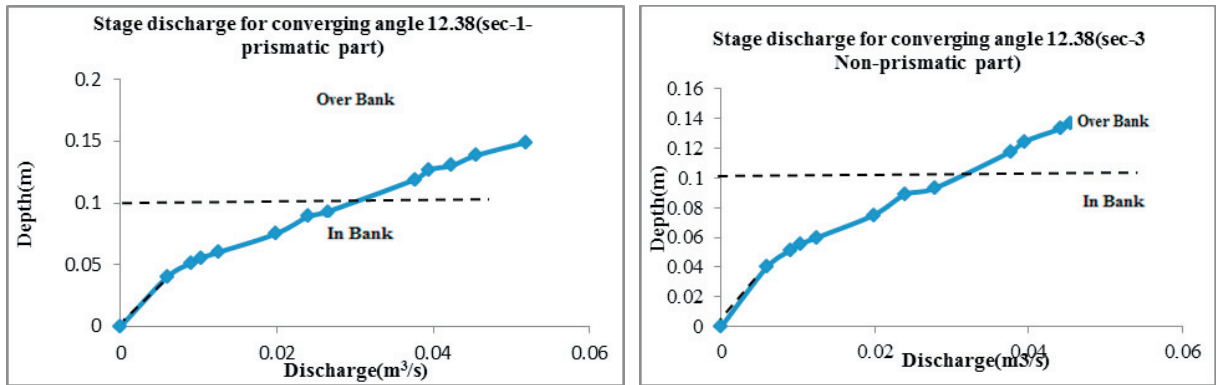


Fig. 2(a). Stage discharge relationship for the converging angle 12.38° (Sec-1 prismatic part) (b). Stage discharge relationship for the converging angle 12.38° (Sec-3- Non-prismatic part)

#### 4. WATER SURFACE PROFILE COMPUTATION AND MODEL DEVELOPMENT

From the literature study, it is seen that water surface profile ( $WP = F(\alpha, \beta, \delta)$ ) for prismatic compound channel, Where  $F$  is the functional symbol. But when all the equations are tested against non-prismatic compound channels of converging sections significant errors are found due variation of geometry. So an attempt has been made here to see the variation of Non prismatic water surface profile with respect to different independent parameters. Non prismatic water surface profile has been derived from a wide range of experimental data sets from three different types of converging compound channels of NIT, Rourkela, India along with three series of converging compound channels data of Rezai (2006) (details of the data sets are given in Table.1) These compound channels have homogeneous roughness both in the main channel and floodplain subsections. Manning’s  $n$  values for all these smooth surfaces are taken as 0.01. A multiple-variable regression model is developed by taking five important dimensionless independent parameters. The dependency of Non dimensional water surface profile ( $NWP$  - Flow depth over floodplain divided by full main channel depth) and the best functional relationships of it have been found out from different plots described below. The relationships may be in the following form

$$NWP = F(\alpha, \beta, \delta, \theta, X_r) \tag{1}$$

The variation of  $NWP$  has been found out for six converging compound channels. The variation of  $NWP$  in terms of relative depth  $\beta$  and relative distance  $X_r$  are plotted for different converging angles  $\theta$  in Fig 4, 5, 6, 7, 8, 9. From these figures it is seen that  $NWP$  increases with increase in relative depth.

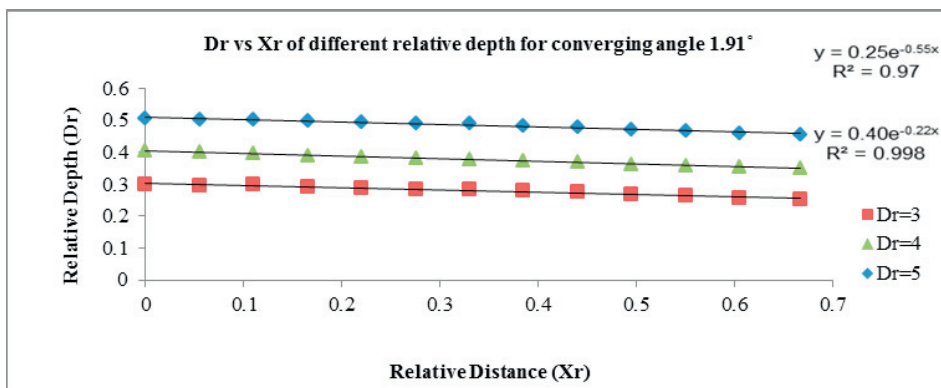


Fig.4. Variation of  $NWP$  along the Non prismatic length for converging angle 1.91°

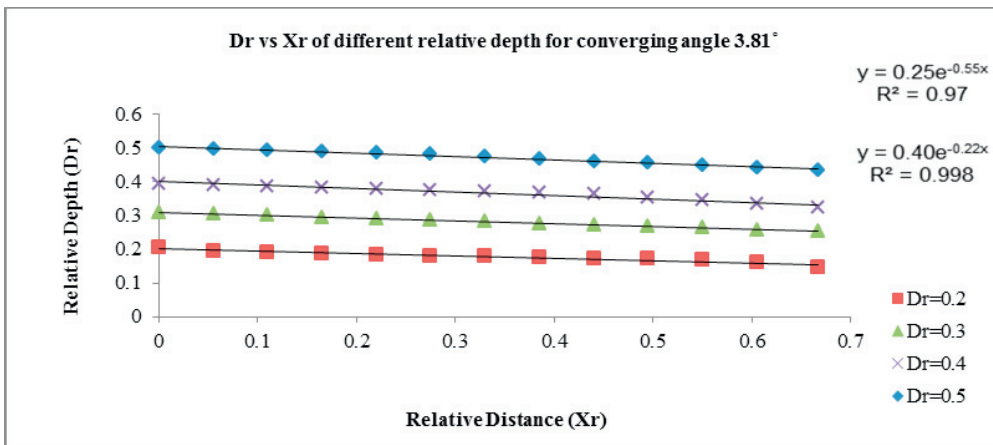


Fig.5. Variation of *NWP* along the Non prismatic length for converging angle 3.81°

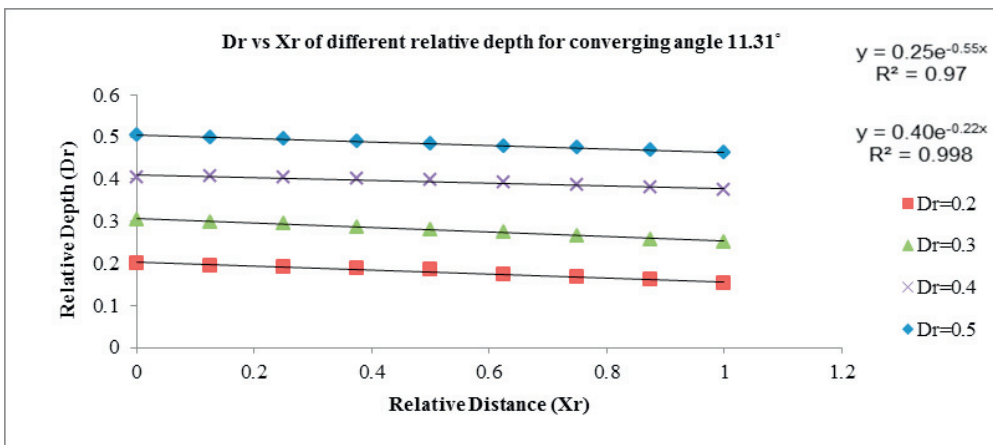


Fig.6. Variation of *NWP* along the Non prismatic length for converging angle 3.81°

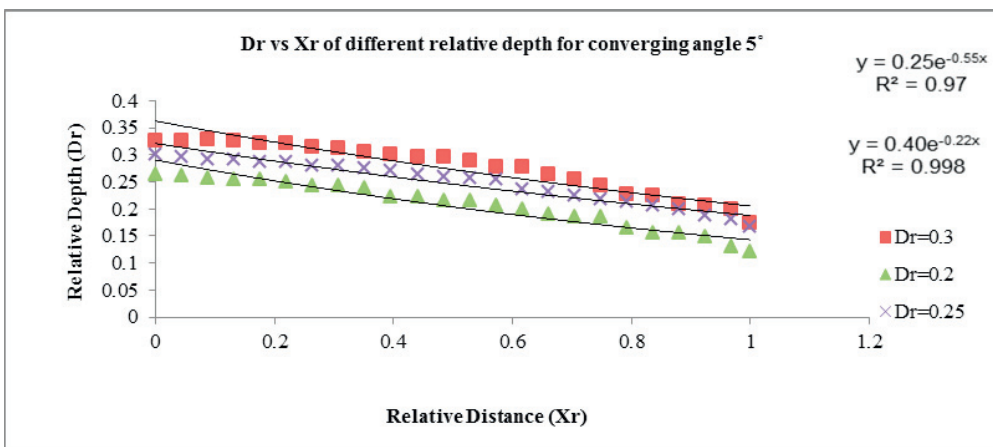


Fig.7. Variation of *NWP* along the Non prismatic length for converging angle 5°

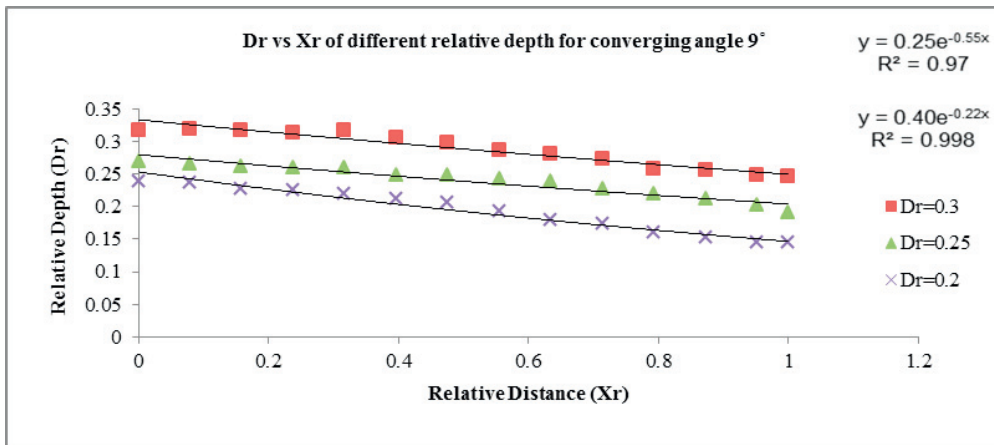


Fig.8. Variation of *NWP* along the Non prismatic length for converging angle 9°

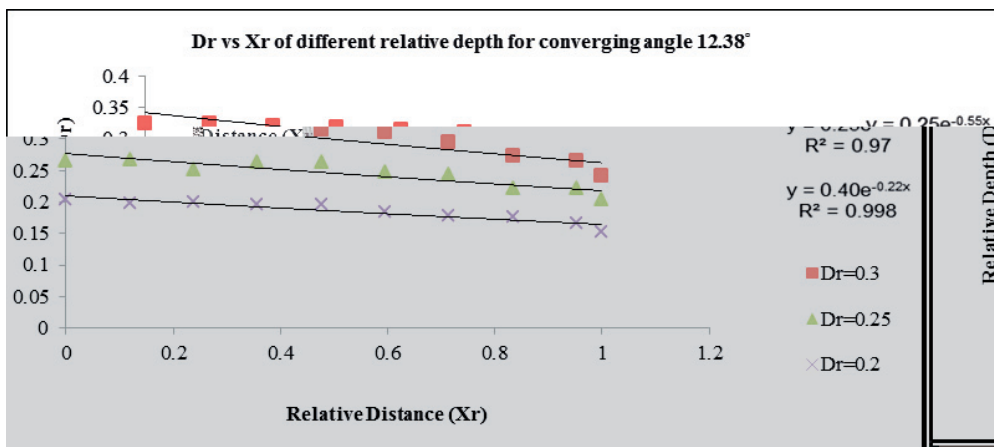


Fig.9. Variation of *NWP* along the Non prismatic length for converging angle 12.38°

By analysing the above plots, the best functional relationships of *NWP* with different non-dimensional geometric and hydraulic parameters for the ranges of overbank flow depths are given by

$$NWP = 0.25 e^{-0.57X_r} \quad \text{for lower Relative flow depth i.e } D_r = 0.2, 0.25, 0.3 \quad (2)$$

$$NWP = 0.40 e^{-0.22X_r} \quad \text{for higher Relative flow depth i.e } D_r = 0.4, 0.5 \quad (3)$$

Here the  $R^2$  value of the chosen functional relationship has been found to be very high and varies from 0.97 to 0.99 (please see the Fig. no. 4, 5, 6, 7, 8, 9). The equations (2) and (3) can be applied to compute the water surface profile of a converging compound channel flow for different converging angles and at different reaches in terms of relative distance from the starting part of non-prismatic reach i.e.  $X_r$ .

5. RESULTS AND DISCUSSION

The *NWP* for all the new non-prismatic compound channels and the data of Rezai (2006) has been computed using equation (2) and (3). The variation between the calculated values of *NWP* of equations (2) and (3) and the corresponding observed values for all the six types of channels are shown in Fig.10 for higher Relative depth and Fig.11 for lower Relative depth. The percentage error *NWP* is less for both Present experimental Channel as well as Rezai (2006) Channel proving the effectiveness of the equation (2) and (3).

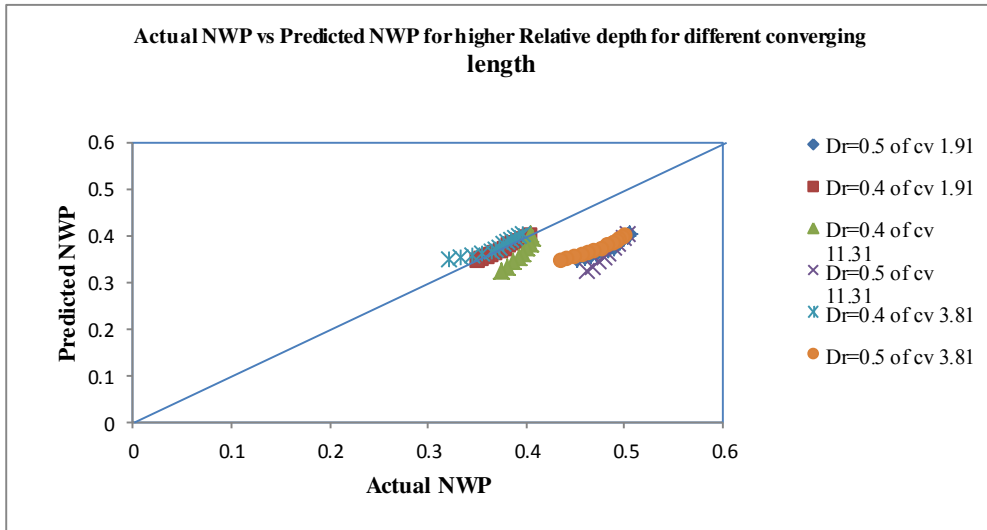


Fig.10. Scatter plot for observed and modelled value of *NWP* for higher  $D_r$ ,

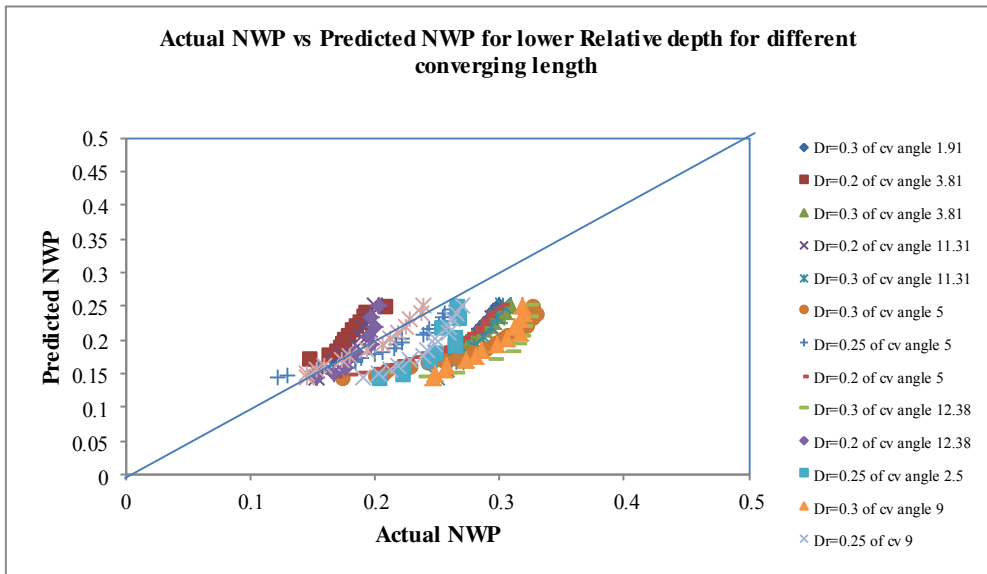


Fig.11. Scatter plot for observed and modelled value of *NWP* for lower  $D_r$ ,

## 6. CONCLUSIONS

The following conclusions can be derived from the above research presented in this work.

- From the experimental results on converging compound channels, the stage discharge of different sections of the converging compound channels is measured.
- The water surface profile along a non-prismatic compound channel are found to increase with increase of Relative depth for converging compound channels of different converging angles and decreases along the converging lengths of the channel under sub-critical flow conditions.
- The dependency of Non prismatic water surface profile is influenced by non-dimensional geometric and hydraulic parameters. The *NWP* in converging compound channel is found to be a non-linear function of all these non-dimensional parameters.
- The present mathematical model for a converging compound channel showing the dependency of *NWP* with relative distance for different flow depths are presented and modelled. The equations are found to provide good results when compared with the observed *NWP*.

## 7. ACKNOWLEDGEMENTS

The author wish to acknowledge thankfully the support from the Institute and the UGC UKIERI Research project (ref no UGC-2013 14/017) by the second authors for carrying out the research work in the Hydraulics laboratory at National Institute of Technology, Rourkela is thankfully acknowledged.

## REFERENCES

- Bousmar D and Zech Y (1999) Momentum transfer for practical flow computation in compound channel J. Hydraul. Eng., 125(7): 696-706
- Bousmar D, Wilkin N, Jacquemart JH and Zech Y (2004) Overbank flow in symmetrically narrowing floodplains. J. Hydraul. Eng., ASCE, 130(4), 305-312
- Proust S, Rivière N, Bousmar D, Paquier A, and Zech Y (2006) Flow in compound channel with abrupt floodplain contraction. J. Hydraul. Eng., 132(9), 958-970
- Rezaei B(2006) Overbank flow in compound channels with prismatic and non-prismatic floodplains. PhD Thesis, Univ. of Birmingham, U.K..
- Knight, D.W., and Shamseldin, A., (2005). "River basin modelling for flood risk mitigation", Taylor & Francis, the Netherlands.
- Rezaei, B., and Knight, D.W., (2009). "Application of the Shiono and Knight Method in compound channel with non-prismatic floodplains" J. Hydraul. Research., 47(6), 716-726.
- Rezaei, B., and Knight, D.W., (2011). "Overbank flow in compound channels with non prismatic floodplains" J. Hydraul. Eng.
- Khatua KK, Patra KC, Mohanty PK (2012) Stage-Discharge prediction for straight and smooth compound channels with wide floodplains. J. Hydraulic. Eng., ASCE, 138(1): 93–99.
- Bousmar, D., and Zech, Y., (2002). "Discussion of two-dimensional solution for straight and meandering overbank flows." by D. A. Ervine, K. Babaeyan-Koopaei and Robert H. J. Sellin, J.H.E., 2000, 126(9). J. Hydraul. Eng., 128(5), 550-551.
- Khiabani, M.H., and Kandasamy, J., (2005). "Friction factor for spatially varied flow with increasing discharge", J. Hydraul. Eng., 131(9), 792-799.

# Realization of FIR Filter using High Speed, Low Power Floating Point Arithmetic Unit

<sup>1</sup>Srikanth Immareddy, <sup>2</sup>Sravan Kumar Talusani, <sup>3</sup>Rayavarapu Prasad Rao

<sup>1</sup>Electronics and Communication Engineering Dept, Methodist College of Engineering and Technology, Hyderabad 500001, India. Email: siri.vlsi@gmail.com.

<sup>2</sup>Electronics and Communication Engineering Dept, Methodist College of Engineering and Technology, Hyderabad 50001, India. Email : sravankumartalusani@gmail.com.

<sup>3</sup>Electronics and Communication Engineering Dept, Avanthi Institute of Engineering and Technology, Viskapatanam, India. Email: prasadrao.rayavarpu@yahoo.com.

**Abstract** - In Digital Signal Processing, filtering is one of the major task, where the inputs to the filter are floating point numbers. This paper discuss about realization of a digital Finite Impulse Response (FIR) filter using high speed, low power floating point arithmetic unit on an Field Programmable Gate Array. High speed is achieved by using a modified normalization unit along with ripple carry adder. A new array multiplier using the concept of carry generation and propagation is used, which reduces the power consumption. The average speed and power requirements of implemented filter are compared with a conventional FIR filter.

**Keyword:** Finite Impulse Response (FIR) Filter, Floating Point Arithmetic Unit(FPAU), Normalization unit, Array multiplier.

## I. INTRODUCTION

Most of the computer applications in recent years need complex computations which demand for accurate results. Example for these kinds of applications includes graphical applications and Digital Signal Processing applications which resulted in the need of including Floating Point Arithmetic Unit (FPAU) [1]-[2]. In Filter design the FPAU is an important block where addition and multiplication operations are frequently used.

Speed is considered as the primary parameter and the power as secondary parameter in designing digital systems nowadays. The feature size of the integrated circuit is reducing almost at nano scale, the motive behind the miniaturization is to improve the speed, but this higher level of integration is increasing the power consumption [3]. Hence heat removal and low power dissipation are the primary goals of the designer and also enhancing the speed of the integrated circuit.

Power reduction can be achieved using different levels of abstraction of a VLSI design. This includes fabrication process level, circuit design level, algorithm level and architecture level. In algorithm level this is achieved with a slight modification in the existing algorithm [4]-[5]. Reduction of threshold voltages will improve the power reduction at circuit level. Parallel and pipelined architectures can be used at architecture level.

A parallel FIR filter is implemented using even symmetric coefficients reducing the number of multipliers, where the multipliers are implemented using adders reducing the hardware requirements [6]. A carry save adder (CSA) is used in implementing FIR filter that gives High Speed and Low power constant multiplier, where the FIR filter is used in

signal processing applications [7]. An FIR filter is designed using the concept of faithfully rounded truncated multipliers, where the emphasis is on the low cost [8]. A modified multiplication technique is proposed that uses redundant multiplication of higher order bits avoided by separating multiplication into higher and lower parts that can reduce the power dissipation in FIR filters in [9]. The aim is to design a FIR filter, with low power consumption and high speed, which can be achieved using a special floating point arithmetic unit.

The logic implementation style of an adder can vary the power dissipation, in order to get high performance and low power, a Bridge style adder is proposed in [10], that uses the concept of high degree of regularity. Hybrid carry-select modified tree adder architecture is investigated to minimize power consumption using multiplexers is proposed in [11]. A carry-look ahead adder technique is used in describing leading-zero count, significantly reduces power consumptions in both static and dynamic CMOS Logic [12]. A scalable leading zero detector is described in [13]. The pass transistor logic is used in leading zero detector design to yield high speed at the cost of high power dissipation is proposed in [14]. The ripple carry adder is selected in this work as it consumes low power than their counterpart adders; the normalization is modified to achieve the speed in the floating point addition.

There are various high-speed multipliers proposed but it should be recognized that power consumption needs to be reduced when there is a tradeoff between speed and power as given in [15]. The multiplication operation can be performed using a Booth multiplier algorithm where the addition can be performed using ripple carry adder, dissipating less power than carry-look ahead adder [16]. The majority of these floating point ALUs can handle at most 32-bit wide floating point numbers particularly, ALUs introduced in DSP processors intended for audio applications [17]-[18]. There are different levels of abstraction where the Low-power multipliers have been studied. In [19]-[20], architecture level method is proposed where clock gating few functional units of a multiplier is carried out. To do the reliable design evaluation, each and every detail of the arithmetic elements needs to be considered rather than going at a high-level approach. For example, the assumption that power consumption in multipliers proportionally varies with the width of data path is not true always [21]. An array multiplier is selected in this work as it is having low hardware requirements which reduce the power consumption.

## II. FLOATING POINT ARITHMETIC UNIT

The Floating point Arithmetic Unit defined in this paper operates on floating point numbers and performs operation such as addition and multiplication. IEEE 754 standard is followed to represent floating point numbers as shown in fig.1 [22]. Here in our discussion we use Single- precision floating point number format, which consists of three fields Sign bit(s), Biased exponent (e) and Mantissa (m). The single-precision number format has 1-bit sign, 8-bit exponent, and 23 bit mantissa. Floating point numbers cover a wide range compared to fixed point numbers. But the complexity of implementation is more.

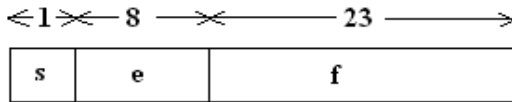


Fig.1 IEEE 754 Single-precision floating point number format.

### A. FLOATING POINT ADDITION

The floating point addition can be performed in five stages they are Exponent difference, pre-alignment, addition, normalization and rounding off stage. Let  $X_1, X_2$  be two floating-point numbers  $X_1 = (S_1, E_1)$  and  $X_2 = (S_2, E_2)$ . The five stages for addition are.

1. Finding the difference between exponents i.e.  $D = E_1 - E_2$ . If  $D < 0$ , then swap the mantissas, the resultant exponent is the larger exponent among  $E_1$  and  $E_2$ .
  2. Pre-aligning the mantissa with lesser exponent by shifting it right by  $D$  bits.
  3. The temporary mantissa is obtained by addition or subtraction of the mantissas based on sign bits of the operand.
  4. Normalization is performed to represent the operand in floating point IEEE 754 standards.
  5. Rounding off is performed on the resultant mantissa.
- The Fig. 2 explains the addition algorithm.

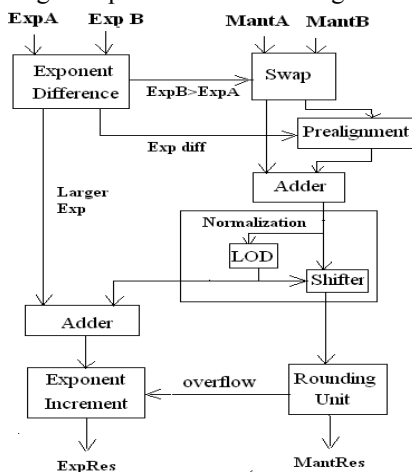


Fig. 2 Floating point Addition data path.

A ripple carry adder is used as adder in FPAU, which consumes less power among all the adders, and the ripple carry adder is simple and slower compared to their counterparts [16]. The Fig.3 is a ripple carry adder used for addition of two 4 bit numbers.

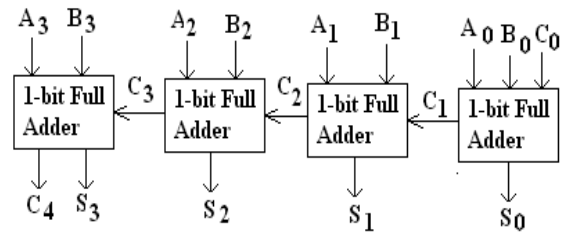


Fig. 3 Ripple carry adder.

### B. FLOATING-POINT NORMALIZATION UNIT:

Normalization unit is an important stage in the floating point addition. Where leading zeros are counted till a first one bit is encountered. A barrel shifter is used to left shift the data depending on the count. The Fig.4 shows about a normalization unit. A modified normalization unit is designed based on partition method is discussed in the next section.

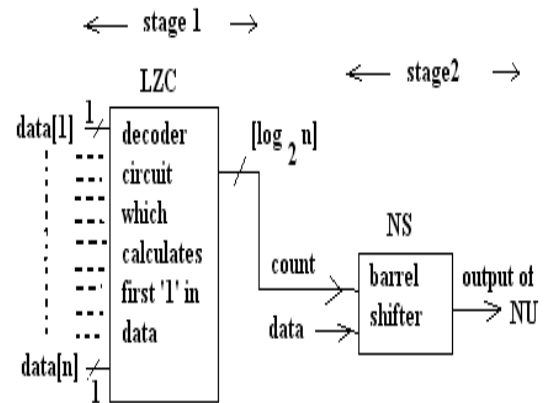


Fig.4. Conventional Normalization Unit.

### C. FLOATING-POINT MULTIPLICATION

Normally the floating point multiplier has a complicated circuit than an adder circuit. Let us assume the floating-point numbers  $X_1 = (s_1, e_1, f_1)$  and  $X_2 = (s_2, e_2, f_2)$ , the resultant number  $X_m = (s_m, e_m, f_m)$  is calculated below in three steps.

1. Calculating the resultant sign  $s_m = s_1 \text{ xor } s_2$ . And exponent  $e_m = e_1 + e_2$ . Multiply the mantissas  $f_m = f_1 * f_2$ .
2. If the result from the multiplier overflows normalization is performed.
3. The mantissa is shifted right by '1' bit and the exponent is incremented by '1' in case of result overflows, in the rounding off step.

The Fig.5 is the algorithm of floating point multiplier. An efficient multiplier improves the overall efficiency of the floating point multiplier.

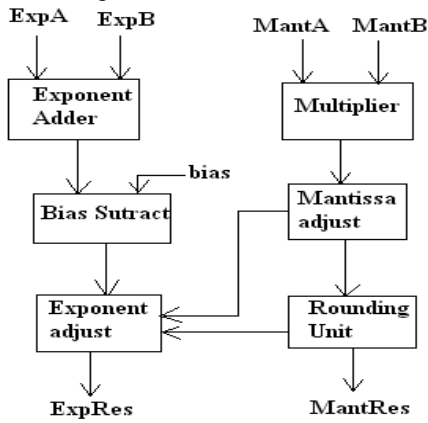


Fig. 5. Floating-point multiplier data path.

An array multiplier is used that consumes less power when compared to all other multipliers [20]. It is simply a shift-add algorithm. The Fig.6 is an array multiplier having two inputs of 4 bit size and an output of 8 bit. A modified array multiplier is used in this paper is explained in this next section.

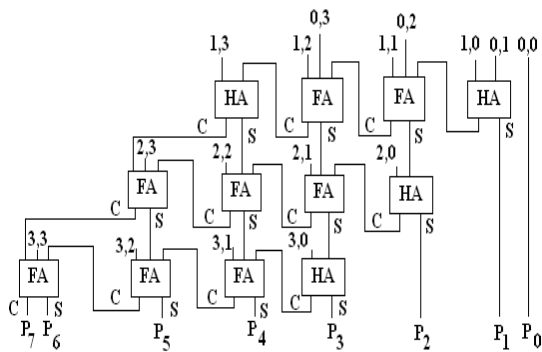


Fig. 6 Conventional 4-bit Array Multiplier.

### III. MODIFIED NORMALIZATION UNIT

The modified Normalization Unit uses the concept of partition the input data. The modified floating-point normalization unit is shown in Fig 7. There are three stages and the computation procedure is explained below.

In stage -1, the 25 bits of input data is partitioned into 5 blocks, with each block consisting of 5 bits each. Each group of 5 bits data is applied as inputs to the OR gate. The 5 OR gates generates outputs as  $y_1, y_2, y_3, y_4, y_5$ . These outputs are applied as inputs to the priority encoder circuit. The priority encoder gives two outputs  $Z$  and  $count$  is 5 bit. In stage-2, the position of first one bit among the input  $Z$  (output of stage-1) is calculated using the conventional NU method. And the sub count is calculated. In stage-3, the output of stage-1, stage-2 is added. This generates the shiftamount. A barrel shifter is used to reduce the delay. The single precision floating point input considered is having 25 inputs. Hence we

select  $m=k= 5$  bits. From the architecture it is observed that  $count=5$  bit,  $subcount= 3$  bit, and  $shiftamount=5$  bit. The barrel shifter is also having 5 bit input.

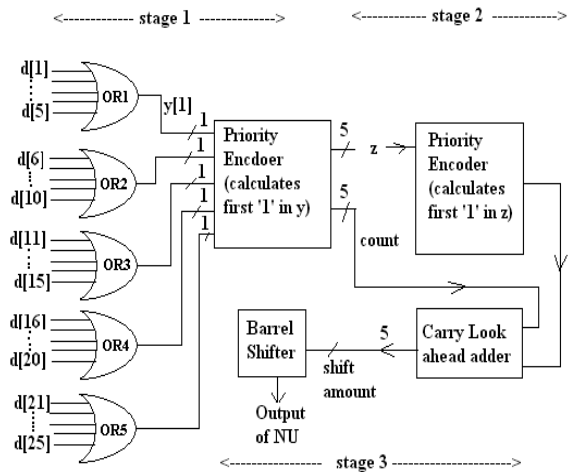


Fig. 7. Modified Normalization Unit.

TABLE I  
COMPARISON OF MODIFIED AND CONVENTIONAL NORMALIZATION UNIT.

Parameter	Conventional NU	Modified NU
Speed (n sec)	39.92	23.63
No. of slices (FPGA)	184	84
Dynamic power(m watts)	34	29

The modified normalization unit using partitioned method shows reduction in average power, number of LUTs and improvement in average speed than the conventional normalization unit. Optimal performance can be achieved when the number of blocks and number of bits in each block are approximately equal. Table I show the comparison between the modified normalization unit and conventional normalization unit.

### IV. MODIFIED ARRAY MULTIPLIER

A Conventional 'n' bit array multiplier gives '2n' bits of output. For Floating point numbers the last 'n' bits contribute to the rounding off process. The modified array multiplier does not calculate these 'n' LSB bits. This reduces the hardware resulting in low power design at the cost of rounding off error. To correct the obtained 'n' bit MSB result, only carry is generated and propagated from the LSB side. By which additional hardware required for computing the sum bits is reduced. In this architecture, changes are made in Lower half of the multiplier by using carry generators in place of Half adders and Full adders.

The carry is generated using carry generation half (CGH) and carry generation full (CGF) circuits using the equation 1, 2.

$$C_{CGH} = A.B \tag{1}$$

$$C_{CGF} = A.B + B.C + A.C \tag{2}$$

The modified array multiplier design has no rounding off step after calculating the output. The rounding off error is ignored as it is of the order of  $10^{-6}$ . The data path after removing this step looks like fig.8.

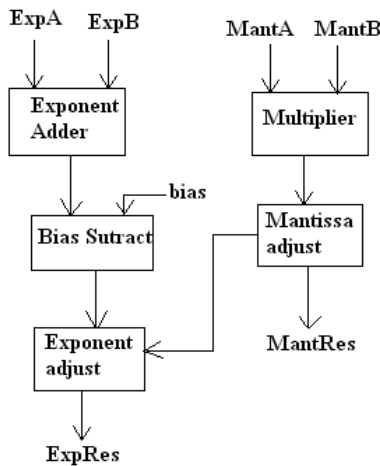


Fig. 8. Modified array multiplier data path.

The modified array multiplier for a single-precision floating point numbers has 24 bit input and output is also 24 bit (MSB), having negligible round off error. The hardware required for generating 24 bit(LSB) is eliminated. The Fig. 9 shown below is the block diagram of modified array multiplier, where the generated carry is propagated to the MSB for reducing the error.

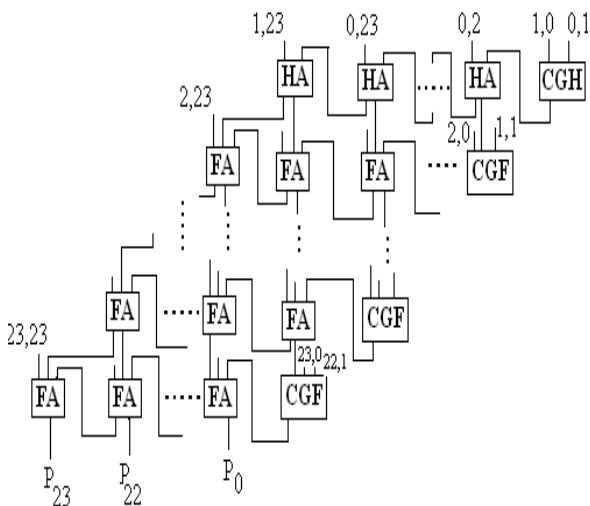


Fig. 9 Architecture of 24 bit Modified Array Multiplier .

In the modified array multiplier architecture as shown in Fig.4.2. The carry generation unit replaces one HA with one CGH, 23 Full adders with 23 CGF. The modified array multiplier is implemented using HDL and simulated. The fig.10 shows the simulations of a sample data.



Fig.10 Simulation of Modified Array Multiplier.

Both the conventional and modified array multiplier is synthesized using Xilinx Spartan. Area and timing information is obtained, the power dissipation information is obtained using Xpower Analyzer. Speed and power dissipation are tabulated in Table II.

TABLE II  
COMPARISON OF CONVENTIONAL ARRAY MULTIPLIER AND MODIFIED ARRAY MULTIPLIER

Parameter	Conventional multiplier	Modified multiplier	Percentage improvement
Speed (ns)	75.2	69.97	2.4 %
Dynamic Power(mw)	993	927	6.7 %

The modified array multiplier design for a single precision floating point input shows an improvement in the power saving.

### V. PROPOSED DIGITAL FIR FILTER

In digital signal processing, a FIR filter is a filter whose response to any finite length input is of finite duration, because it settles to zero in finite time. The FIR filter is computed mathematically as summation of input data multiplied with filter coefficients. The input data and filter coefficients are generally floating point numbers. Let us assume  $X[n]$  is the input data vector and  $H[n]$  is the filter coefficients vector, the output vector of digital FIR filter is  $Y[n]$ ,

The 'm<sup>th</sup>' output of a Digital FIR is computed as

$$Y[m] = X[n].H[0] + X[n-1].H[1] + X[n-2].H[2] + \dots + X[n-m].H[m] \quad (3)$$

The number of taps of the filter is given by 'm'. So for each value of m the input data is multiplied by a filter coefficient and the result is accumulated with the previous sum as shown in Eq.3. The main idea is to multiply and add. This multiplication and Addition is achieved using the Floating Point Arithmetic Unit. The operation of multiply and add is not only restricted to FIR filter, this is used in many signal processing concepts like convolution, IIR filter, Fourier transforms etc.

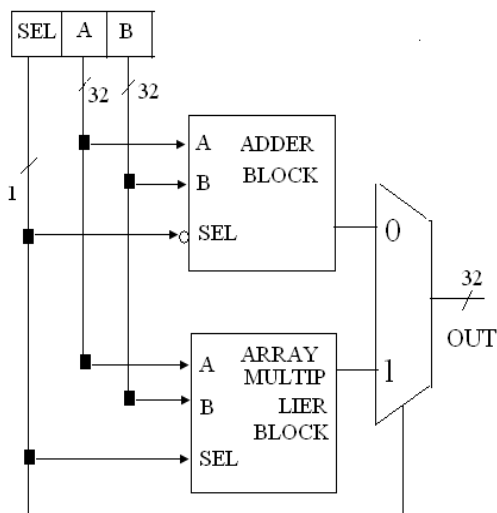


Fig. 11 Modified Floating point Arithmetic Unit.

The adder block and multiplier block of a FPAU makes use of modified Normalization Unit and modified multiplier as shown in the fig.11. The SEL bit of the instruction tells about the operation type. The adder block is designed using ripple carry adder and modified Normalization Unit. An array multiplier is used in the multiplier block. The FPAU operates on floating point numbers. The conventional and proposed FIR filter are simulated and synthesized on XILINX SPARTAN-3 FPGA board. The results of average speed and power dissipation of conventional and proposed FIR filter are graphically represented in Fig.12 and table III.

TABLE III  
COMPARISON OF CONVENTIONAL FIR FILTER AND MODIFIED FIR FILTER.

Parameter	Normal FIR	Modified FIR	Percentage Enhancement
Speed (ns)	105.5	80.5	23.1 %
Dynamic Power(mw)	7.17	5.76	20.5 %

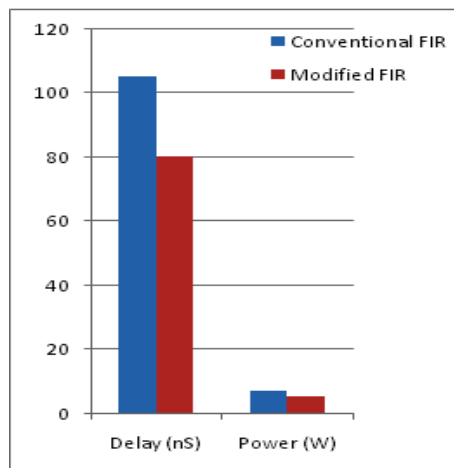


Fig.12 Delay and Power comparison of conventional and Proposed FIR filters.

An FIR filter is realized using the floating point Arithmetic Unit and is implemented on Xilinx FPGA Spartan board. Average speed and power consumption are compared to conventional techniques. This proposed FIR filter has resulted in an average speed enhancement and a power reduction.

## VI. CONCLUSION

In this paper we have designed a digital Finite Impulse Response (FIR) filter using a floating point arithmetic unit (FPAU). The addition unit of the FPAU consists of a ripple carry adder and a modified normalization unit which uses a partitioning technique, enhances the speed of arithmetic unit. The multiplication is performed using a modified array multiplier where the hardware required is reduced, resulting in low power consumption. The FIR filter design is implemented on a FPGA, that resulted in an average speed enhancement of 23.1% and an average power reduction of 20.5% compared with conventional FIR filter.

## VII. REFERENCES

- [1] Nabeel Shirazi, Al Walters, Peter Athanas. "Quantitative Analysis of Floating Point Arithmetic on FPGA based Custom Computing Machines". *IEEE Symposium on FPGAs for Custom Computing Machines*. Apr.1995, pp.155-162.
- [2] Gokhale, Maya, Jonathan Cohen, Yoo, W. Marcus Miller, Arpith Jacob, Craig Ulmer, and Roger Pearce, "Hardware Technologies for High-Performance Data-Intensive Computing." *Computer*, vol. 41, no. 4, pp. 60-68, Apr.2008.
- [3] P.Lapsley, J.Bier, A.Shoham, and E.Lee, "DSP Processor Fundamentals Architectures and Features". *Piscataway, NJ: IEEE Press*, 1997.
- [4] G.K.Yeap, "Practical Low Power VLSI Design", Kluwer Academic Publishers, 1998.
- [5] M. Pedram, "Power minimization in IC Design: Principles and applications," *ACM Transactions on Design Automation of Electronic Systems*, vol.1, pp. 3-56, Jan. 1996.

[6] Shikha jain , Prof. Ravi Koneti and Rita Jain, "Analysis of Fast FIR Algorithms based Area Efficient FIR Digital Filters", *International Journal of Computer Science and Information Technologies*, Vol.5,2014, pp . 4124-4127.

[7] V. Anand Kumar and S. Saranya " Less Overhead High Performance Adder Tree for FIR filter architecture in Speech Processing Applications.", *International Journal of Computer Science and Mobile Computing*, Vol.3 Issue.11, November- 2014, pp. 344-350.

[8] T. Sandhya Pridhini, Diana Alosius, Aarthi Avanthiga and Rubesh Anand , "Design of Multiple Constant Multiplication algorithm for FIR filter ", *International Journal of Computer Science and Mobile Computing*, Vol.3 Issue.3, March- 2014, pp. 438-444.

[9] R. De Mori, "Suggestion for an IC Fast Parallel Multiplier," *Electronics Letters*, vol. 5, pp.50-51, Feb. 1969.

[10] Haibing Hu, Tianjun Jin, Xianmiao Zhang; Zhengyu Lu, Zhaoming Qian, "A Floating point Coprocessor Configured by a FPGA in a Digital Platform Based on Fixed-point DSP for power Electronics" *IEEE 5th conference on Power Electronics and Motion Control Conference*, 2006.

[11] T.K. Callaway and Jr. Swartzlander, "Power delay characteristics of CMOS multipliers," in *Proc.13th Int. Symp. Computer Arithmetic*, pp.26-32, 1997.

[12] Giorgos Dimitrakopoulos, Kostas Galanopoulos, Christos Mavrokefalidis and Dimitris Nikolos," Low-Power Leading-Zero Counting and Anticipation Logic for High-Speed Floating Point Units", *In IEEE Transactions on VLSI Systems*, vol.16, no. 7, pp. 837-850, July 2008.

[13] V.Oklobdzija, 'Comments on leading-zero anticipatory logic for high-speed floating point addition,' *IEEE J. Solid State Circuits*, pp. 292-293, Feb. 1997.

[14] N. Quach and M. Flynn, "Leading one prediction implementation, generation, and application." *Technical Report CSL-TR-91-463 Stanford University*, March 1991.

[15] Zhijun Huang and M.D.Ercegovac, "High-performance left-to-right array multiplier design," in *Proceedings of the 16th IEEE Symposium on Computer Arithmetic*, pp. 4-11. 2003.

[16]. Sneha Manohar Ramteke, Yogeshwar Khandagre, Alok Dubey "Implementation of Low Power Booth's Multiplier by Utilizing Ripple Carry Adder " , *International Journal of Scientific & Engineering Research*, Volume 5, Issue 5, May-2014 , pp. 145-150.

[17]. J.Eiler, A.Ehliar, D.Liu, "Using Low Precision Floating Point Numbers to Reduce Memory Cost for MP3 Decoding," *Proc. IEEE International Workshop on Multimedia Signal Processing*, Siena, Italy, Sep. 2004.

[18]. J. Fridman, Z. Greenfield, "The Tiger SHARC DSP Architecture," *Proc. IEEE* , pp. 66-76, Jan.-Feb. 2000.

[19] J. Hoffman, G. Lacaze, and P. Csillag, "Iterative Logical Network for Parallel Multiplication," *Electronics Letters*, vol. 4, pp. 178, 1968.

[20] M.S.Elrahaa, I.S. Abu-Khater, M.I. Elmasry, "Advanced Low Power Digital Circuits Techniques", Kluwer Academic Publ., 1997.

[21] P. Burton and D.R. Noaks, "High-Speed Iterative Multiplier," *Electronics Letters*, vol. 4, p. 262, 1968.

[22]. IEEE Standard Board, "IEEE Standard for Binary Floating-point Arithmetic," *The Institute for Electrical and Electronics Engineers*, 1985.

[23] M.Jayaprakash, M.Peer Mohamed and Dr.A.Shanmugam "Design and Analysis of Low Power and Area Efficient Multiplier", *International Conference on Electronic Devices Systems and Applications*, 2011.



**SRIKANTH IMMAREDDY**  
Received the Bachelor degree in Electronics and Communication Engineering (ECE) from the JNTU Hyderabad India and Master degree in Digital Systems from Osmania University, India in 2009. He is working as Assistant Professor in ECE Dept at Methodist College of Engineering and Technology, India His main interests are in the fields of Very Large Scale Integration and Digital Signal Processing.



**SRAVANKUMAR TALUSANI**  
Received the Bachelor degree in Electronics and Communication Engineering (ECE) from Osmania University, India and Master degree in Digital Systems & Computer Electronics from JNTU Ananthapur, India. He is working as Assistant Professor in ECE Dept at Methodist College of Engineering and Technology, India His major interests are in the fields of Analog Electronics and Signal Processing.



**RAYAVARAPU PRASADRAO**  
Received the Bachelor degree in Electronics and Communication Engineering (ECE) from Andhra University, India and Master degree from JNTU, Hyderabad. Pursuing Ph.D from Gitam University, India. He is working as Associate Professor in ECE Dept at Avanthi Institute of Engineering and Technology, India. His major interests are in the fields of Digital Electronics.

## **Experimental and Numerical Study of Flow in Prismatic and Non-prismatic Section of a Converging Compound Channel**

**Abinash Mohanta<sup>1</sup>, Bandita Naik<sup>2</sup>, K.C. Patra<sup>3</sup> and K.K. Khatua<sup>4</sup>**

*<sup>1,2,3,4</sup>Department of CIVIL Engg, National Institute of Technology,  
Rourkela, Odisha, India.*

### **Abstract**

Rivers have fascinated engineers and scientists for decades while providing water supply for domestic, irrigation, and industrial consumption or transportation and recreation use. As a result of topography changes along the open channels, designing the converging compound channel is an essential. Water surface prediction is an important task in flood risk management in urban area. In this paper based on the principle of the momentum balance, a one dimensional method is investigated to predict the water surface elevations in non-prismatic compound channels. The numerical method is then applied to calculate water surface elevation in non-prismatic compound channel configurations, the results of calculations show good agreement with the experimental data. In this paper a complete three-dimensional and two phase CFD model for flow distribution in a converging compound channel is investigated. The finite volume method (FVM) with a dynamic Sub grid-scale was carried out for convergence condition. The volume of fluid (VOF) method was used to allow the free-surface to deform freely with the underlying turbulence. The accuracy of the model was analyzed with observed data from experimental studies of a converging compound channel as the qualitative reference and the computed results of the present study were validated. The predicted results for the flow characteristics are in reasonable agreement with the experiment data.

**Keywords:** Experimental model, Numerical model, FVM method, VOF method, prismatic and non prismatic section, converging compound channel.

## 1. Introduction

Prediction of conveyance capacity in open channel flows is complex and requires adequate modeling of flow features such as secondary circulation cells and, specifically for over-bank channels, the momentum exchange that occurs at the main channel/floodplain interface. One of the significant characteristic attributes of flow in an open-channel bend is its secondary flow and therefore the helical motion that is the main reason of the winding river morphology and the tendency to create a succession of shoals and deeps along its way. Due to the existence of secondary flow, flow characteristics in channel bends are much more complicated than those in straight channels. In other words, close to the inner wall and also at the channel bed, pressure gradient exceeds centrifugal force and conveys water in a transverse direction towards the inner wall. At the free surface, centrifugal force drives the flow to the outer wall. This kind of flow is known as the secondary flow (Lien et al., 1999). Super-elevation, secondary flows and their tending to redistribute the mean velocity, permuting the boundary shear stress, bank erosion and shifting, flow separation (that its presence coming together with vortex bar formation decreases the channel width and conveyance capacity), and bed migration in mobile boundary channels have made the study of the non-prismatic open channels of a high interest in the field of river engineering.

A step has been taken to do numerical analysis on a non prismatic compound channel flow .The work will help to simulate the different flow variables in such type of complex flow geometry. Booij (2003) and VanBalen et al. (2008) modeled the flow pattern at a mildly-curved 180° bend and assessed the secondary flow structure using large eddy simulation (LES). Lu et al. (2004), Bodnar and Pihoda (2006) and Omid Seyedashraf, AliAkbar & Milad Khatib Shahidi(2012) applied a three-dimensional numerical model to simulate secondary flows, the distribution of bed shear stress, the longitudinal and transversal changes of water depth and the distribution of velocity components at bend using the standard  $k-\epsilon$  turbulence model. B. K. Gandh, H.K. Verma and Bobby Abraham (2010) determined the velocity profiles in both the directions under different real flow conditions and investigated the effects of bed slope, upstream bend and a convergence / divergence of channel width of velocity profile. Ahmed Kassem; Jasim Imran and Jamil A. Khan analyzed from the three-dimensional modeling of negatively buoyant flow in a diverging channel with a sloping bottom and modified the  $k-\epsilon$  turbulence model for the buoyancy effect. Anthony G. Dixon (2012) simulated CFD software with fluid flow interactions between phases. Other studies have been also conducted by researchers in this area (e.g. Ervine and Jasem (1995), Jasem (1990), James & Brown (1977), Elliott (1990), Bousmar (2002) and Bousmar et al. (2004a) Bahram Rezaei (2006)).

In the present work, an effort has been made to investigate the velocity profiles for prismatic and non-prismatic section of a convergent compound channel by using a commercial computational fluid dynamics(CFD) code, namely FLUENT. The CFD model developed for a real open-channel was first validated by comparing the velocity profile obtained from it with that obtained by actual measurement in the same channel

using preston tube. The CFD model has been the used to analyze the effects of upstream bend, convergence of channel width and bed slope, and to study the variations in velocity profiles along the horizontal and vertical directions.

### 2. Experimental Setup

Experiments was conducted in non-prismatic compound channels with varying cross section built inside a concrete flume measuring 15m×.9m×0.5m at National Institute of Technology Rourkela Hydraulic laboratory. The width ratio of the channel is  $\alpha \leq 1.8$  and the aspect ratio is  $\delta \geq 5$ . The converging angle of the channel is 12.38°. Converging length of the channel is 0.84m. The channel is made up of cement concrete. Water will be supplied through a Centrifugal pumps (15 hp) discharging into a RCC overhead tank. In the downstream end there will be a measuring tank followed by a sump which will feed to over head tank through pumping thus completing recirculation path. Fig.1 shows the schematic diagram of experimental setup and dimensions of channel with test section respectively. Fig.2 shows the plan view of two different experimental sections. Water was supplied to the flume from an underground sump via an overhead tank by centrifugal pump (15 hp) and recirculate to the sump after flowing through the compound channel and a downstream volumetric tank fitted with closure valves for calibration purpose. Water entered the channel bell mouth section via an upstream rectangular notch specifically built to measure discharge in the laboratory channel. An adjustable vertical gate along with flow straighteners was provided in upstream section sufficiently ahead of rectangular notch to reduce turbulence and velocity of approach in the flow near the notch section. At the downstream end another adjustable tail gate was provided to control the flow depth and maintain a uniform flow in the channel. A movable bridge was provided across the flume for both span wise and stream wise movements over the channel area so that each location on the plan of compound converging channel could be accessed for taking measurements. The broad parameters of this channel such as aspect ratio of main channel ( $\delta$ ), width ratio ( $\alpha$ ).

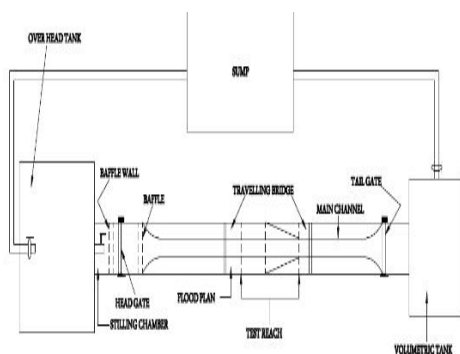


Fig. 1: Plan view of Experimental Set up

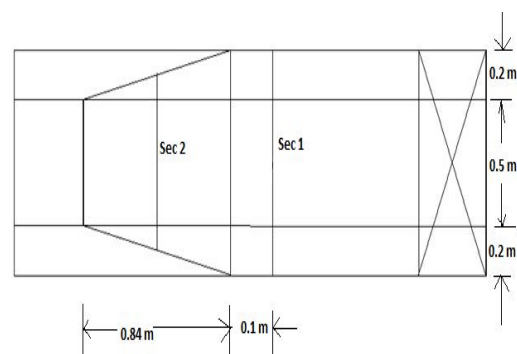


Fig. 2: Plan view of two different experimental section

### 3. Validation of CFD Model

For validation of CFD simulation, the velocity profile across the width of a channel is measured by a preston tube and compared with the numerical results. A long converging water conveying non prismatic channel has been selected for this purpose. The channel width is divided into cells of 0.05 m size for measurement of velocity at the centre of each cell by Preston tube. For CFD simulation, the flow domain is initially discretized with hexahedral elements of face length equals to 0.01 m for analysis. Flow is assumed to be steady, turbulent and three-dimensional. Experimental velocity profile was measured by preston tube and velocity contour was drawn by SURFER and then validated with CFD prediction.

Discharge evaluated from the two velocity profiles using velocity-area integration method are as under:

Discharge from Preston tube measurement data = 0.051 m<sup>3</sup>/s

Discharge from CFD simulation data = 0.063 m<sup>3</sup>/s

### 4. Results and Discussion

Results have been shown to demonstrate the performance of commercial generic CFD package when applied to open channel flows. In cases where the channel geometry is more complex and varies along the channel, the secondary flow is more as a result of the geometry than the turbulence. Thus the usefulness of CFD and applicability of the models for the problem under consideration depends very much upon the type of geometry and particularly on the nature of dominant forces.

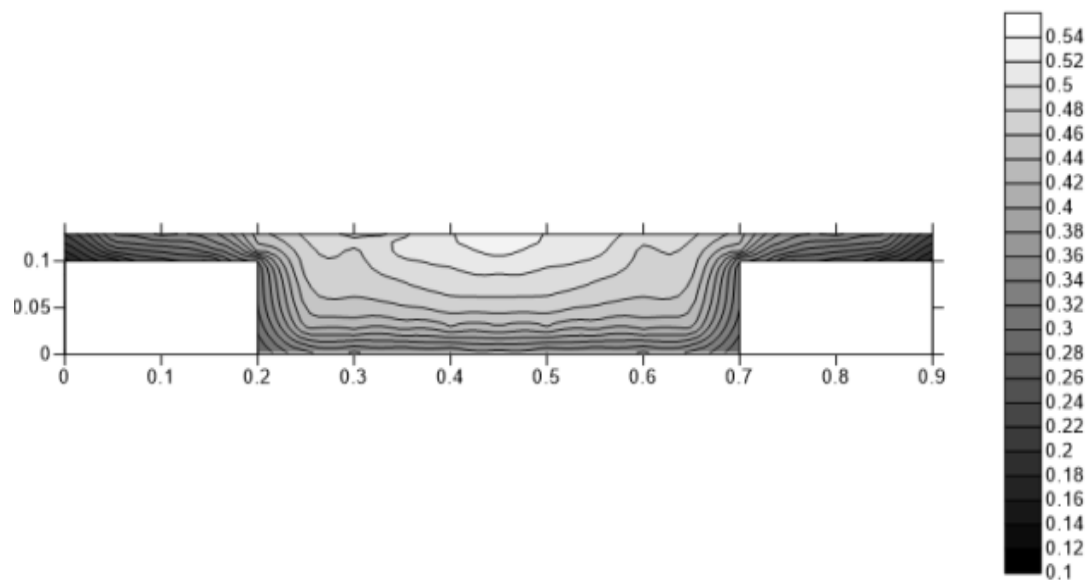


**Fig.3 (a)** Contour of Sec 1 of experimental results.

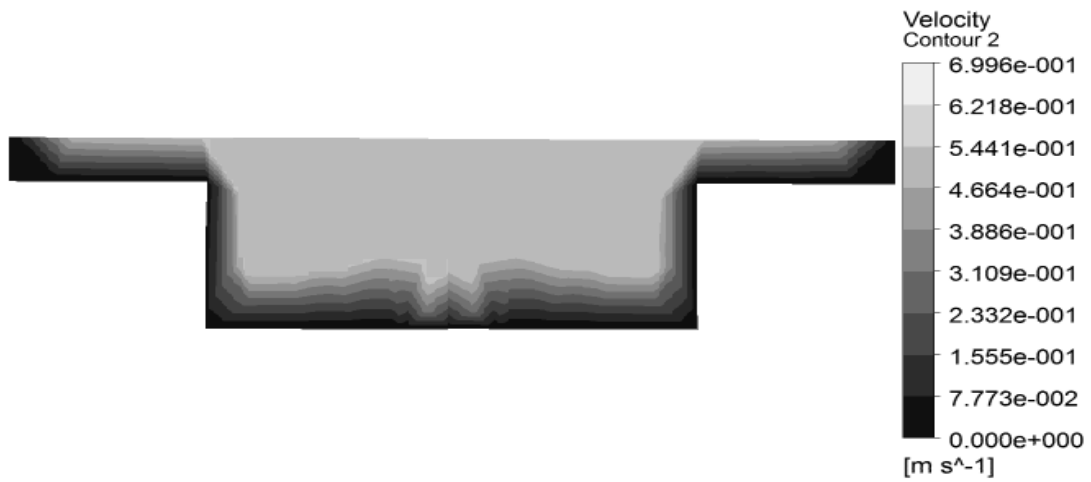


Fig.3 (b) Contour of Sec 1 by CFD simulation.

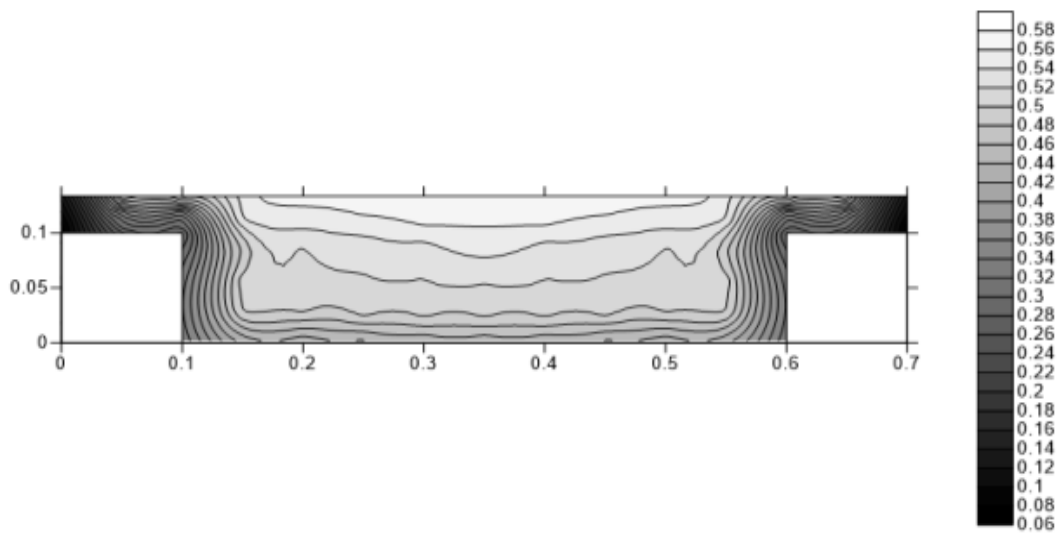


Fig. 4 (a) Contour of Sec 2 of experimental results.

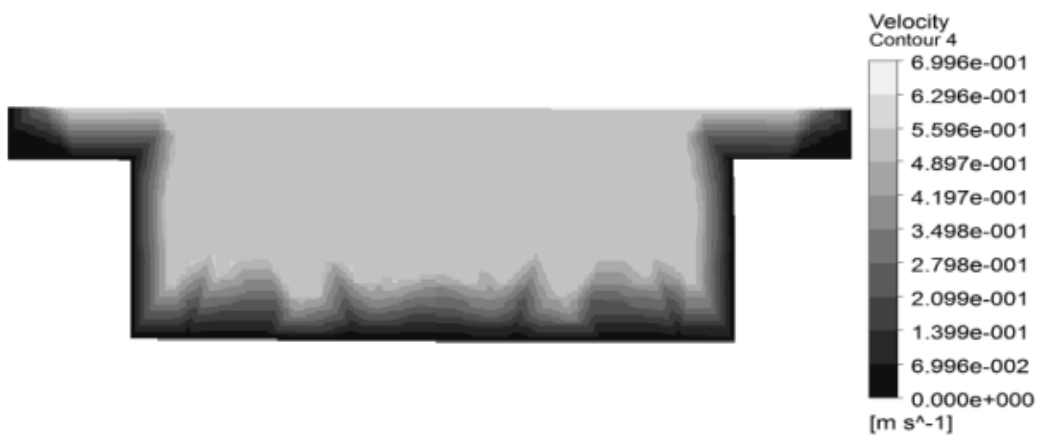
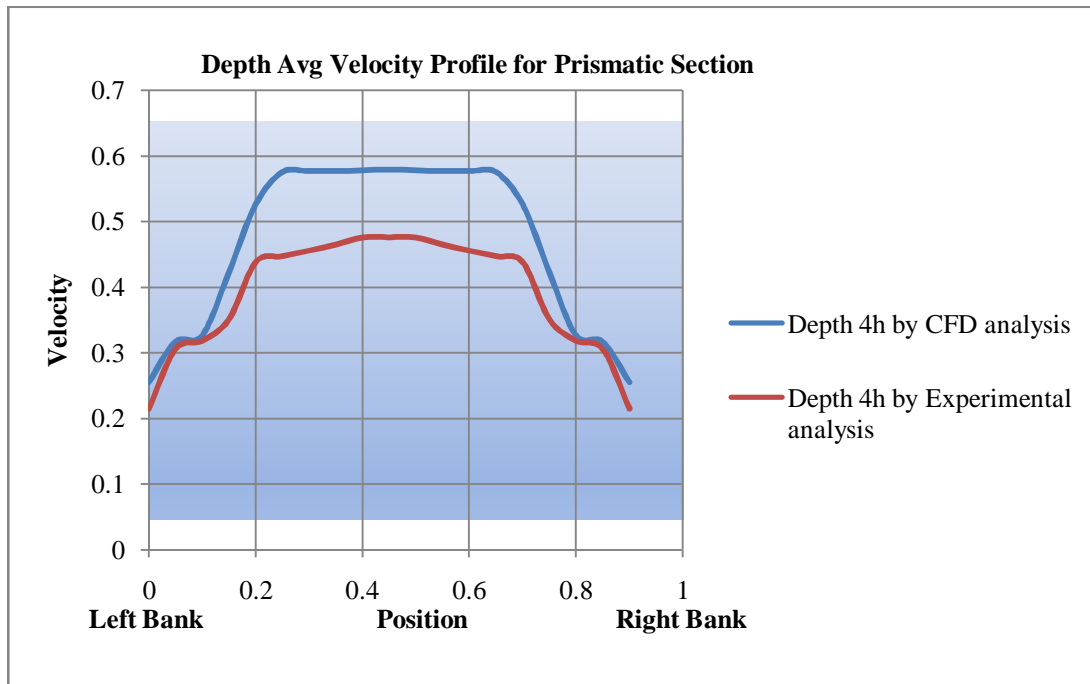
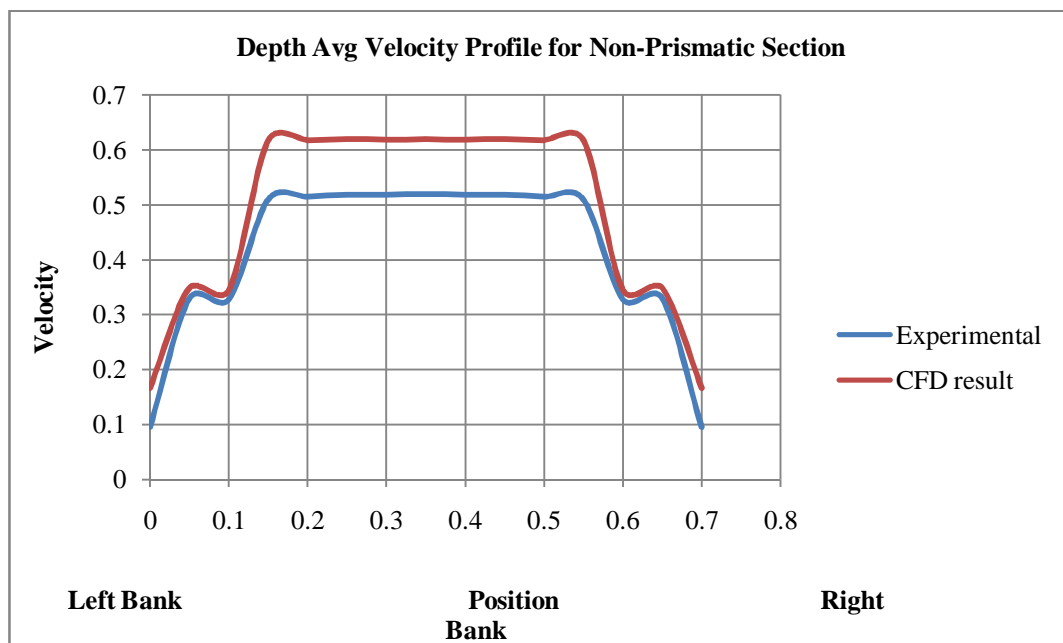


Fig. 4 (b) Contours of sec 2 by CFD simulation.



**Fig. 5:** Depth average velocity profile for sec 1 (by both experimental and Computational results)



**Fig. 6:** Depth average velocity profile for section 2 (by both experimental and Computational results).

## 5. CONCLUSIONS

1. Fig.3 (a) and Fig.4 (a) shows the velocity contours for sec-1 & sec-2 obtained by experimental results. Fig.3 (b) and Fig.4 (b) shows the velocity contours for sec- 1 &2 by Numerical analysis. Fig.5 and Fig.6 shows the both experimental and Computational depth average velocity profile for sec-1 & sec-2. 2. The results show that the CFD predictions accurately predict the velocity and depth average velocity for LES turbulence model.3. In both the cases velocity was over predicted when smooth walls were applied as expected. In this paper the flow velocity profile in non prismatic compound channel has been numerically modeled. The CFD model has been validated by comparing the results with actual measurement carried out with Preston tube.

## References

- [1] ANSYS, Inc. (2010, November), *ANSYS Workbench User's Guide*, Canonsburg, Pennsylvania, United States of America.
- [2] Ahmed Kassem, Jasim Imran, and Jamil A. Khan (2003), Three-Dimensional Modeling of Negatively Buoyant Flow in Diverging Channel, **10.1061/ASCE 0733-9429-2003/129/12936**
- [3] Bakker, A. (2008, February 3), Computational Fluid Dynamics Lectures: *Lecture 14*, Multiphase flow, Retrieved from The Colorful Fluid Mixing Gallery: <http://www.bakker.org/dartmouth06/engs150/>
- [4] Bodnar, T. and Prihoda (2006), Numerical simulation of turbulent free-surface flow in curved channel. *Journal of Flow Turbulent Combust* **76**, 429-442
- [5] Booij (2003), Measurements and large eddy simulation in some curved flumes, *Journal of turbulence- 4*, **8-16**
- [6] Bousmar, D., Wilkin, N., Jacquemart, J.H., Zech, Y., (2004), Overbank flow in symmetrically narrowing floodplains, *J. Hydraul. Eng., ASCE*, **130(4)**, 305-312.
- [7] Bousmar, D., Denis, B. &Zech, Y. (2004), Coherent flow structures in a converging compound channel, *Proc. River Flow 2004 Conference*, Naples, Italy, 1, **423-430**.
- [8] Bousmar, D., and Zech, Y., (2002), Discussion of two-dimensional solution for straight and meandering overbank flows, *J. Hydraul. Eng.*, **128(5)**, 550-551.
- [9] B. K. Gandhi, H.K. Verma and Bobby Abraham(2010)Investigation of Flow Profile in Open Channels using *CFDIGHEM-2010*, **21-23**, AHEC, IIT Roorkee, India
- [10] Ervine, D.A &Jasem, H.K. (1995), Observations on flows in skewed compound channels, *J. Wat. Marit. En. ICE*, **112**, 249-259.
- [11] Fluent Inc. (2006), *FLUENT 6.3 User's Guide*, Lebanon, New Hampshire, United States of America.
- [12] Ferziger, J. H., and Peric, M. (2002), *Computational methods for fluid dynamics*, 3rd Ed., Springer, New York.

- [13] *Gambit 2.2* tutorial guide.
- [14] Knight, D.W. & Shiono, K. (1990), Turbulence measurements in a shear layer region of a compound channel, *J. Hydr. Res., IAHR*, **28(2)**, 175-196.
- [15] Khazaei, M. Mohammadiun (2012), Effect of flow field on open channel properties using numerical investigation and experimental comparison, pp.617-628.
- [16] Lien, H.C., Hsieh, T.Y., Yang, J.C. and Yeh, K.C. (1999), Bend flow simulation using 2D depth-averaged model, *Journal of Hydraulic Engineering-ASCE* **125**, 1097-1108.
- [17] Lu, W.Z, Zhang, W.S, Cui, C.Z. and Leung, A.Y.T. (2004), A numerical analysis of free surface flow in curved open channel with velocity-pressure-free-surface correction, *Computational Mechanics-* **33**, 215-224.
- [18] Omid Seyedashraf, Ali Akbar Akhtari, Milad Khatib Shahidi (2012), Numerical Study of Channel Convergence Effects on Flow Pattern in 90 Degree Bends, *9th International Congress, IUT*, Isfahan, Iran.
- [19] Ramamurthy, A., Han, S., and Biron, P. (2013), Three-Dimensional Simulation Parameters for 90° Open Channel Bend Flows, *Journal of Computing in Civil Engineering-ASCA* **27(3)**, 282-291.
- [20] Rasool Ghobadian, Kamran Mohammadi (2011), Simulation of subcritical flow pattern in 180° uniform and convergent open-channel bends using SSIIM 3-D model, *Water Science and Engineering*, **4(3)** 270-283
- [21] Rezaei, B. (2006), Overbank flow in compound channels with prismatic and non-prismatic floodplains, *PhD Thesis, Univ. of Birmingham*, U.K.

## Flow Analysis for a Converging Compound Channel

**B. Naik, K.K. Khatua, Rahul Sahoo and Shiba Shankar Satapathy**

*Department of Civil Engineering, N.I.T. Rourkela, INDIA.*

### Abstract

In overbank flow, due to interaction mechanism between the main channel and floodplain, the flow properties of the compound sections are greatly affected. The complexity raises more when dealing with a compound channel with converging floodplains. In converging compound channels, due to change in floodplain geometry, there is either severe change of momentum exchanges if the geometry of transition is contraction or expansion. Many investigators have studied and explained the complexity of such compound geometry in predicting the flow variable. In this paper, some experimental results in compound channels with converging floodplains are described and compared. The variations of flow properties for both prismatic and non-prismatic floodplains of different convergence angles are studied and analysed.

**Keywords:** compound channel, converging angle, water surface profile, flow depth, velocity.

### 1. Introduction

Open Channels are classified either Prismatic open channels or non-prismatic channels. The open channels in which shape, size of cross section and slope of the bed remain constant are said to be as the prismatic channels otherwise said to be non-prismatic channels. In non-prismatic compound channels with converging/diverging floodplains, due to continuous change in floodplain geometry along the flow path, the resulting interactions and momentum exchanges is increased. This extra momentum exchange is very important parameter and should be taken into account in the overall flow modelling of a river. As natural river data during flood are very difficult to obtain, research on such a topic is generally done in laboratory flumes. The present study focuses on converging compound channels. In a converging compound channel if the

flood plain is contracted, the flow is forced to leave the flood plains and enter to the main channel because of change in cross section area. New experiments have been conducted at the Hydraulics and Fluid mechanics Laboratory of Civil Engineering Department of NIT, Rourkela to analyse the behaviour of flow effect due to change in flood plain geometry in terms of converging angle.

## 2. Experimental Work

### 2.1 Experimental Setup

Experiments have been conducted in non-prismatic compound channels with varying cross section built inside a concrete flume measuring 15m long  $\times$  9.5m width  $\times$  0.55m depth. The width ratio of the channel is  $\alpha > 1.72$  and the aspect ratio is  $\delta > 5.78$ . The converging angle of the channel is taken as  $12.38^\circ$ . Converging length of the channel is found to be 0.84m. The channel is made up of cement concrete. Water was supplied through a Centrifugal pumps (a 15 hp) discharging into a RCC overhead tank. In the downstream end there lies a measuring tank followed by a sump which feed the water to the overhead tank through pumping.. Water was supplied to the flume from an underground sump via an overhead tank by centrifugal pump (15 hp) and recirculated to the sump after flowing through the compound channel and a downstream volumetric tank fitted with closure valves for calibration purpose. An adjustable vertical gate along with flow straighteners was provided in upstream section sufficiently ahead of rectangular notch to reduce turbulence and velocity of approach in the flow near the notch section. At the downstream end another adjustable tail gate was provided to control the flow depth and maintain a uniform flow in the channel. A movable bridge was provided across the flume for both span wise and stream wise movements over the channel area so that each location on the plan of compound converging channel could be accessed for taking measurements.

Water surface measurements were measured directly with point. The measurements were made each 5mm and 10mm in converging flume of 840 mm length. Point velocities were measured along verticals spread across the main channel and flood plain so as to cover the width of entire cross section. Also at a no. of horizontal layers in each vertical, point velocities were measured. Measurements were thus taken from mid-point of main channel to the left edge of floodplain. The lateral spacing of grid points over which measurements were taken was kept 5cm inside the main channel and the flood plain. Velocity measurements were taken by pitot static tube (outside diameter 4.77mm) and two piezometers fitted inside a transparent fibre block fixed to a wooden board and hung vertically at the edge of flume the ends of which were open to atmosphere at one end and connected to total pressure hole and static hole of pitot tube by long transparent PVC tubes at other ends.. Steady uniform discharge was maintained the run of the experiment and several runs were conducted for overbank flow with relative depth varying between 0.05-0.51. The discharge varied between  $39259.768\text{cm}^3/\text{s}$  to  $146672.3\text{cm}^3/\text{s}$ . Point depth average velocity were made at a depth of  $0.4H$  from the bed in the main channel and  $0.4(H-h)$  on the flood plains.

**Table 1:** Hydraulic parameters for the experimental runs.

Sl. No. of Runs	Discharge Q in cm <sup>3</sup> /s	Overbank depth H in cm	Relative depth $D_r=(H-h)/H$	Froude no.(Fr)	Reynolds no.(R)
1	39259.36	10	0.05	0.677465	34138.57
2	51338.78	11.7	0.19	0.537911	43360.45
3	62014.92	14.02	0.32	0.353251	50402.24
4	92108.59	15.83	0.4	0.259969	72721.13
5	146672.3	19.4	0.51	0.205241	109620.5

After obtaining the point velocities at various grid points representing the whole compound channel flow cross section, velocity contours were drawn. The velocity contours were drawn by normalizing the point velocities with the cross sectional means velocities for the respective overbank depth of flow

### 3. Result and Discussion

The new experimental results from non-prismatic compound channels are presented in this section. Velocity contour of prismatic non prismatic section are shown in **Fig1(a,b)**The stage discharge curve at experimental section-1&2 was plotted and shown in **Fig 2(a&b)** . The water surface profile of different relative depth are shown in **Fig 3(a)**.The depth average velocity of different converging part of relative depth of 0.5 are shown in the **Fig 4(a,b,c)**.. The boundary shear stress of different converging part of relative depth of 0.5 are shown in the **Fig 5(a,b,c)**.

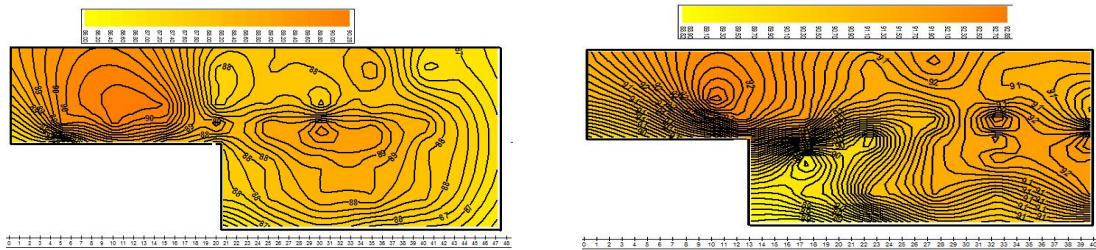


**Fig. 1:** (a)Velocity contour of sec-1 (b)Velocity contour of sec-2

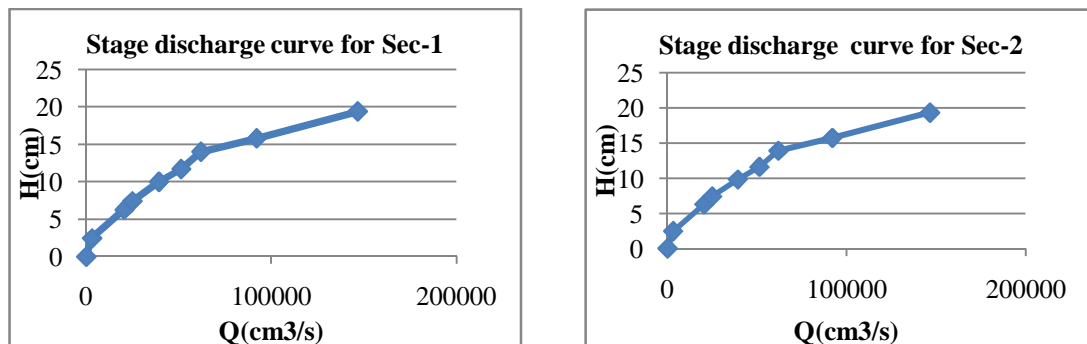


**Fig. 2:** (a,b)Stage discharge curve for Prismatic and Non prismatic section.

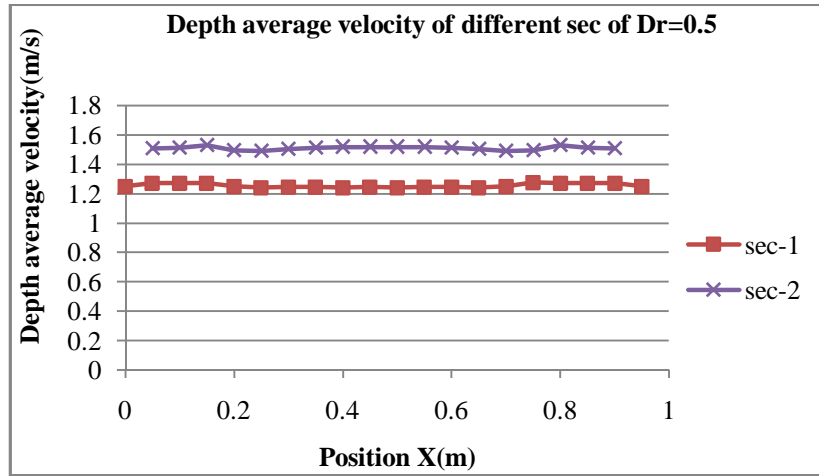
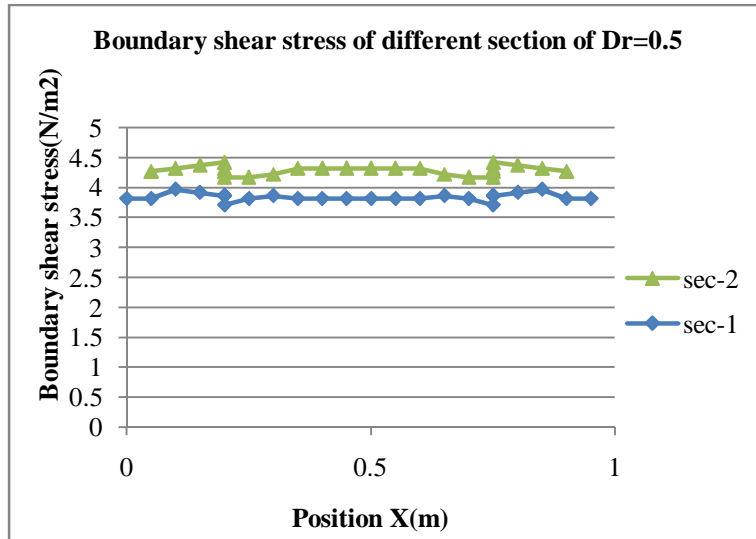


Fig. 3: (a) shows the Depth average velocity.



(b) shows the boundary shear of Prismatic and Non prismatic section

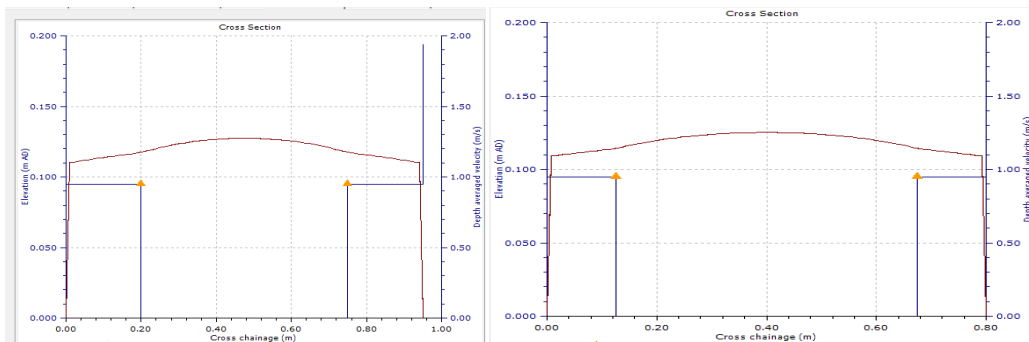
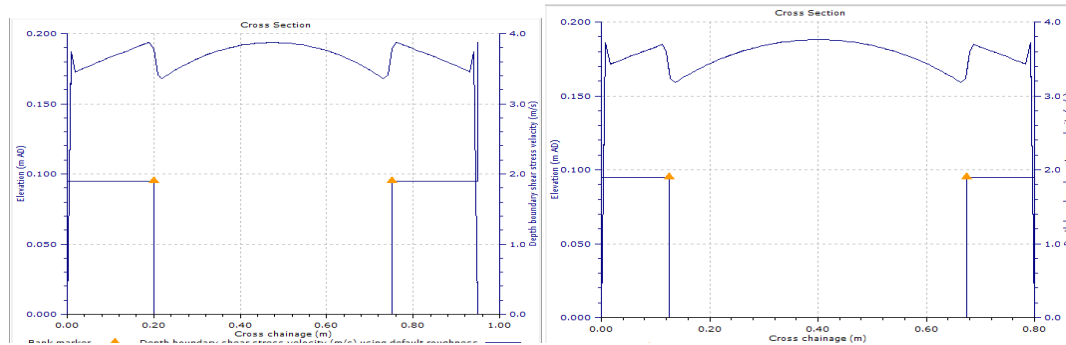


Fig. 4: (a) Depth average velocity of sec-1 (b) Depth average velocity of sec-2 by CES



**Fig. 5:** (a) Boundary shear stress of sec-1 (b) Boundary shear stress of sec-2 by CES

#### 4. Conclusions

1. Experiments are conducted to study the effect of flow variables for converging and non-converging compound channels.
2. From the Velocity contours of the experimental channels, it is seen that at section 1 the higher velocity contours occur both at the middle of flood plain and interface of main channel. At section 2 the occurrence of higher magnitude velocity contours happens same for floodplain however in the main channel region it is again at central region.
3. From the stage discharge curve it is seen that non of the methods is good agreement with the actual stage discharge.
4. From the water surface profile curve it is seen that the depth of flow start decreases from mid section of the converging part. It is clearly distinguish at higher relative depth
5. From the depth average velocity curve and boundary shear stress curve it is seen that both increases along the narrowing part of the flume.
6. In CES also the depth average velocity and boundary shear stress increase along the narrow part of the flume.

#### References

- [1] Ackers P. (1993). "Stage–discharge functions for two-stage channels" the impact of new researches. *Inst Water Environ Manage*, 7, pp.52–61
- [2] Bousmar, D., and Zech, Y., (1999). "Momentum transfer for practical flow computation in compound channel" *J. Hydraul. Eng.*, 125(7), 696-706.
- [3] Bousmar, D., and Zech, Y., (2002). "Discussion of two-dimensional solution for straight and meandering overbank flows." *J. Hydraul. Eng.*, 128(5), 550-551.
- [4] Bousmar, D., Wilkin, N., Jacquemart, J.H., Zech, Y., (2004). "Overbank flow in symmetrically narrowing floodplains." *J. Hydraul. Eng.*, ASCE, 130(4), 305-312.

- [5] Chow VT. (1959). "Open- channel hydraulics". New York: Mc. Graw-Hill Book Co, .Hydraul. Eng., 137(8), 815-824
- [6] Elliott, S.C.A & Sellin, R.H.J. 1990. "SERC floo channel facility: skewed flow experiments", J. Hydr. Res., IAHR, 28(2), 197-214
- [7] James, M. & Brown, B.J. 1977. Geometric parameters that influence floodplain flow, Report WES-RR-H-77-1, USACE, Vicksburg, USA.
- [8] Knight, D.W., and Hamed, M.E., (1984), "Boundary Shear in Symmetrical Compound Channels", Journal of the Hydr. Eng., ASCE, Vol.110, No.HY10, Paper 19217, pp.1412-1430.
- [9] Khatua K.K, Patra K.C, and Mohanty P.K. (2012). "Stage-Discharge Prediction for Straight and Smooth Compound Channels with Wide Floodplains" J. Hydr. Engg, ASCE
- [10] Rezaei, B. (2006). "Overbank flow in compound channels with prismatic and non-prismatic floodplains." PhD Thesis, Univ. of Birmingham, U.K.
- [11] Rezaei, B., and Knight, D.W., (2009). "Application of the Shiono and Knight Method in compound channel with non-prismatic floodplains" J. Hydraul. Research. 47 (6), 716-726.
- [12] Rezaei, B., and Knight, D.W., (2011). "Overbank flow in compound channels with non-prismatic floodplains" J. Hydraul. Research
- [13] Sellin, R.H.J., (1964), "A Laboratory Investigation into the Interaction between Flow in the Channel of a River and that of its Flood Plain", La Houille Blanche, No.7, pp.793-801.
- [14] Wormleaton, and Hadjipanous, P., (1985), "Flow Distribution in Compound Channels", Journal of the Hydr. Engg., ASCE, Vol.111, No.7, pp. 1099-1104.

the cross-over (around 9% of the total shear force). Then the value goes on increasing towards the next bend apex. Similarly as seen in figure 7, at the outer wall, the shear force carried by the bend apex is less (about 8% of the total shear force) which first slightly decreases and then increases to reach maximum value at the cross-over (about 11% of the total shear force). On moving from the cross-over, the shear force at the outer wall starts decreasing and then somewhat increases towards the other bend apex. From figure 6, it is observed that there is a significant difference in the shear force sharing among the inner and outer walls of all the reaches. But, there is less variation among the inner and outer walls of the cross-over section G. Figure 6 demonstrates that the shear force carried by the bed of the channel throughout the meander path is found to remain more or less constant. The bed is observed to carry about 80% of the total shear force while the rest is being shared by the inner and outer walls.

#### 4. CONCLUSIONS

The following conclusions can be presented in this work

1. The present research work is providing information for getting shear stress variation of a meandering channel of sinuosity more than 4.
2. An experimental investigation has been carried out to measure the boundary shear stress and shear force distribution along the bed and the side slopes of a highly meandering compound channel at different reaches along the meander path.
3. From the results of shear stress measurements it is found that the shear stress at the inner wall always remains higher as compared to that at the outer wall. The boundary shear stress distribution is prominent in the bend apex section while the difference gradually decreases on travelling from the bend apex to the cross-over. Boundary shear stress distribution at the cross-over section is found to be more or less uniform throughout.
4. The shear force carried by the inner wall is found to decrease up to the cross-over section and then goes on increasing. The shear force at the inner wall is also found to always remain higher than the shear force at the outer wall. The shear force carried by the bed of the all the channel section is found to be nearly uniform throughout the meander path.
5. From the shear force distribution results, the sharing among the inner and outer walls is not uniform at all reaches along the meander path. Whereas there is very less variation between the shear force sharing at inner and outer walls at the cross-over section.
6. The above observation can be applied in the study of hydraulic problems such as channel design, channel migration, interaction losses, erosion and depositional pattern study of a meandering channel. Bed shear forces which are useful for the study of bed load transfer and wall shear forces which represent a general view of channel migration pattern can be analysed.

#### 5. ACKNOWLEDGEMENTS

The authors wish to acknowledge thankfully the support received by the fourth author from DST India, under grant no.

SR/S3/MERC/066/2008 for conducting experimental research works.

#### REFERENCES:

- i. Khatua, K. K. (2008), "Interaction of flow and estimation of discharge in two stage meandering compound channels". Thesis Presented to the National Institute of Technology, Rourkela, in partial fulfilment of the requirements for the Degree of Doctor of philosophy.
- ii. Khatua, K.K. and Patra, K.C. (2010). Evaluation of boundary shear distribution in a meandering channel. Proceedings of ninth International Conference on Hydro-Science and Engineering, IIT Madras, Chennai, India, ICHE 2010, 74.
- iii. Knight, D. W. (1981). "Boundary shear in smooth and rough channels." *J. Hydraul. Div., Am. Soc. Civ. Eng., 107(7)*, 839–851.
- iv. Knight D. W. and Demetriou J.D. (1983). "Floodplain and main channel flow interaction." *J. Hydraul. Eng., ASCE, 109(8)*, 1073–92.
- v. Knight, D.W., Yuan, Y.M., and Fares, Y.R. (1992). "Boundary shear in meandering channels." Proceedings of the Institution Symposium on Hydraulic research in nature and laboratory, Wuhan, China (1992) Paper No.11017, Vol. 118, Sept., pp. 151-159.
- vi. Patel, V.C. (1965). "Calibration of the Preston tube and limitations on its use in pressure gradients." *Journal of Fluid Mechanics, 23(01)*, 185-208.
- vii. Patra, K.C, and Kar, S. K. (2000). "Flow Interaction of Meandering River with Floodplains". *Journal of Hydr. Engrg., ASCE, 126(8)*, 593–604.
- viii. Pradhan, A. (2014). "Analysis of Flow along the Meander Path of Highly Sinuous Rigid Channel". Thesis Presented to the National Institute of Technology, Rourkela, in partial fulfilment of the requirements for the Degree of Master of Technology.
- ix. Preston, J. (1954). "The determination of turbulent skin friction by means of Pitot tubes." *Journal of the Royal Aeronautical Society, 58(518)*, 109-121.
- x. Rajaratnam, N., and Ahmadi, R.M. (1979). "Interaction between Main Channel and Flood Plain Flows." *Journal of Hydraulic Division, ASCE, Vol..105, No. HY5, pp. 573-588.*

#### Effect Of Cylindrical Staggered Vegetation On Roughness Prediction In An Open Channel

K. Panigrahi<sup>1</sup> K.K.Khatua<sup>2</sup> B. Naik<sup>3</sup>

<sup>1</sup>M.Tech (Research), Department of Civil Engineering, N.I.T. Rourkela, 769008, India

<sup>2</sup>Associate Professor, Department of Civil Engineering, N.I.T. Rourkela, 769008, India

<sup>3</sup>Ph. D. (scholar), Department of Civil Engineering, N.I.T. Rourkela, 769008, India

Email: [kajalpanigrahi@yahoo.in](mailto:kajalpanigrahi@yahoo.in)

**ABSTRACT:** A laboratory study to explore the effect of vegetation in terms of rigid cylindrical roughness on the hydraulics of flow in an open channel is presented. The study consists of flume experiments for flows with unsubmerged rigid cylindrical stems of a concentration and diameter arranged in a regular staggered configuration. Vegetation in an open channel retards the flow of water by causing a loss of energy through turbulence and by exerting additional drag

*forces on the moving liquid. Because of this complex nature, it is difficult to develop a flow model. Vertical profile of longitudinal velocity in vegetated channels reflects complex mechanics of flow vegetation interactions and determines the bulk flow velocity and flow rate. Velocity coefficient is found to vary with the non-dimensional hydraulic, geometric and surface parameters such relative depth ratio of water depth  $h$  to stem height  $h_s$ , Reynolds's number ( $Re$ ) and Froude's number ( $Fr$ ) etc. Parameters determining the velocity distribution are discussed and results are summarised and presented. Graphs of velocity vs. hydraulic parameters are presented. In addition, vegetation characteristics were shown to influence the height of maximum velocity.*

**Key Words:** *Vegetative channel, cylindrical roughness, Manning's coefficient, Reynolds's number ( $Re$ ) and Froude's number ( $Fr$ ), Relative depth.*

## 1. INTRODUCTION

The establishment of a satisfactory waterway for handling runoff from agricultural area is probably the most difficult problem encountered by the farmers in planning an economical and effective conservation system. While vegetated waterways have long been employed for terrace outlets, very little uses until recent years have been made of grasses in artificial waterways, but dependence has been placed more on the mechanical structures. So need for research of design of effective vegetated waterways is imminent. Design of effective vegetated waterways needs that various hydraulic characteristics of vegetated channels be studied. The most important hydraulic characteristic is the retardance coefficient mainly called as Manning's  $n$ . The retardance coefficient varies from vegetation to vegetation and also for the same vegetation it varies according to the stage of growth, depth of submergence etc. So effective design of grassed waterways needs a closely approximate value of retardance coefficient to be determined. If we underestimate the value of the roughness coefficient ( $n$ ) then the canal section will be over designed as the low value of  $n$  will lead to high velocity and hence to high discharge capacity of the channel. Similarly if we overestimate the value of the retardance coefficient and use this value in design problems then we underestimate the discharge. The excess discharge therefore frequently spoils the downstream areas of channel by overtopping. This clearly indicates that the retardance coefficient of the grasses used for channel need to be determined before this value is used for the design purposes.

Vegetation in an open channel retards the flow of water by causing a loss of energy through turbulence and by exerting additional drag forces on the moving liquid. Because of this complex nature, it is difficult to develop a flow model. The scope of the present work includes determination of the various hydraulic characteristics i.e. resistance offered to the flow by the vegetation, protection offered by the channel bed and effect of the vegetation on the flow characteristics in the channel. In addition to the above mentioned points, other aspects like velocity distribution relations, Froude's number and Reynolds's number calculation and design of grass-lined channels are studied.

The degree of influence in a vegetative channel further depends on the other vegetation characteristics such as (a) vegetation species, (b) distribution, (c) flexibility, (d) degree of submergence and (e) the vegetation density (Abood et al. 2006). In a vegetative open channel flow, the average water velocity in the cross section tends to decrease at a higher rate, due to flow resistance from the stems and leaves of the vegetation which generally increases roughness of surfaces (Fishenich 2000). For calculating flow velocity, Manning's formula is generally used. It is also widely used in vegetated waterways to solve in related hydraulic applications. The formula states:

$$V = \frac{K}{n} R_h^{2/3} S^{1/2} \quad (1)$$

Where,  $V$  is the cross-sectional average velocity ( $L/T$ ; m/s);  $K$  is a conversion factor of ( $L^{1/3}/T$ ),  $1 \text{ m}^{1/3}/\text{s}$  for SI unit);  $n$  is the Gauckler–Manning coefficient (frequently called as Manning's roughness coefficient);  $R_h$  is the hydraulic radius ( $L$ ;  $m$ ) which is the ratio of cross sectional area of flow to wetted perimeter and  $S$  is the slope of the hydraulic grade line ( $= h_f/L$ ), which is the same as the channel bed slope when the water depth is constant and  $h_f$  is called difference of hydraulic head across a cross section of channel of length  $L$ . Manning's roughness coefficient is found to vary largely in a vegetated waterway. It depends on depth of flow in the channel and slope of the channel; when the slope of the channel increases, roughness coefficients decreases (Diaz 2005).

The present study focuses on straight simple vegetated rectangular channel. New experiments have been conducted at the Hydraulics and Fluid mechanics Laboratory of Civil Engineering Department of National Institute of Technology, Rourkela to analyse the behaviour of flow effect due to rigid cylindrical vegetation.

## 2. MATERIALS AND METHODS

### 2.1 Experimental Setup

Experiments have been conducted in a straight simple rectangular channel with varying cross section built inside a metallic flume measuring 12 m long  $\times$  .60 m width  $\times$  0.45 m depth and the aspect ratio is  $\delta > 5.00$ . Water was supplied through a centrifugal pump (a 15 hp) discharging into a RCC overhead tank. In the downstream end there lies a measuring tank followed by a sump which feed the water to the overhead tank through pumping. Water was supplied to the flume from an underground sump via an overhead tank by centrifugal pump (15 hp) and recirculated to the sump after flowing through the experimental channel and a downstream volumetric tank fitted with closure valves for calibration purpose. An adjustable vertical gate along with flow straighteners was provided in upstream section sufficiently ahead to reduce turbulence and velocity of approach in the flow near the initial section. At the downstream end another adjustable tail gate was provided to control the flow depth and maintain a uniform flow in the channel. A movable bridge was provided across the flume for both span wise and stream wise movements over the channel area so that each location on the plan of the experimental channel could be accessed for taking

measurements. The whole channel was fabricated by using 19 mm thick water resistant ply wood in the bed. Iron rods of diameter 6.5 mm, each raised to a height of 10 cm were pre-drilled into the plywood in a staggered pattern with spacing of 10 cm. Section of study with vegetation was limited to 6 m. Figure 1 represents the view of the experimental channel. Point velocities were measured along verticals spread across the main channel so as to cover the width of entire cross section. Also at a number of horizontal layers in each vertical, point velocities were measured. Measurements were thus taken from mid-point of main channel to the left edge of the channel boundary. The lateral spacing of grid points over which After obtaining the point velocities at various grid points representing the cross section of whole rectangular channel flow, velocity contours were drawn. The velocity contours were drawn by normalizing the point velocities with the cross sectional means velocities for the respective overbank depth of flow.

**Table-1:** Hydraulic parameters for the experimental runs

Sl. no. of Runs	Discharge Q in m <sup>3</sup> /s	Depth H in m	Manning's n	Froude no. (Fr)	Reynolds' s no. (Re)
1	0.002345	0.017	0.021	0.648	3695.83
2	0.00287	0.018	0.022	0.622	4517.08
3	0.003638	0.021	0.024	0.618	5661.44
4	0.005287	0.029	0.025	0.563	8029.79
5	0.007255	0.033	0.026	0.548	10864.35
6	0.007898	0.041	0.029	0.504	11576.96
7	0.009327	0.051	0.035	0.430	13285.61
8	0.010264	0.060	0.042	0.363	14219.52
9	0.010711	0.067	0.048	0.322	14561.58
10	0.011206	0.075	0.054	0.288	14925.72

The new experimental results from rectangular vegetated channel are presented in this section. Velocity contours of cross sections without vegetation are shown in figure 2(a,b). From the figure it is seen that both at sections 2 and 4 the higher velocity contours occur at central region. The Stage-Discharge curve of the straight vegetated channel was plotted and shown in figure 3. Five cross sections are taken for the detail study purpose. Sections 1 and 5 are having 4 vegetations, section 3 consists of 5 vegetations, sections 2 and 4 do not consist of vegetation. The depth average velocity curves of two cross sections without vegetation (section-2 and section-4) and with vegetation (section-1, section-3 and section-5) of the experimental channel

measurements were taken was kept 5 cm inside the main channel. Velocity measurements were taken by pitot static tube (outside diameter 4.77 mm) and two piezometers fitted inside a transparent fibre block fixed to a wooden board, hung vertically at the edge of flume. The ends were open to atmosphere at one side and connected to total pressure hole and static hole of pitot tube by long transparent PVC tubes at other side. Steady uniform discharge was maintained during the running of the experiment and several runs were conducted. The discharge varied between 0.002345 m<sup>3</sup>/s to 0.013564 m<sup>3</sup>/s. Point depth average velocity were made at a depth of 0.4H from the bed in the main channel

11	0.012636	0.091	0.064	0.243	16142.68
12	0.013171	0.095	0.065	0.237	16654.79
13	0.013564	0.103	0.072	0.217	16812.13



are shown in the figure 4(a,b,c,d and e). From the figure it is seen that the vegetated cross sections are observed to have higher depth average velocities when compared to the cross sections without any cross sections in agreement with the depth average velocity curves. The curves of non-dimensional parameter i.e. Inverse Aspect Ratio Vs. Froude's Number, Reynolds's Number, Manning's n are shown in Figure 5(a,b and c) respectively. From the figure it is seen that the Froude's Number decreases as the Inverse Aspect Ratio increases while the Reynolds's Number increases alongwith the increase in Inverse Aspect Ratio. Again Manning's n is also seen to be rising according to the rise in Inverse Aspect Ratio.

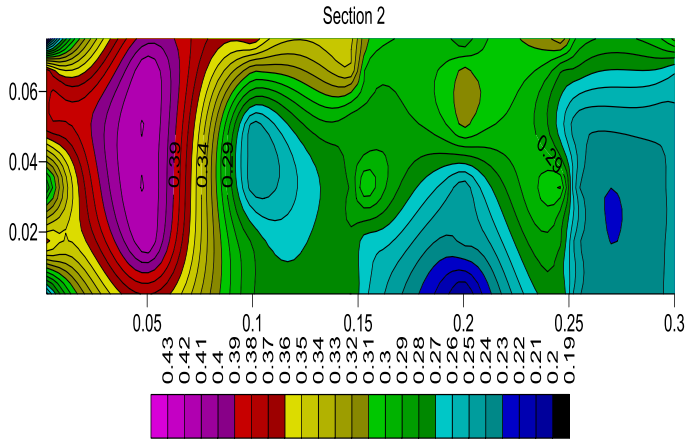


Figure-2(a): Velocity contour of section-2

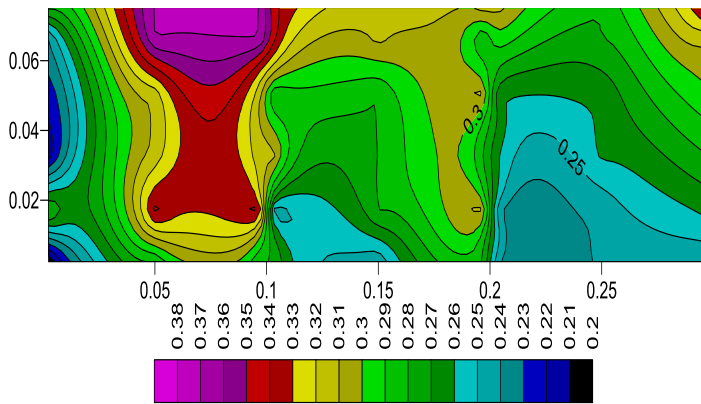


Figure-2(b): Velocity contour of section-4

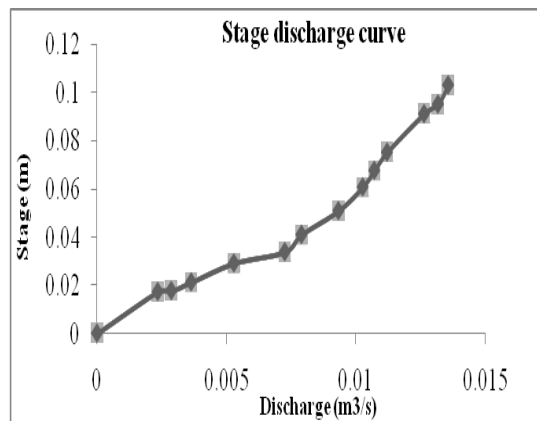


Figure-3: Stage-Discharge curve for the vegetated channel

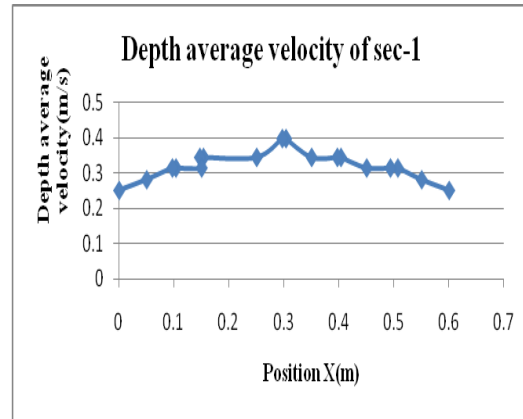


Figure-4(a): Depth average velocity curve of section-1 with 4 vegetations

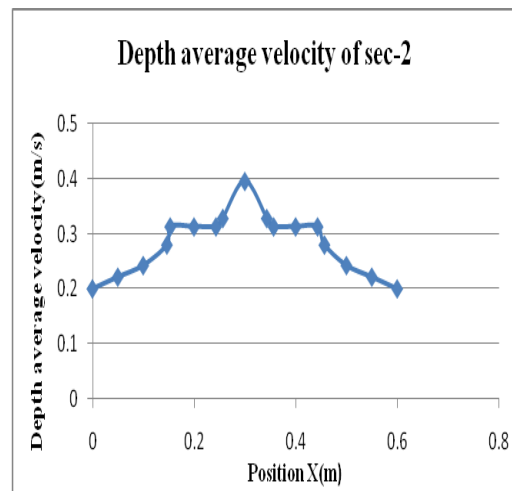


Figure-4(b): Depth average velocity of section-2 without vegetation

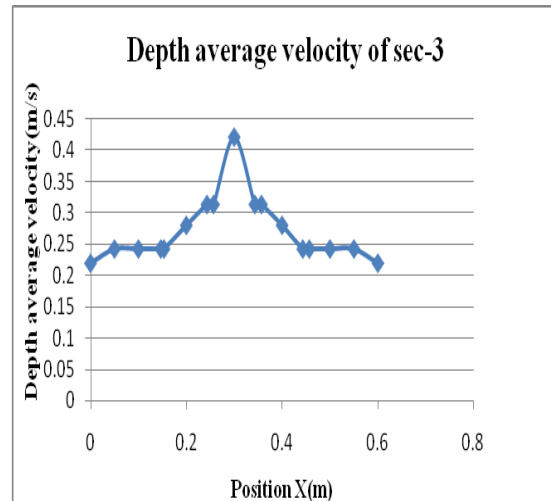


Figure-4(c): Depth average velocity curve of section-3 with 5 vegetations

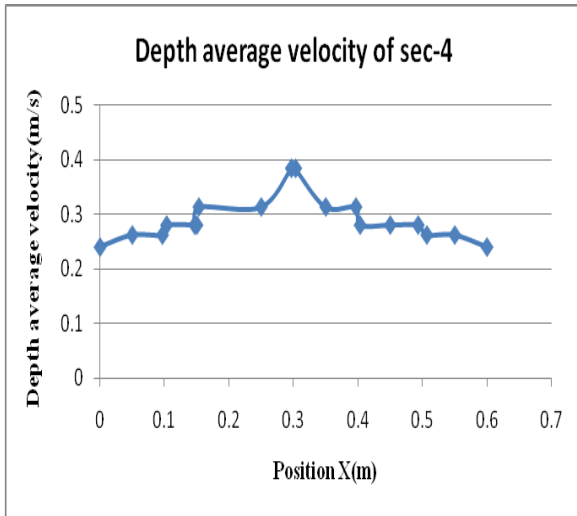


Figure-4(d): Depth average velocity curve of section-4 without vegetation

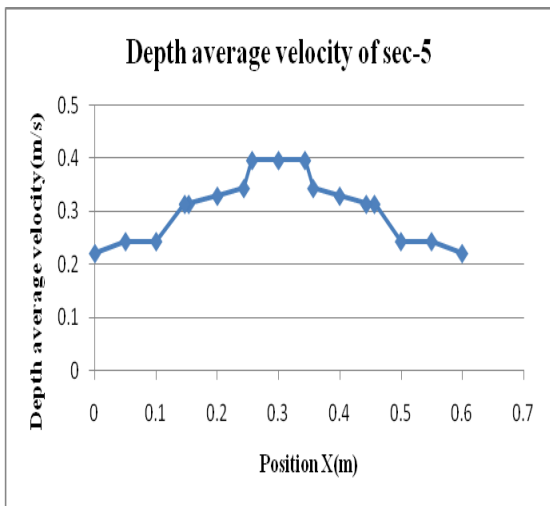


Figure-4(e): Depth average velocity curve of section-5 with 4 vegetations

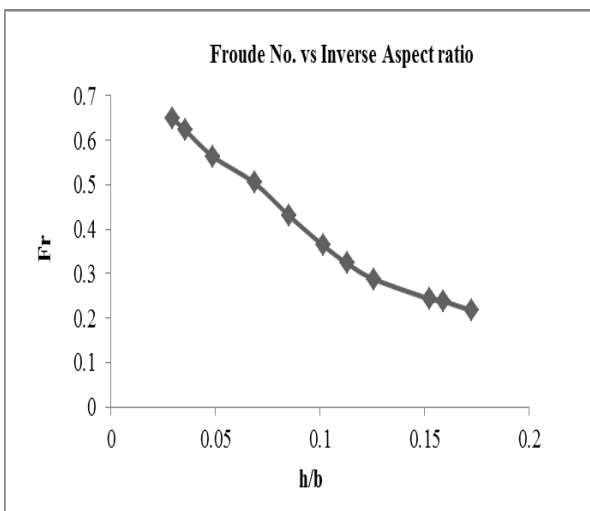


Figure-5(a): Froude's Number vs Inverse Aspect Ratio

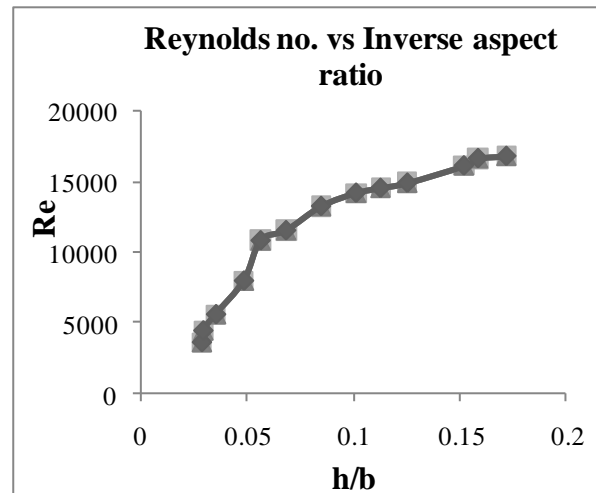


Figure-5(b): Reynolds's Number vs Inverse Aspect Ratio

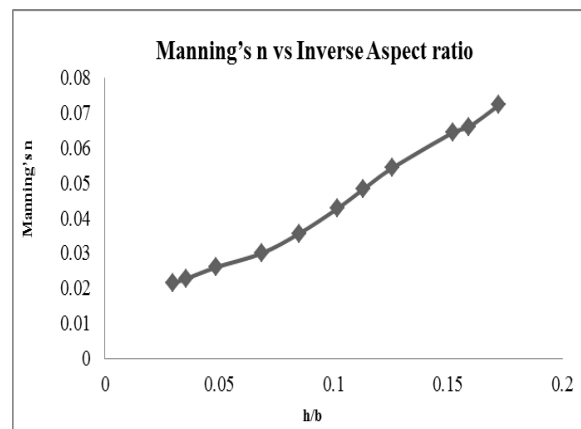


Figure-5(c): Reynolds's Number vs Inverse Aspect Ratio

#### 4. CONCLUSIONS

Experiments are conducted to study the effect of flow variables for simple straight rectangular channel with rigid cylindrical vegetation arranged in a staggered pattern. From the velocity contours of the experimental channels, it is seen that both at sections 2 and 4 the higher velocity contours occur at central region. The vegetated cross sections are observed to have higher depth average velocities when compared to the cross sections without any cross sections in agreement with the depth average velocity curves. The nature of the Froude's Number and the Reynolds's Number are found to be exactly opposite when plotted against Inverse Aspect Ratio. The Froude's Number decreases as the Inverse Aspect Ratio increases while the Reynolds's Number increases alongwith the increase in Inverse Aspect Ratio. Again Manning's n is also seen to be rising according to the rise in Inverse Aspect Ratio.

## 5. REFERENCES

- i. B. Panigrahi, "Hydraulic Characteristics of Grass-Lined Channel," Unpublished M. Engineering. Thesis, Asian Institute of Technology, Bangkok, Thailand, Dec. 1987.
- ii. B. Panigrahi, B.P. Behera and S.D. Sharma, "Retardance coefficients for flow in vegetated waterways," *J. of Indian Water Resources Society*, Vol. 13, pp. 206-211, 1993
- iii. E. Žic1, M. Vranješ, N. Ožanič1 "Methods of roughness coefficient determination in natural riverbeds," in *International symposium on water management and hydraulic engineering*, 2009, Paper: A01.
- iv. E.Žic, "The roughness coefficient analysis on the example of Butoniga river bed in Istria," master's thesis in the making, Rijeka 2008
- v. F.C. Wu, H.W. Shen and Y.J. Chou, "Variation of roughness coefficient for un-submerged and submerged vegetation," *J. of Hydraulics Engineering*, ASCE, Vol. 125(9), pp. 934-942, 1999.
- vi. F. Maghdam and N. Kouwen, "Non-rigid, non-submerged vegetation roughness on flood plains," *J. of Hydraulics Engineering*, ASCE, Vol. 123(1), pp. 51-56, 1997.
- vii. J.C. Fishenich, "Resistance due to vegetation," *EMRRP Technical Notes Collection (ERDC TN-EMRRP-SR-07)*, U.S. Army Engineer Research and Development Center, Vicksburg, MS, p. 9., 2000.
- viii. K.V.N.Sharma and S.R. Sasikantah, "Evaluation of Manning's n for steady and non-uniform flow," in *Proc. Second Australian Conference on Hydraulics and Fluid Mechanics*, 1965 pp. A177-A187.
- ix. M. Rightetii and A. Armanini, "Flow resistance in open channel flows with sparsely distribution bushes," *J. of Hydrology*, Vol (269), pp. 55-64, 2002.
- x. M.M. Abood, B. Yusuf, T.A. Mohammed and A.H. Ghazali, "Manning Roughness Coefficient for Grass-Lined Channel," *Suranaree J. Sci. Technol.*, Vol.13(4), pp. 317-330, 2006.
- xi. M.W. Abdelsalam, F.A. Khattab, A.A. Khalifa and F.M. Bakry, "Flow capacity through wide and submerged vegetation channels," *J. of Irrigation and Drainage*, ASCE, Vol. 150(5), pp. 25-44, 1992.
- xii. M.A. Sadeghi, M.S. Bajestan and M. Saneie, "Experimental investigation on flow velocity variation in compound channel with son-submerged rigid vegetation in floodplain," *World Applied Sciences J.*, Vol. 9 (5): 489-493, 2010.
- xiii. N. Kouwen and R.M. Li, "Biomechanics of vegetative channel linings," *J. of Hydraulic Division*, ASCE, Vol. 106 (HY 6), pp. 1085-1103, 1980.
- xiv. N. Kouwen and E.T. Unny, "Flexible roughness in open channels," *J. of Hydraulics Division*, ASCE, Vol. 99(5), pp.713-729, 1973.
- xv. N. Kouwen, "Effect of riparian vegetation on flow resistance and flood potential discussion," *J. of Hydraulic Engineering ASCE*, Vol. 126 (12), pp. 954, 2004.
- xvi. R.G. Diaz, "Analysis of Manning coefficient for small-depth flows on vegetated beds," *Hydrological Processes*, Vol. 19, pp. 3221-3233, 2005.
- xvii. R.N. Fenzl and J.R.Davis, "Hydraulic resistance relationships for surface flows in vegetated channels," *Trans. of the ASAE*, vol. 7(1), pp. 46-51 and pp.55, 1964.
- xviii. R. Li and H.W. Shen, "Effect of tall vegetation on flow and sediment," *J. of the Hydraulic Division*, ASCE, Vol. 99 (HY 5), pp. 793-813, 1973.
- xix. S. Petryk and G. Bosmajian III, "Analysis of flow through vegetation," *J. of the Hydraulic Division*, Proc. ASCE, 1975, Vol. 101, (HY 7), pp. 871-884.
- xx. S.F. Shih and G.S. Rahi, "Seasonal variations of Manning's roughness coefficient in subtropical marsh," *Trans. of ASAE*, Vol. 25(1), pp. 116-119, 1982.
- xxi. T.Murota, M.Fukuhara, "Sato: Turbulence structure in vegetated open channel flows," *J. of Hydro science and Hydraulic Engineering*, Vol. 2 (1), pp. 47-61, 1984.

xxii.

xxiii.

## An Improved Approach for Flow Prediction in Compound Open Channel Flow of Uniform Roughness Pradhan Siprarani<sup>1</sup>Khatua Kishanjit K. <sup>2</sup>

<sup>1</sup>Ph.D. Research Scholar Department of Civil Engineering,  
N.I.T. Rourkela, India

<sup>2</sup>Associate Professor, Department of Civil Engineering, N.I.T.  
Rourkela, India.

Email: [pradhan.siprarani@gmail.com](mailto:pradhan.siprarani@gmail.com),  
512ce1006@nitrkl.ac.in.

**ABSTRACT:** Most natural rivers consist of a main channel and the adjacent floodplains. The various subdivision methods fail to determine the discharge capacity in rivers with overbank flow because of the ignorance of the strong interaction between the main channel and the shallow floodplains. An experimental investigation is performed to study the effect of momentum transfer in terms of an apparent shear stress in rough and smooth compound channels for different hydraulic, geometric conditions and roughness ratios. A new method to calculate flow in compound channels is proposed. The approach is based on a new model on the momentum transfer coefficient at the vertical interface and the horizontal interface between adjacent flow compartments, typically between the main channel and floodplain of a two-stage channel. The new approach is found to give better results as compared to the other approaches when applied to the present experimental data sets, large channel of FCF data sets and some natural river data sets.

**Keywords:** Compound Channels, Momentum Transfer coefficient, Stage-Discharge relationship, Apparent shear stress

## 1. INTRODUCTION

A major area of uncertainty in river channel analysis is that of accurately predicting the capability of river channels with floodplains, which are termed compound channels. Cross-sections of these compound channels are generally characterized by a deep main channel, bounded on one or both sides by a relatively shallow floodplain, which is rougher and has slower velocities than as compared to that of main channel. Due to interaction between the main channel and floodplains, there are bank of vertical vortices found in many experiments by Myers (1990), Knight and Shiono (1991), along the vertical interface between the main channel and the flood plain, which lead to extra resistance in terms of consumption a lot of energy. Due to this extra resistance, the prediction of stage-discharge curve become difficult and more difficult when there is large different roughness between the main channel and floodplain. There, flow structure and flow resistance become very complex and flow shows very strongly three-dimensional characteristics, see Knight (1999), Rameshwaran and Naden (2003). In predicting the flood-water level, conventional methods for estimating the discharge capacity of a compound channel have

## Chapter – 10

# Boundary Shear Stress Distribution Along The Converging Floodplain of A Non Prismatic Compound Channel Flow

B. Naik<sup>1</sup>, Kishanjit K. Khatua<sup>2</sup>, Shiba Shankar Satapathy<sup>3</sup>

<sup>1,3</sup> Research Scholar, Department of Civil Engineering, National Institute of Technology  
Rourkela, India.

<sup>2</sup> Associate Professor, Department of Civil Engineering, National Institute of Technology  
Rourkela, India.

---

*Abstract : The boundary shear force distributions in open channel flow is needed for various purposes such as the flow resistance relationship, the mechanism of sediment transport, for designing stable channels and calculation of energy losses. During floods, river overtops the main channel and flow over the flood plain located to its sides. Once a river stage is out of banks, the cross sectional geometry of flow is changed. For such compound channels, the flow structure becomes complicated due to the transfer of momentum between the deep main channel and the adjoining floodplains that magnificently affects the shear stress distribution in floodplain and main channel sub sections. Due to the rapidly growing population and to the consequent demand for food and accommodation more and more land on floodplain regions of a river system has been used for agriculture and settlement. This also causes floodplain geometry to vary along the length of the flow called converging compound channel. Again the momentum transfer is more complicated due to the converging flood plain. In this paper an experimental investigation concerning the distribution of shear stress in the main channel and floodplain of the converging compound channels are presented. Based on the experimental results of boundary shear, a new equation is developed for predicting boundary shear stress distribution in terms of non-dimensional geometric and flow variables.*

*Keywords: compound channel, boundary shear, discharge, divided channel method, non-dimensional flow parameters*

---

### 1. INTRODUCTION

Compound channels are common configuration of rivers during floods. These are very important for environmental, ecological and design issue. So it is very essential to study the flow mechanism of rivers both in in bank and overbank conditions due to the velocity difference between the main channel and flood plains. Sellin(1964) first investigated through laboratory investigations the momentum transfer phenomena. After that several investigators found that the momentum transfer was responsible for the non-uniformity in the boundary shear stress distribution across the section perimeter (e.g. Ghosh and Jena (1971); Knight and Hamed(1984); Patra et al. (2004). Knight and Hamed(1984) developed a relation for shear stress distribution of a compound channel following the works of Knight and Demetriou(1983) and extended the relation to discharge estimation. Their model has been shown to be adequate by Knight and Hamed(1984) for compound channels having

smaller width ratio ( $\alpha$  value up to 4). Khatua and Patra(2007)based on more experimental observations carried forward the study and developed a model for channels with  $\alpha$  value up to 5.25. Mohanty and Khatua (2014)again developed a new model for channel with  $6.67 \leq \alpha \leq 11.96$ .Both prismatic and meandering compound channels geometrieswere extensively investigated in laboratory flumes. However, when the compound section data of prismatic compound channelsof Knight and Hamed (1984),Khatua and Patra(2007),Mohanty and Khatua(2014)were compared with non-prismatic compound channels significant errors inestimation of  $\%S_{fp}$  were noticed due tonon-inclusion of extra mass and momentum transfer.In Converging compound channels water flow on the floodplain crosses over water flow in the main channel, resulting in increased interactions and momentum exchanges, as explained by Bousmar and Zech(1999), Bousmar et al. (2004), and Proust et al. (2006). This extra momentum exchange should also be taken into account in the flow modeling. Most of hydraulic formulae assume that the boundary shear stress distribution is uniform over the wetted perimeter. Distribution of boundary shear stress mainly depends upon the shape of the cross section and the structure of the secondary flow cells.So new models are necessary to be developed for the non-prismatic compound sections. New experiments on non-prismatic compound channels were conducted inthe Fluid Mechanics and Hydraulics laboratory of NIT, Rourkela, India. After that stage-discharge measurement, point to point velocity measurements and point to point boundary shear measurements at different sections of the non-prismatic compound channels are taken andnew relationships are developed between  $\% S_{fp}$ and  $\%A_{fp}$ .by taking different non dimensional geometric, hydraulic and surface parameters.

## 2. EXPERIMENTAL WORKS

### 2.1 Experimental Setup

Experiments had been conducted at the Hydraulics and Fluid mechanics Laboratory of Civil Engineering Department of National Institute of Technology, Rourkela, India. Two sets of non-prismatic compound channels with varying cross sections were built inside a concrete flume measuring 15m long  $\times$  0.90m width  $\times$  0.55m depth and flume with perspex sheet of same dimensions. The width ratio of the channel was  $\alpha = 1.8$  and the aspect ratio was  $\delta = 5$ . Keeping the geometry constant, the converging angles of the channels were varied as  $12.38^\circ$ ,  $9^\circ$  and  $5^\circ$  respectively. Converging length of the channels fabricated were found to be 0.84m, 1.26m and 2.28m respectively. Longitudinal bed slope of the channel was 0.0011; it was satisfying subcritical flow conditions at different sections of the non-prismatic compound channels. Roughness of the floodplain and main channel were identical and the Manning's n was determined as 0.011 from the experimental runs in the channel. A re-circulating system of water supply was established with pumping of water from an underground sump to an overhead tank from where water flows under gravity to the experimental channel. Adjustable vertical gates along with flow strengtheners were provided in upstream section sufficiently ahead of rectangular notch to reduce turbulence and velocity of approach in the flow near the notch section. An adjustable tailgate at the downstream end of the flume helps to maintain uniform flow over the test reach. Water from the channel was collected in a volumetric tank that helps to measure the discharge rate. From the volumetric tank water runs back to the underground sump. Figure 1(a) shows the plan view of experimental

setup. Figure 1(b) shows the typical grid showing the arrangement of velocity measurement points along horizontal and vertical direction at the test section.

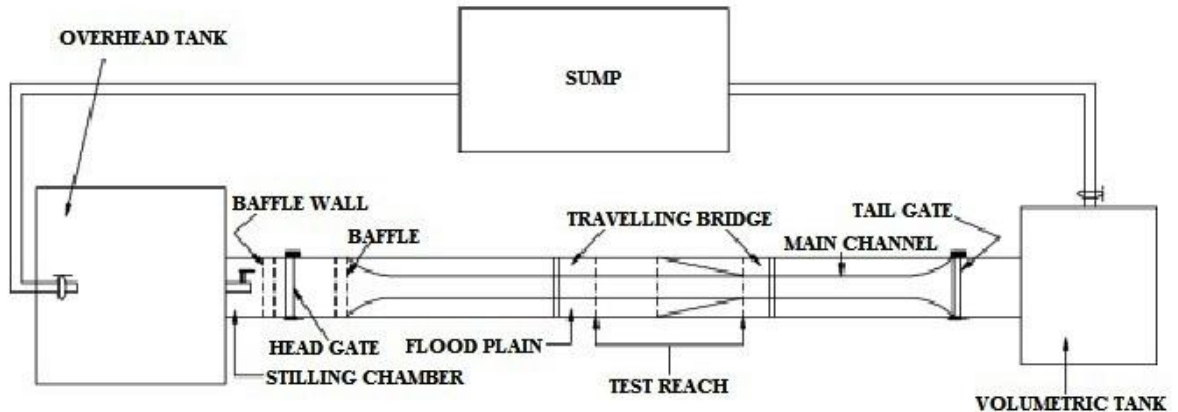


**Figure 1(a).** Plan view of Experimental Setup

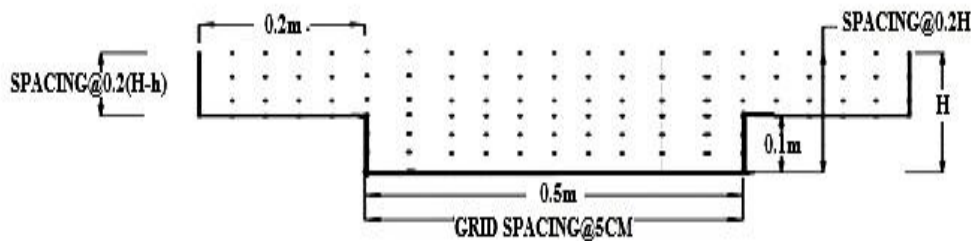


**Figure 1(b).** Typical grid showing the arrangement of velocity measurement points at the test section

A movable bridge was provided across the flume for both span wise and stream wise movements over the channel area so that each location on the plan of compound channel could be accessed for taking measurements. The broad parameters of this channel are aspect ratio of main channel ( $\delta$ ), width-ratio ( $\alpha$ ). A micro-Pitot tube of 4.77 mm external diameter in conjunction with suitable inclined manometer was used to measure velocity at these points of the flow-grid. The Pitot tube was physically rotated with respect to the main stream direction till it gave maximum deflection of the manometer reading. A flow direction finder having a least count of  $0.1^\circ$  was used to get the direction of maximum velocity with respect to the longitudinal flow direction. The angle of limb of Pitot tube with longitudinal direction of the channel was noted by the circular scale and pointer arrangement attached to the flow direction meter. The overall discharge obtained from integrating the longitudinal velocity plot and from volumetric tank collection was found to be within  $\pm 3\%$  of the observed values. Using the velocity data, the boundary shear at various points on the channel beds and walls were evaluated from a semi log plot of velocity distribution. Boundary shear stresses were also obtained from the manometric readings of the head differences of Preston tube techniques

using Patel's (1965) relationship. Error adjustments to the shear value were done by comparing the corresponding shear values obtained from the energy gradient approach. The results so obtained were found to be consistently within  $\pm 3\%$  the value.

**Table 1.** Hydraulic parameters for the experimental channel data

Verified test channel	Types of channel	Angle of convergent ( $\Theta$ )	Longitudinal slope ( $S$ )	Cross sectional geometry	Total channel width ( $B$ )	Main channel width ( $b$ )	Main channel depth ( $h$ )	Width ratio (sec-1) $B/b$ ( $\alpha$ )	Converging length ( $X_r$ )	Aspect Ratio $b/h$ ( $\delta$ )
					Meter	Meter	Meter		Meter	
Rezai (2006)	Convergent (CV2)	11.31°	0.002	Rectangular	1.2	0.398	0.05	3	2	7.96
Rezai (2006)	Convergent (CV6)	3.81°	0.002	Rectangular	1.2	0.398	0.05	3	6	7.96
Rezai (2006)	Convergent (CV6)	1.91°	0.002	Rectangular	1.2	0.398	0.05	3	6	7.96
N.I.T. Rkl	Convergent	5°	0.001	Rectangular	0.9	0.5	0.1	1.8	2.28	5
N.I.T. Rkl	Convergent	9°	0.001	Rectangular	0.9	0.5	0.1	1.8	1.26	5
N.I.T. Rkl	Convergent	12.38°	0.001	Rectangular	0.9	0.5	0.1	1.8	0.84	5

### 3. EXPERIMENTAL RESULTS

The boundary shear distribution for relative depth 0.15 for converging angle 12.38° and for relative depth 0.5 for the converging angle 11.31° Rezai (2006) are shown in Figure 2(a) and 2(b). Various boundary elements of the compound channel comprising the wetted parameters are labeled as (1), (2), (3) and (4) as shown in Figure (3). Label (1) denotes the two vertical walls of floodplain of length  $[2(H-h)]$ , and (2) denotes floodplain beds of length  $(B-b)$ . Label (3) denotes the two main

channel walls of length ( $2h$ ) and the bed of the main channel of length  $b$  is represented by label (4) (where  $H$  is the total depth of the compound channel,  $h$  is the main channel height,  $B$  is the total width of the compound channel). Experimental shear stress distributions at each point of the wetted perimeter are numerically integrated over the respective sub-lengths of each boundary element (1), (2), (3), and (4) to obtain the respective boundary shear force per unit length for each element. Sum of the boundary shear forces for all the beds and walls of the compound channel is used as a divisor to calculate the shear force percentages carried by the boundary elements. Percentage of shear force carried by floodplains comprising elements (1) and (2) is represented as  $\%S_{fp}$ .

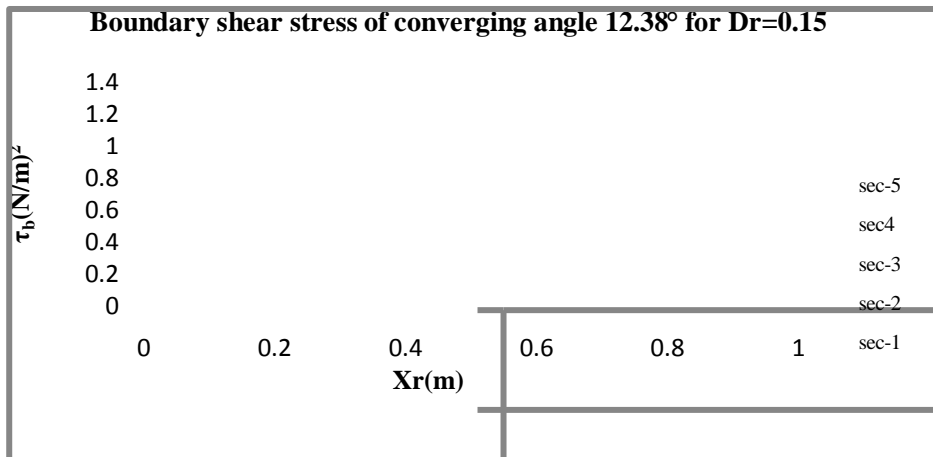


**Figure 2(a).** Boundary shear distribution for the present experimental channel of relative depth 0.15 (for converging angle  $12.38^\circ$ )

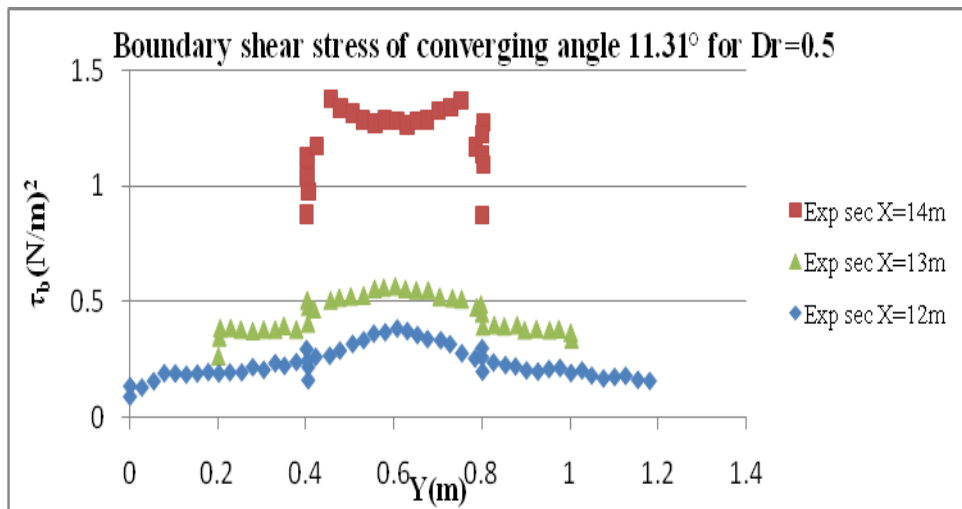


**Figure 2(b).**Boundary shear distribution for the Rezai(2006) experimental channel of relative depth 0.5(for converging angle 11.31°)

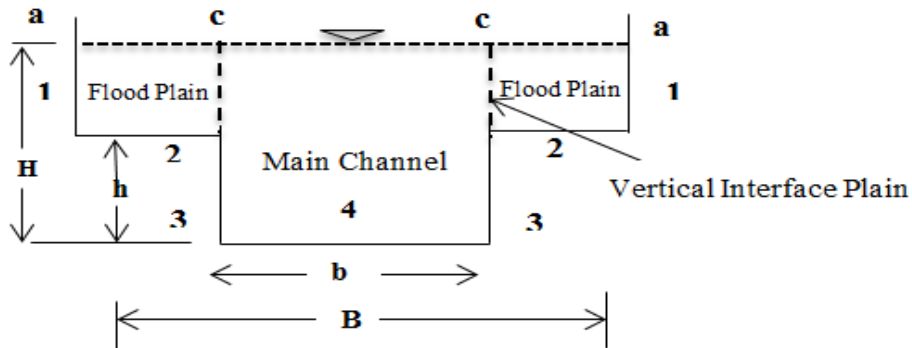


**Figure3.** Interface planes dividing a compound section into sub areas

#### 4. THE BOUNDARY SHEAR STRESS MODEL

For a straight and smooth compound channel section of any given over-bank flow depth, both  $\alpha$  and  $\beta$  are known then the  $\%S_{fp}$  can be calculated by using the equation of Knight and Hamed(1984) i.e

$$\%S_{fp} = 48(\alpha - 0.8)^{0.289} (2\beta)^m \quad (1)$$

Equation (1) is applicable for the channels having equal surface roughness in the floodplain and main channel. For non-homogeneous rough channels equation (1) is improved by Knight and Hamed (1984) as

$$\%S_{fp} = 48(\alpha - 0.8)^{0.289} (2\beta)^m [1 + 1.02\sqrt{\beta \log \gamma}] \quad (2)$$

Where  $\alpha$  = width ratio,  $\beta$  = relative depth =  $(H - h)/H$ ,  $\gamma$  = the ratio of Manning's roughness of the floodplain ( $n_{fp}$ ) to that for the main channel ( $n_{mc}$ ),  $b$  = width of main channel,  $B$  = total width of compound channel,  $h$  = bank full depth and  $H$  = total depth of flow.

The exponent  $m$  is evaluated from the relation

$$m = 1/[0.75e^{0.38 \alpha}] \quad (3)$$

Equation (1) is good for  $\alpha \leq 4$ . Khatua and Patra (2007) further improved equation (2) and proposed an equation for  $\%S_{fp}$  as

$$\%S_{fp} = 1.23(\beta)^{0.1833} (38L_n\alpha + 3.6262)[1 + 1.02\sqrt{\beta \log \gamma}] \quad (4)$$

In a simple open channel flow the boundary shear per unit length ( $SF$ ) is generally assumed to be uniform and is expressed as  $SF = \rho g AS$ , where  $\rho$  is density of water and  $g$  is acceleration due to gravity. The parameters  $\rho$ ,  $g$  and  $S$  are assumed constant for a given channel. Only the flow area ( $A$ ) varies with flow depth. So it can be stated that  $SF$  is a function of  $A$ . The percentage of the area occupied by floodplain subsections obtained by vertical interfaces (Fig 3),  $\%A_{fp} = 100 \times A_{fp}/A$ . Then  $\%S_{fp}(100 \times S_{fp} / SF)$  should be a function of  $\%A_{fp}$ . Due to the momentum transfer in a compound

channel, it has been shown that  $S_{fp}$  doesn't vary linearly with  $A_{fp}$  (e.g. Knight and Hamed (1984), Patra and Kar (2004)). Therefore, a functional relationship between  $\%S_{fp}$  and  $\%A_{fp}$  has been derived. This equation has been obtained by curve fitting between  $\%A_{fp}$  and  $\%S_{fp}$  which gave the highest regression coefficient. Khatua and Patra (2007) have shown the validity of Equation (4) for  $\alpha$  up to = 5.25. Again for  $\alpha=6.67$  Khatua et al (2012) obtained a new relation for percentage shear carried by the flood plain as

$$\%S_{fp} = 4.1045(\%A_{fp})^{0.691} \quad (5)$$

Considering the relative depth  $\beta = (H - h)/H$  and width ratio  $\alpha = B/b$ , so for rectangular channel and floodplains, Equation (5) is simplified as

$$\%S_{fp} = 4.105 \left[ \frac{100\beta(\alpha-1)}{1+\beta(\alpha-1)} \right]^{0.691} \quad (6)$$

For width ratio up to 12, from regression analysis, Equation (5) is further modified by Mohanty et al (2014)

$$\%S_{fp} = 3.3254(\%A_{fp})^{0.746} \quad (7)$$

From the literature study, it is seen that  $\%S_{fp} = F(\alpha, \beta, \delta)$  for prismatic compound channel, Where  $F$  is the functional symbol. But when all the equations are tested against non-prismatic compound channels of converging sections significant errors are found due variation of geometry. So an attempt has been made here to see the variation of  $\%S_{fp}$  with respect to different independent parameters.  $\%S_{fp}$  has been derived from a wide range of experimental data sets from three different types of converging compound channels of NIT, Rourkela, India along with three series of converging compound channels data of Rezai (2006) (details of the data sets are given in Table.1) These compound channels have homogeneous roughness both in the main channel and floodplain subsections. Manning's  $n$  values for all these smooth surfaces are taken as 0.01. A multiple-variable regression model is developed by taking five important dimensionless independent parameters. The dependency of  $\%S_{fp}$  and the best functional relationships have been found out from different plots described below. So it is in the following form

$$\%S_{fp} = F(\alpha, \beta, \delta, \theta, X_r) \quad (8)$$

The variation of  $\%S_{fp}$  has been found out for six converging compound channels. The variation of  $\%S_{fp}$  in terms of relative depth  $\beta$  is plotted for different converging angles  $\theta$  in Fig (4). From the figure (4) it is seen that  $\%S_{fp}$  increases with increase in relative depth. The variations of  $\%S_{fp}$  in terms of relative distance  $X_r$  are plotted for different relative depth in Fig (5). From the figure (5) it is seen that the shear force percentage carried by flood plains ( $\%S_{fp}$ ) are found to decrease from section to section of all the converging compound channels of different converging angles. The variation of  $\%S_{fp}$  in terms of different converging angles for different relative depth are shown in Fig (6), from this it is seen that shear force percentage carried by flood plains are found to increase with increase of overbank flow depth.

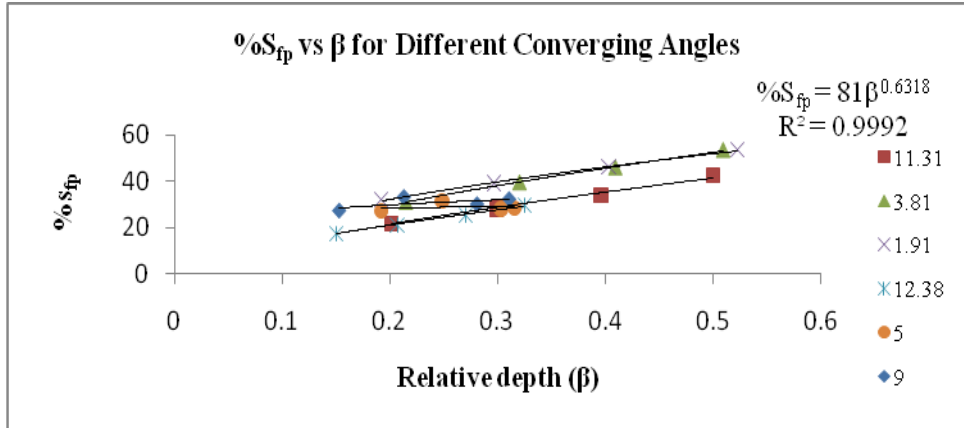


Figure4 .Variation of  $\%S_{fp}$  of non-prismatic compound channel at typical sections

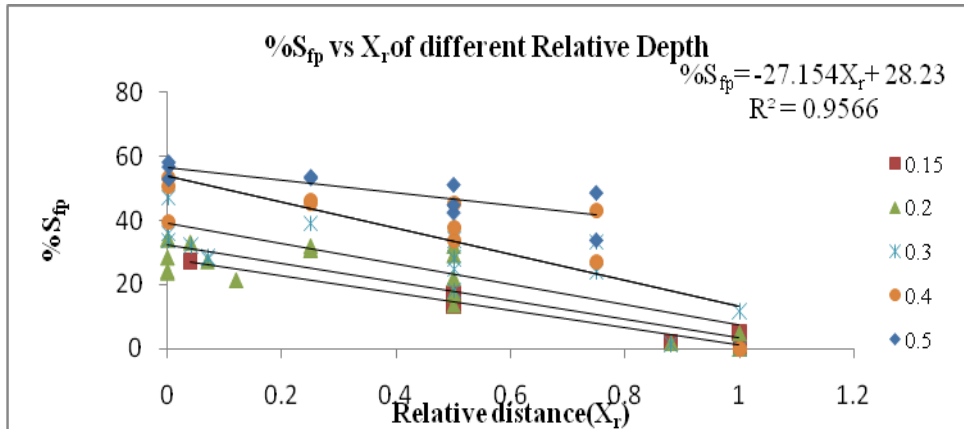


Figure5. Variation of  $\%S_{fp}$  of floodplain shear with section to section along the converging angle and prismatic channel width

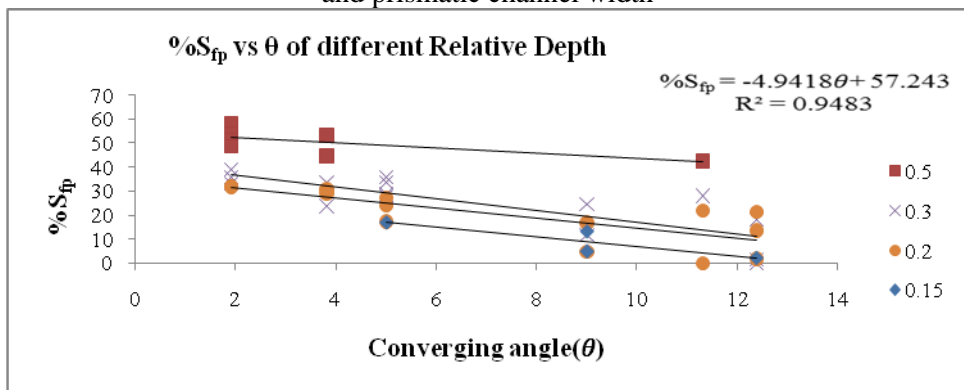


Figure6. Variation of  $\%S_{fp}$  of floodplain shear with converging angles for constant relative depth

By analyzed the above plots, percentages of boundary shear stress in floodplain region i.e. corresponding functional relationships  $\%S_{fp}$  of with different non-dimensional geometric and hydraulic parameters are

$$\%S_{fp} = A(\beta)^{0.63} \quad (9)$$

$$\%S_{fp} = A(X_r) + c \quad (10)$$

$$\%S_{fp} = A(\theta) + c \quad (11)$$

$$\%S_{fp} = F(\delta) \quad (12)$$

$$\%S_{fp} = F(\alpha) \quad (13)$$

From the above graphs (Fig. no.4,5,6) it is shown that  $R^2$  value is very high and varies from 0.95 to 0.99. By using above relationships we compile to developed a mathematical model by using the theregression analysis software. From the regression analysis an empirical formulation is formulated. These equations (equation no. 9, 10, 11, 12, 13) show the relation between  $\%S_{fp}$ , with width ratio, relative depth, aspect ratio, converging angle, relative distance.

**Table 2.** Unstandardized Coefficient and Regression Statistics

	Coefficients	Regression Statistics	
Intercept	-22.985	Multiple R	0.911
$\beta$	0.767	R Square	0.831
Xr	0.899	Adjusted R Square	0.826
$\theta$	0.281	Standard Error	7.154

Table 2 data represent the result of linear regression analysis. From the above table the corresponding co-efficient are found and a mathematical empirical relation is created and it shows in equation 14. After then by putting the different dependent variables from the above graph (Fig 4 to Fig 6) then it will give a relation in a modified form which shows in equation 15 in accurate linear form.

$$\%S_{fp} = -22.985 + 0.767(D_r) + 0.899(X_r) + 0.281(\theta) \quad (14)$$

After simplify the above equation

$$\%S_{fp} = 18.505 + 62.140D_r^{0.631} - 24.42(X_r) + 1.38(\theta) \quad (15)$$

After formulation of the new mathematical model, an attempt has been taken to validate with the data of other investigators and present experimental channel data sets. So in the present study the necessary validation is carried out with previous known data sets. The results are as follows.

## 5. RESULTS AND DISCUSSION

### 5.1. Error Analysis

The variation between the calculated values of ( $\%S_{fp}$ ) using equations (1), (5) and (7) and the corresponding observed values for all the five types of channels are shown in Fig.7. The percentage error in estimated shear carried by flood plains ( $\%S_{fp}$ ) is less when compared to previous models for both Present experimental Channel as well as Rezai(2006) Channel .

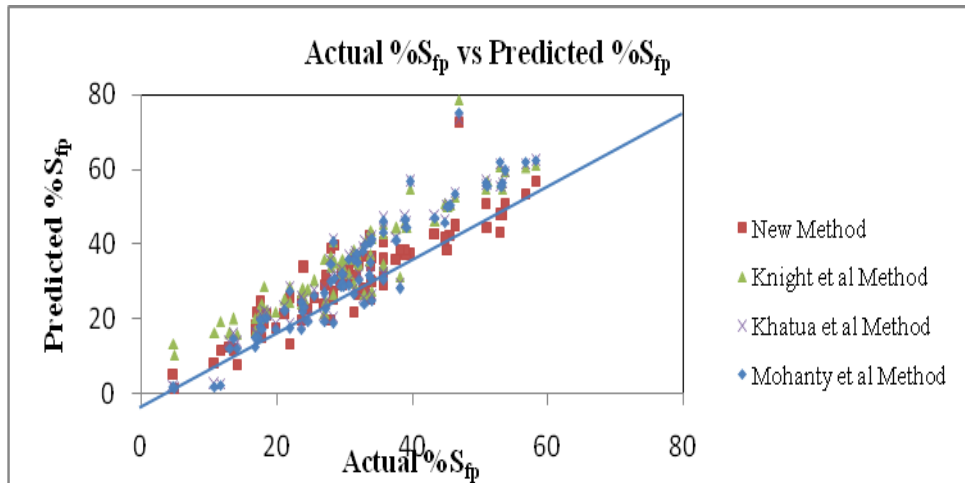


**Figure 7.**Scatter plot for observed and modeled value of  $\%S_{fp}$

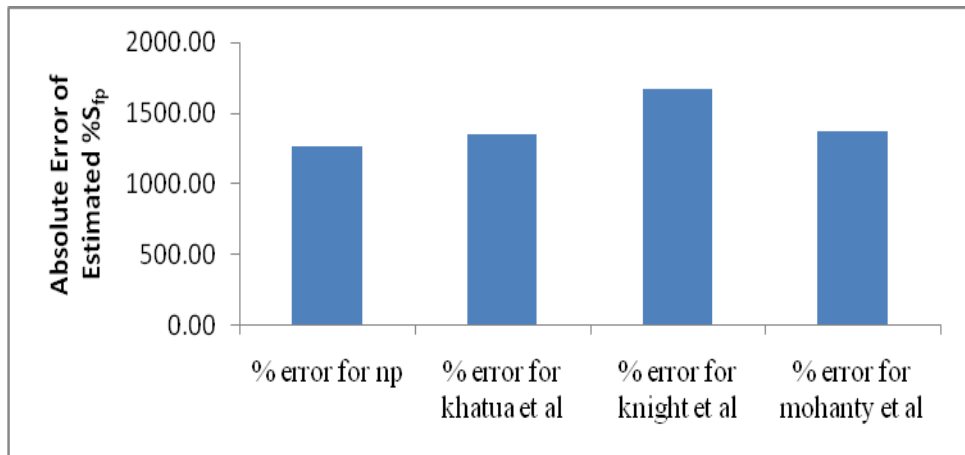


**Figure 8.**Absolute Error by standard approaches applied to Present experimental channel data

Using the new equation, various conventional methods is estimated for the flow cases considered in Present experimental Channel of Rourkela and Rezai (2006)Channel. The methods considered areKhatuaet’al(2012), Knight et’ al(1984), Mohanty et’ al(2014).The percentage in error in estimating the discharge is computed as

$$Absolute\ Error(\%) = \frac{100\%}{N} \sum \left| \frac{Sf_{p_{calc}} - Sf_{p_{act}}}{Sf_{p_{act}}} \right| \quad (16)$$

Where  $Sf_{p_{calc}}$  is the estimated discharge,  $Sf_{p_{act}}$  is actual discharge;  $N$  is the total number of data. Figure (8) shows the comparison among various methods in Present experimental Channel of Rourkela and Rezai(2006) channel cases. In Figure (8), the New Method appears to be the best method.

**Table 3.** Statistical error analysis of different methods

Methods Stastical parameters	New Method	Khatua et.al	Knight et.al method	Mohanty et.al method
MSE	28.78119	35.62421	45.33	39.95373
RMSE	5.364811	5.968602	6.73	6.320896
MAE	3.734498	4.759234	5.31	4.746045
MAPE	13.43366	17.19923	21.63	17.4745

In order to know the efficiency of the newly developed model different statistical error analysis for the different methods are presented in Table 3. MSE, RMSE, MAE, MAPE of new method are less as compare to other methods.

## 7. CONCLUSIONS

The following conclusions can be derived from the above research presented in this work.

1. From the experimental results on converging compound channels, the boundary shear at point of the wetted perimeter of different sections of the converging compound channels are measured and the distribution of shear force carried by flood plains and in main channel perimeters were calculated.
2. The shear force percentage carried by flood plains ( $\%S_{fp}$ ) is found to decrease from section to section of all the converging compound channels of different converging angles. For the channels of the same angle, the shear force percentage carried by flood plains is found to increase with increase of overbank flow depths.
3. The dependency of shear force percentage carried by flood plains with five most influencing non-dimensional geometric and hydraulic parameters of a converging compound channel are

evaluated and modeled. The  $\%S_{fp}$  in converging compound channel is found to be a non-linear function of all these non-dimensional parameters.

4. Different standard models to predict the shear force percentage carried by flood plains are applied to the present channel and the channels of other investigators. The present mathematical model presented for  $\%S_{fp}$  of a converging compound channel gives least error when compared with other models applied at different reaches of the channels.
5. Error analysis in terms of MSE, RMSE, MAE and MAPE are performed for all data series by all the models to predict the shear force percentage carried by converging flood plains showing the efficacy of the present model.

## 8. ACKNOWLEDGEMENTS

The author wish to acknowledge thankfully the support from the Institute and the UGC UKIERI Research project (ref no UGC-2013 14/017) by the second authors for carrying out the research work in the Hydraulics laboratory at National Institute of Technology, Rourkela is thankfully acknowledged.

## REFERENCES

- Bousmar D and Zech Y (1999) Momentum transfer for practical flow computation in compound channel. *J. Hydraul. Eng.*, 125(7): 696-706
- Bousmar D, Wilkin N, Jacquemart JH and Zech Y (2004) Overbank flow in symmetrically narrowing floodplains. *J. Hydraul. Eng., ASCE*, 130(4), 305-312
- Ghosh S., Jena SB (1971) Boundary shear stress distribution in open channel compound. *Proc. Inst. Civil Eng.*, 49: 417-430
- Knight DW, Demetriou JD (1983) Flood plain and main channel flow interaction. *J. Hydraul. Eng., ASCE*, 109 (8):1073-1092
- Knight DW., Hamed ME (1984) Boundary shear in symmetrical compound channels. *J Hydraul. Eng., ASCE*, 110(10):1412
- Khatua KK, Patra KC (2007) Boundary shear stress distribution in compound open channel flow. *J. Hydraul. Eng., ISH*, 12 (3):39-55
- Khatua KK, Patra KC, Mohanty PK (2012) Stage-Discharge prediction for straight and smooth compound channels with wide floodplains. *J. Hydraulic. Eng., ASCE*, 138(1): 93-99
- Patel VC (1965) Calibration of the Preston tube and limitations on its use in pressure gradients. *J. Fluid Mech.* 231:85-208. Cambridge University Press
- Patra KC, Kar SK, Bhattacharya AK (2004) Flow and velocity distribution in meandering compound channels. *J. Hydraul. Eng., ASCE*, 130(5):398-411
- Proust S, Rivière N, Bousmar D, Paquier A, and Zech Y (2006) Flow in compound channel with abrupt floodplain contraction. *J. Hydraul. Eng.*, 132(9), 958-970

Boundary Shear Stress Distribution Along the Converging Floodplain of A Non Prismatic  
Compound Channel Flow

---

- Prabir K Mohanty, Kishanjit Khatua, Saine S Dash(2014) Flow prediction in two stage wide compound channels. Journal of Hydraulic Engineering, ISH
- Rezaei B(2006) Overbank flow in compound channels with prismatic and non-prismatic floodplains. PhD Thesis, Univ. of Birmingham, U.K..
- Sellin RHJ (1964) A laboratory investigation into the interaction between flow in the channel of a river and that of its flood plain, La HouilteBlanche, 7:793–801
- Wormleaton PR, Allen J, and Hadjipanos P (1982) Discharge assessment in compound channel flow. J. Hydraul. Div., 108 (9):975–994

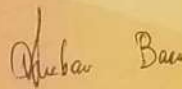


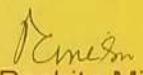
INTERNATIONAL CONFERENCE  
ON  
HIGH PERFORMANCE COMPUTING AND APPLICATIONS  
अन्तरराष्ट्रीय सम्मेलन : उच्च प्रदर्शन अभिकलन (ICHPCA-2014)  
22-24 DECEMBER, 2014

CERTIFICATE OF PARTICIPATION

This is to certify that Laranya Pamulaparty  
of Jawaharlal Nehru Technological University, Hyderabad, India  
has actively participated and presented a paper entitled A Novel approach for avoiding overload  
in the web crawling

in the conference organized by C.V. Raman College of Engineering, Bhubaneswar, India, held from 22<sup>nd</sup> to 24<sup>th</sup> December 2014.

  
Dr. Anirban Basu  
General Chair  
ICHPCA-2014

  
Prof. Rachita Misra  
Convener  
ICHPCA-2014

  
Prof. K.C. Patra  
Director  
C.V. Raman College of Engineering



Scanned with  
CamScanner  
IEE  
KOLKATA SECTION  
Technical Sponsor



DIV-V  
Education & Research  
Technical Sponsor



Government of India  
Department of Atomic Energy  
BRNS



Department of Biotechnology  
Government of India

TATA  
CONSULTANCY  
SERVICES  
Gold Sponsor



International Conference  
on  
**INTELLIGENT COMPUTING, COMMUNICATION & CONVERGENCE**  
(ICCC-2014)

Paper Id : 277

27<sup>th</sup>-28<sup>th</sup> December, 2014

Organized by  
**IIMT RESEARCH NETWORK**  
BHUBANESWAR, ODISHA, INDIA

*Certificate*

This is to certify that Prof./Dr./Mr./Mrs. Lavanya Pamulaparty has participated /presented a paper entitled "**XNDDF: Towards a Framework for Flexible Near-Duplicate Document Detection Using Supervised and Unsupervised Learning**" in the International Conference on **Intelligent Computing, Communication & Convergence (ICCC-2014)**, Bhubaneswar, Odisha on 27<sup>th</sup>-28<sup>th</sup> December, 2014.

Program Chair  
ICCC-2014



# MULTI LEVEL HUFFMAN TEST DATA COMPRESSION WITH MULTIPLE SCAN CHAIN METHOD

<sup>1</sup>Srikanth Immareddy, <sup>2</sup> Sravan Kumar Talusani

<sup>1</sup> *Electronics and Communication Engineering Dept, Methodist College of Engineering and Technology, Hyderabad 500001, India.*

<sup>2</sup> *Electronics and Communication Engineering Dept, Methodist College of Engineering and Technology, Hyderabad 50001, India.*

## Abstract

The present paper focuses on the compression system using Huffman compression algorithm for data compression. The rate of data decompression is more time consuming during the decoding of these compressed data. Various works have proposed for the enhancement of compressed data decoding. In this paper the realization and implementation of a High speed decoding Huffman coding system is proposed and the proposed architecture shows an improvement with respect to the speed of decoding operation based on multiple scan method and multi level decoder partitioning concept. As a part of the above work the existing Huffman coding system is also implemented and its performance in terms of speed and area are compared with the proposed work.

*Keyword:* Data compression, Huffman coding, Multi-level, Multiple-scan high speed Decoder

## I. INTRODUCTION

Data compression is one of the major challenges involved in testing and has been difficult to master and also tough to implement. Coding is often referred as a special representation of data, without loss of required information. The Information theory is defined to be the study of efficient coding and it affects the transmission speed, memory required for storage and error probability. A new data compression algorithm is being presented in this work analyzing the existing Huffman coding system. Data compression involves in transforming a stream of bits into a new stream of bits, by reducing the length using the Huffman coding algorithm.

The problem of compressing the test data and reducing test time for core-based Silicon on chip has been discussed in several different angles in recent Literature [1], [6], [7], [8]. The time required for test data between a workstation across a network and a tester off the chip is reduced using scan chain architectures maximizing the bandwidth utilization are presented in [1]. Novel approaches for compressing test data using the Burrows–Wheeler transform and run-length coding were presented in [7], [8]. A new scan vector using cyclical

decompressor and run-length coding is described for compression and decompression of scans vectors in [9]. A modular built-in self-test (BIST) approach that allows sharing of BIST control logic among multiple cores is presented in [3]. A novel Technique for combining BIST and external testing across multiple Cores are described in [12]. The statistically encoding test data idea was presented in [2]. A statistical coding using comma codes similar to Huffman codes is described for nonscan BIST scheme circuits is presented in [5]. A technique that uses a linear combinational expander circuit is presented in [2]. The use of Frequency directed run length (FDR) and Golomb codes for test data compression has been demonstrated [4]–[6]. A Parallel Serial Full Scan (PSFS) approach for reduction of test time in cores is presented in [5]. A virtual scan chains for specially designed cores is presented in [5] for reduction in test time and test data. Various types of run length coding have been discussed in the above surveys which are not the efficient coding method.

A Huffman code with variable length input is proposed in [11] for System on chip SOC test data compression. Increase in test data bandwidth has been presented in [9] using a technique for reusing scan chains for other cores in an SOC. An automatic test pattern generation (ATPG) techniques have been described in [10] for producing test cubes that are suitable for encoding. A fixed-to-fixed block-encoding scheme is described in [7]. A fault simulation-based technique to reduce the entropy of the test vector set by pattern transformation is described in [8]. Such transformations increase the amount of compression that can be achieved on the transformed test set using statistical coding. ATPG algorithms for producing test vectors that can more effectively be compressed using statistical codes have been described in [2]. Huffman coding algorithms are used for automatic test pattern generation for system on chip have been discussed.

A test-data compression method based on multi level Huffman coding, has been presented for IP cores of unknown structure, that improves compression result, area over ahead for decompressor is presented in [13]. A multilevel Huffman test-data

compression approach for IP cores with multiple scan chains has been presented with a decompression architecture that can generate clusters of test bits in parallel. This new method reduces test-application times and achieves high compression ratios, and also the sizes of the encoded data blocks are made independent of the slice size that can be applied to multiple scan-chain cores has been presented in [14]. An efficient decoder for decompressing the compressed data is implemented using Xilinx and simulated on Active HDL enhances the speed of decoding operation has been presented in [15]. The present paper implements and realizes the high speed Huffman decoder with the concept of multi level Huffman using the multi scan chain method.

## II. DATA COMPRESSION

Data compression is a way of encoding digital data so it takes up less storage space and requires less network bandwidth to be transmitted. An effective encoding technique minimizes the average length of a data. Consider data containing  $m$  unique patterns  $A_1, A_2, \dots, A_m$  with probabilities of occurrence  $P_1, P_2, \dots, P_m$  respectively [3]. The entropy  $H$  is defined intuitively as the minimum average number of bits required to represent a pattern, is given by

$$H(DS) = - \sum P_i \log_2 P_i \quad (1)$$

Therefore, an optimal encoding technique is one in which the average number of bits needed to represent a pattern is closest to the entropy bound. Among all statistical encoding techniques the Huffman code is having the shortest average codeword that assign a unique binary codeword to each pattern [12]. In fact, if  $L_H$  is the average length of a Huffman-encoded pattern in  $D_S$ , then

$$H(DS) \leq L_H \leq H(DS) + 1. \quad (2)$$

In addition, Huffman codes possess the prefix-free property, i.e., no codeword is the prefix of a longer codeword [15]. It can be shown that this property is important for decoding. Table-III illustrates the Huffman code for an example data set with sixteen unique patterns out of a total of 384. Column 1 of Table-III lists the sixteen patterns, column 2 lists the corresponding number of occurrences (Occ) of each pattern  $X_i$ , and column 3 lists the corresponding probability of occurrence  $p_i$ , given by  $Occ / D_S$ . Finally, column 4 gives unique pattern to each corresponding Huffman code. Using a state diagram approach, as shown in Figure 1, performs Huffman decoding. In conventional Huffman decoding each incoming bit is compared with entries of the lookup table of the code vectors. The original or the encoder

transmitted data from is retrieved from the lookup table, which consists of all the unique words and their corresponding code vectors.

Once the Huffman coding is performed, the encoded data is serially transmitted to the decoder. In a conventional decoder, these single bit data is accepted and the state of decoder is changed based on the data that can be either '0' or '1'. Once the data is received at the decoder, it is compared with each entries of the code vectors from the lookup table. If the received data matches with any of the code vectors in the lookup table, the unique word of the matched code vector corresponding to the transmitter encoder data is decoded by the decoder. If a mismatch occurs, the decoder accepts the next received data and repeats the above procedure. When all the states of the decoder are traversed and a unique word of the received data pattern is identified, the control is transferred to the initial state, indicating that the unique word for the data pattern has been matched and the decoder wait for the next incoming data. If unmatched, control is transferred to next state as shown in the figure and again process repeats. The decoding process continues till the encoder stops transmitting the data.

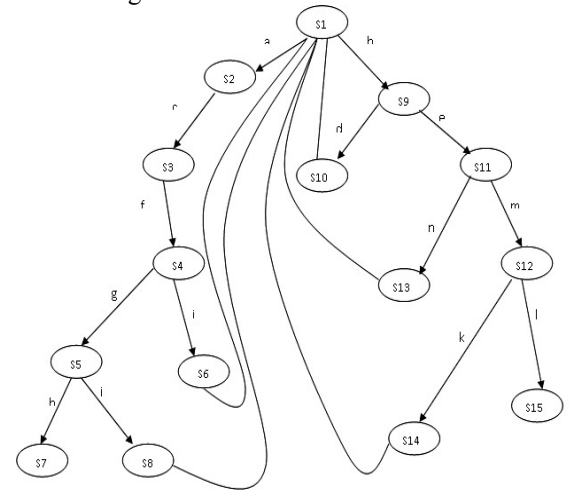


Fig. 1. State Transition of a conventional Huffman Decoder

Once the complete data has been received, decoding of the compressed data is done as said earlier by the state diagram approach and the decoded data is decompressed and the complete process of decoding is called as decompression of data. Figure 1 shows the state diagram for Huffman decoding. Each bit of data after reception is compared with the code vectors of the look up table if a match occurs between the test code and code word of LUT then the state is returned to its initial state returning the corresponding symbol for that code word. Else on not matching the state moves to next state. For example the transition of state starts with 'S1' state called initial state and

proceeds to next states based on the code bits received. On a match, the state 'S1' results a symbol 'a' or 'b' starting again with initial state. If a non-match occurs the state goes to the next state depending on the received code bit.

### III. HIGH SPEED HUFFMAN DECODER ARCHITECTURE

The block diagram of high speed Huffman decoder architecture is shown in Figure 2. The proposed decoder receives the input bit stream in serial from the encoder. The received serial data is passes to the N-bit shifter which converts the serial data into parallel data. The length decoder and the symbol decoder accepts the parallel data from the Shifter, decodes the original data back from the decoding code words. The code words of equal length are shorted and aligned in the look up table (LUT) of a codebook. The symbol decoder consists of partitioned codebooks of equal length code words.

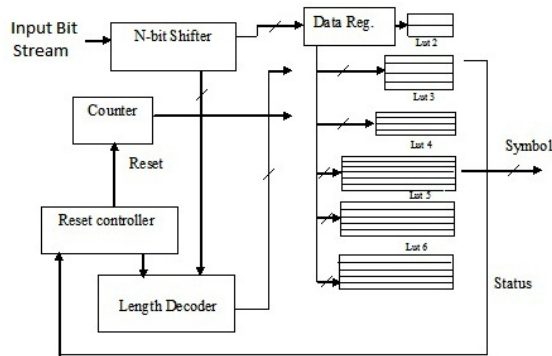


Fig. 2. Architecture of High speed Huffman Decoder

The length decoder calculates the length of the received code word and the high-speed decoder scans the LUT with the received code depending on its length. The scanning time of tracing is reduced as each LUT consists of specific length codes. For Example, if the code word for '1111' is '11' during encoding the '1111' will be represented as '11' and transmitted. In the decoding of a normal tree based Huffman decoder the two clock cycles are utilized in storing these two bits. As the actual data is of size four bits, additionally 16 clock cycles are utilized by the system for tracing out the code word from code book. Hence a tree based decoder utilizes 34 clock cycles (2+16+16=34) for decoding.

Whereas the proposed Multi-scan decoder utilizes 2 clock cycles for scanning LUT-1 which is of one bit length, if the matching fails, the next code bit is latched i.e. '11' and the scanning is performed on LUT-2 which is of length 2. It takes maximum of

four clock cycles for scanning LUT-2. Hence it utilizes maximum of 8 (2+2+4) clock cycles, which is comparatively faster than the existing conventional Huffman decoding system.

The counter is used in controlling the decoding operation. Selection of the LUT depends on the length decoder in the symbol decoder unit. The selection of the code word is done sequential manner based on the count value from the counter unit. The length decoder output helps in selecting one among the six LUT's for tracing the code word from the LUT. The reset generation unit generates the reset signal for the counter and the length decoder unit; they get reset to initial value. The reset generator generates the reset signal when the status signal goes high. The status signal is generated from the symbol decoder when a match of code word occurs. Under every 6-clock cycles the shift register receives 6 coded bits and transfers it to data register of symbol decoder and length decoder.

While the symbol decoder process on data registers value the shift register keep receiving the next code bits from the encoder unit. This gives the decoder unit to work simultaneously while receiving the data bits. This gives a faster operation compared to existing tree based decoding where the encoded bits are latched for decoding. The output of the symbol decoder and the received code bits are applied to the length decoder which generates the count length starting from L1 to the maximum of the received code bit length. Depending on either L1 or L2 or L3 etc one of the LUT among the 6 LUT is selected.

The count generation is stopped by length decoder once it receives a reset signal; this completely disables the decoding system from further decoding. For example, if the Code words received at the end are not of 6-bit length, in such cases the decoder generates a count up to the existing code bits only. Table 1 generates length count from L1 to L6 for selecting the LUT.

TABLE I  
TRUTH TABLE FOR LENGTH DECODER.

L1	L2	L3	L	L5	L6
1	0	0	0	0	0
0	1	0	0	0	0
0	0	1	0	0	0
0	0	0	1	0	0
0	0	0	0	1	0
0	0	0	0	0	1

## IV. SIMULATION RESULTS

The proposed architecture is simulated on Active HDL 8.1 v, with the data bits as given in table II. The sample data used for simulation are the compacted test cubes.

TABLE II  
DATA DIVIDED INTO 4-BIT BLOCKS

1111	0101	0011	1111	1011	1110	1101	1011
1111	1111	1111	1111	0000	0000	0000	0000
1001	0010	0110	0111	1110	1101	0110	1110
1111	1111	1110	0110	1111	1001	1111	1011
1111	1111	0111	1010	1111	1111	0111	1111
0010	1110	1000	0100	1111	1111	1111	1111
0110	1011	1011	1011	1101	0111	1011	0111
1100	1000	1010	0111	0101	1011	1111	1101
1011	0100	1101	1101	1110	1111	1111	1111
1111	1011	0111	0101	1111	0111	1111	1101
1100	1101	1001	1110	1110	1101	1011	0110
0111	0010	1111	1111	0111	1111	1011	1111

This section illustrates the statistical encoding for the given set of data. To encode the given data, it is divided into 4-bit blocks; each block is a 4-bit pattern. The dataset consist of 15 unique words divided in 4-bit block each. To reduce the number of unique words the data is partitioned into size of 4, which reduces the complexity of the decompression circuit. This also increases the speed of decompression. Each block pattern is mapped into a variable length code word. The length of the code word depends on the probability with which each pattern occurs in the data set.

TABLE III  
PROBABILITY AND CODE TABLE

i	X <sub>i</sub>	Occurrence	Probability	Huffman code
1	1111	30	0.3125	11
2	1011	12	0.1250	100
3	0111	10	0.1042	010
4	1101	09	0.098	000
5	1110	08	0.0833	1011
6	0110	05	0.0521	0011
7	0000	04	0.0417	10101
8	0010	03	0.0313	01111
9	1001	03	0.0313	01110
10	0101	03	0.0313	01101
11	1100	02	0.0208	01100
12	0100	02	0.0208	00101
13	1000	02	0.0208	00100
14	1010	02	0.0208	101001
15	0011	01	0.0104	101000
16	0001	0	0	UUUU
# States of FSM				15

The Table III shows the probabilities (pi) of occurrence of each unique pattern [xi] in the data of Table II. Following simulation results shows the data compression and decompression using Huffman coding. The result shows the compression in memory location required for data storage.

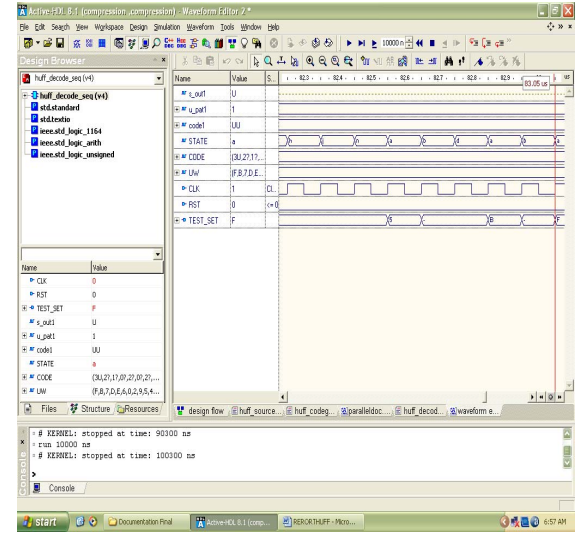


Fig.3. Simulation of the existing Huffman decoding system.

The Figure 3 shown above indicates the simulation result obtained for the existing Huffman coding system. From the simulation result it is observed that a total of 83.15 $\mu$ s is taken for the decoding of complete encoded data set. The signal 'Test set' shows the decoded data set retrieved for the obtained encoded data bits.

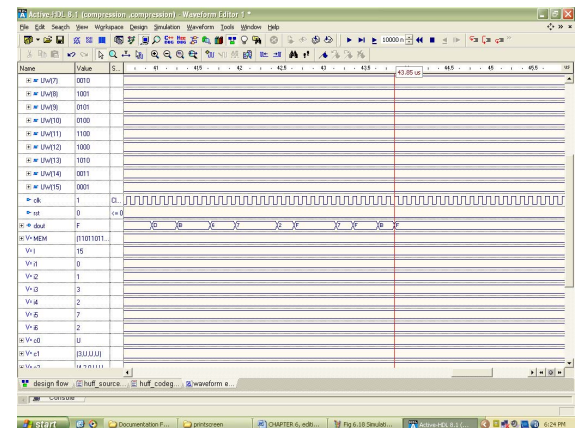


Fig.4.Simulation waveform of the High speed Huffman decoding system.

The Figure 4 shows the simulation result for the final timing simulation result obtained for the decoding of the complete data set. From the simulation result it is obtained that a total of 43.75 $\mu$ s simulation time period is taken for the decoding of

the complete data set. It is observed that about 50% of the time is reduced during the decoding process of the given data set using high speed Huffman decoder.

## V. IMPLEMENTATION RESULTS

The proposed High speed decoding Huffman coding system design and the existing Huffman coding are implemented on to the targeted FPGA Cyclone EP1C20F324C6 using Quartus II. The chip planner resource utilization of the targeted FPGA for the high speed Huffman decoder system results about 63 % utilization, i.e. use a total of 13,280 Logic cells out of available 20,600 logic cells is shown in figure5.

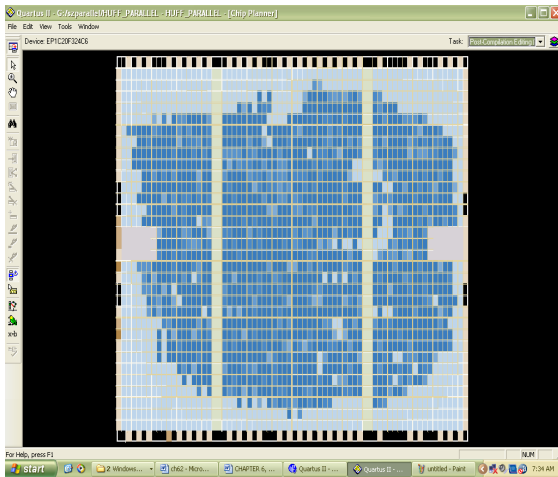


Fig.5. FPGA Chip planner resource utilization.

The Routing is carried out using FPGA Editor. It is observed that the average interconnects usage is 31% of the available device resources and the Peak interconnects usage is 57% of the available device resources.

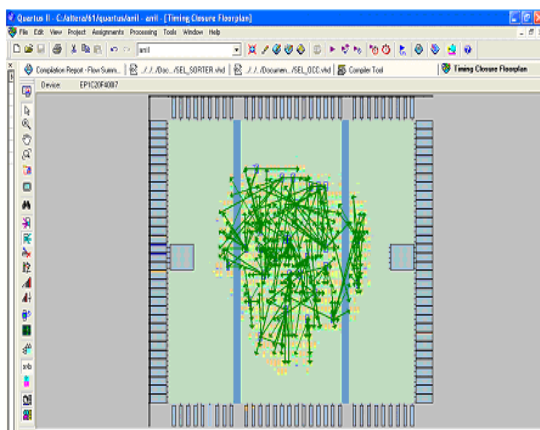


Fig.6. Timing closure floor plan using Chip Planner.

The Floor plan timing closure is shown in Figure-6. The timing closure report gives the Total cell delay = 102.658 ns (33.86 %) and the Total interconnect delay = 187.876 ns (63.14 %) for the Proposed system.

TABLE IV  
COMPARISON OF IMPLEMENTATION RESULTS

Sl No	Parameter	Existing system	Proposed system
1	Logic cell	347	563
2	LC register	738	905
3	LUT only LC	128	218
4	Register only LC	133	160
5	LUT/ Register LC's	185	185
6	Critical Path Delay	316 nsec	309 ns
7	Total cell delay	112 nsec	103 ns
8	Total interconnect Delay	191 nsec	187 nsec

From the Table IV it can be observed that the Proposed System requires more resources on the FPGA than the Existing Huffman system.

## VI. CONCLUSION

In this paper a high speed Huffman decoder is implemented using the concept of efficient partitioning of the multiple length code to isolated code register based on their length. The multi level Huffman decoder with multiple scan improves the scanning time for a test data set having less code length. We conclude that the High speed Huffman decoding system takes 50 % less time for decoding when simulated using Active HDL 8.1v and 33% more FPGA resources when implemented using Quartus II implementation tool compared to the existing Huffman decoding system.

## REFERENCES

- [1] J. Aerts and E. J. Marinissen, "Scan chain design for test time reduction in core-based ICs," in Proc. Int. Test Conf., 1998, pp. 448–457.
- [2] I. Bayraktaroglu and A. Orailoglu, "Test volume and application time reduction through scan chain concealment," in Proc. Design Automation Conf., 2001, pp. 151–155.
- [3] F. Brglez, D. Bryan, and K. Kozminski, "Combinational profiles of sequential benchmark circuits," in Proc. Int Symp. Circuits Syst., 1989, pp.1929–1934.
- [4] A. Chandra and K. Chakrabarty, "Test data compression for system-on-a-chip using Golomb codes," in Proc. VLSI Test Symp., 2000, pp.113–120.

[5] Efficient test data compression and decompression for system-on-a-chip using internal scan chains and Golomb coding,” in Proc. Design Automation, Test Eur., 2001.

[6] “Frequency-directed run-length codes with application to system-on-a-chip test data compression,” in Proc. VLSI Test Symp., 2001, pp. 42–47.

[7] “Reduction of SOC test data volume, scan power and testing time using alternating run-length codes,” in Proc. Design Automation Conf., 2002, pp. 673–678.

[8] R. Chandramouli and S. Pateras, “Testing systems on a chip,” IEEE Spectrum, pp. 42–47, Nov. 1996.

[9] R. Dorsch and H.-J. Wunderlich, “Reusing scan chains for test pattern decompression,” in Proc. European Test Workshop, 2001, pp. 124–132.

[10] “Tailoring ATPG for embedded testing,” in Proc. Int. Test Conf., 2001, pp. 530–537.

[11] P. Gonciari, B. M. Al-Hashimi, and N. Nicolici, “Improving compression ratio, area overhead, and test application time for systems-on-a-chip test data compression/decompression,” in Proc. Design Automation Test Eur., 2002, pp. 604–611.

[12] I. Hamzaoglu and J. H. Patel, “Test set compaction algorithms for combinational circuits,” in Proc. Int. Conf. Computer-Aided Design, 1998, pp. 283–289.

[13] Xrysovalantis Kavousianos, Emmanouil Kalligeros, and Dimitris Nikolos,” Multilevel Huffman Coding: An Efficient Test-Data Compression Method for IP Cores”, in IEEE Transactions on Computer-Aided Design of Integrated Circuits and Systems, VOL. 26, NO. 6, June 2007.

[14] Xrysovalantis Kavousianos, Emmanouil Kalligeros, and Dimitris Nikolos,” Multilevel-Huffman Test-Data Compression for IP Cores With Multiple Scan Chains”, IEEE Transactions on VLSI SYSTEMS, VOL. 16, NO. 7, July 2008.

[15] K. Ashok Babu and V. Satish Kumar, “Implementation of Data Compression Using Huffman Coding”, International Conference on Methods and Models in Computer Science ICM2CS-2010, 2010, pp 65-70



**SRIKANTH  
IMMAREDDY**

Received the Bachelor degree in Electronics and Communication Engineering (ECE) from the JNTU Hyderabad India and Master degree in Digital Systems from Osmania University, India in 2009.

He is working as Assistant Professor in ECE Dept at Methodist College of Engineering and Technology, India His main interests are in the fields of Very Large Scale Integration and Digital Signal Processing.



**SRAVANKUMAR  
TALUSANI** Received the Bachelor degree in Electronics and Communication Engineering (ECE) from Osmania University, India and Master degree in Digital Systems & Computer Electronics from JNTU Ananthapur, India.

He is working as Assistant Professor in ECE Dept at Methodist College of Engineering and Technology, India His major interests are in the fields of Analog Electronics and Signal Processing.